



# **PHASE EQUILIBRIA OF REFRIGERANT GAS HYDRATE SYSTEMS IN THE PRESENCE OF SUCROSE**

**By**

**Aimee Smith**

BScEng (Chemical)

University of KwaZulu-Natal

This dissertation is submitted in fulfillment of the academic requirements for the degree of Master of Science in Engineering (Chemical) at the School of Engineering, University of KwaZulu-Natal

**Supervisor:** Prof. Deresh Ramjugernath

**Co-Supervisors:** Dr. Paramespri Naidoo

Prof. Amir H. Mohammadi

**January 2015**

DECLARATION

I, Aimee Smith, declare that:

- (i) The research reported in this thesis, except where otherwise indicated, is my original work.
- (ii) This thesis has not been submitted for any degree or examination at any other university.
- (iii) This thesis does not contain other persons' data, pictures, graphs or other information, unless specifically acknowledged as being sourced from other persons.
- (iv) This thesis does not contain other persons' writing, unless specifically acknowledged as being sourced from other researchers. Where other written sources have been quoted, then: a) their words have been re-written but the general information attributed to them has been referenced; b) where their exact words have been used, their writing has been placed inside quotation marks, and referenced.
- (v) Where I have reproduced a publication of which I am an author, co-author or editor, I have indicated in detail which part of the publication was actually written by myself alone and have fully referenced such publications.
- (vi) This thesis does not contain text, graphics or tables copied and pasted from the internet, unless specifically acknowledged, and the source being detailed in the thesis and in the References sections.

\_\_\_\_\_  
Aimee Smith

\_\_\_\_\_  
Date

As the candidate's supervisor I agree/do not agree to the submission of this thesis.

\_\_\_\_\_  
Prof. Deresh Ramjugernath

\_\_\_\_\_  
Date

**ABSTRACT**

The South African sugar industry has the potential to be one of the largest suppliers of renewable energy into the national energy grid. The majority of the sugar mills obtain their fuel requirements by burning of final bagasse produced during sugar cane processing. In some cases, surplus energy is produced which can often go to waste. However, if this surplus energy could be injected into the national energy grid, it will not only increase the industry's profitability, but also assist in meeting government's renewable energy targets. One such area of the sugar milling process where excess energy could be recovered is the highly energy-intensive evaporation process. This study investigates gas hydrate technology as a possible aqueous solution separation process. It investigates gas hydrate technology as a feasible technique for increasing the solids content in aqueous carbohydrate systems. The aim of this study is to obtain hydrate dissociation conditions of various refrigerant hydrates in the presence of sucrose. The hydrate-vapour-liquid (HVL) phase equilibrium measurements were performed using the isochoric pressure search method with a newly developed high-pressure apparatus. In order to verify the temperature and pressure calibrations, vapour pressure measurements for 1,1,1,2-tetrafluoroethane (R134a), R410a and R507 were performed. The experimental apparatus and method were verified by conducting hydrate-vapour-liquid equilibrium measurements on known test systems. These include CO<sub>2</sub> (1) + water (2) + {0 or 20} wt.% sucrose. New systems measured include 1,1,1,2-tetrafluoroethane (1) + water (2) + {12 or 15} wt.% sucrose (3), R410a (1) + water (2) + {12 or 15} wt.% sucrose (3) and R507 (1) + water (2) + {12 or 15} wt.% sucrose (3). In addition, a sucrose sample supplied by the Sugar Milling Research Institute (SMRI) was also investigated.

From the measurements performed in this study, it is found that the presence of sucrose exhibits an inhibition effect on hydrate formation. This is seen by the shift of the H-V-L equilibrium phase boundary to either higher pressures or lower temperatures. Additionally, through measurements performed on the SMRI sample it can be seen that the presence of additional carbohydrates (glucose and fructose) in the system increases the effect of inhibition on hydrate formation.

The van der Waals-Platteeuw solid solution theory is used to model the hydrate phase (Parrish and Prausnitz, 1972). For systems containing carbon dioxide, the vapour phase is modeled using the Peng-Robinson Equation of State (Peng, 1976), while for systems containing refrigerants, the vapour phase is assumed ideal based on the assumptions of Eslamimanesh et al. (2011). In all systems, the liquid phase is modeled using the UNIFAC model. The inhibition effect of sucrose is accounted for by using a purely empirical correction method proposed by Englezos and Hall (1994). The predicted results compare well to the experimental results.

## **ABSTRACT**

An approximate cost analysis, based on the findings of Heist and Barron (1983) was also performed. This analysis determined that the capital costs associated with the construction of a hydrate separation technology would amount to approximately R33 million with the operations and maintenance costs amounting to approximately R0.08 per kg of feed processed. These figures compare well to the costs associated with evaporation processes.

In order for hydrate separation technologies to be implemented in the sugar industry, crystal size and quality need to be determined. Therefore, investigations regarding such properties should be conducted. Possible methods to be investigated include Spectroscopy, X-ray Diffraction and Laser Scattering. In addition, techniques to determine the concentration of the final solution, such as centrifugation of the hydrate slurry, need to be established.

**ACKNOWLEDGEMENTS**

My deepest thanks must first go to my Lord and Saviour, Jesus Christ, for accompanying me on this journey and forever being my pillar of hope.

I would like to express my sincere thanks to my supervisors Prof. Deresh Ramjugernath, Dr Paramespri Naidoo and Prof. Amir H. Mohammadi for their continuous support and guidance. This study would not have been possible without their help.

In addition, I would like to thank Thokozani Ngema for his endless patience, kind support and assistance throughout my master's study as well as all of the members of the Thermodynamic Research Unit. I would also like to thank Wayne Nelson and Leon Augustine for the design and construction of my equipment, and Ayanda Khanyile and Lindinkosi Mkhize for all of the assistance during equipment commissioning.

I would like to express my overwhelming thanks to my parents, Sandra McHendry and John McHendry, and Jean-Marc Strydom and Leigh McClelland. I would not be here today without their love and support throughout all of my academic years. Finally, heartfelt thanks must go to my husband, Lloyd Smith, for his love and care. Without his support, I would have not been successful in my study and research.

TABLE OF CONTENTS

**DECLARATION .....i**

**ABSTRACT .....ii**

**ACKNOWLEDGEMENTS .....v**

**TABLE OF CONTENTS .....vi**

**LIST OF FIGURES.....x**

**LIST OF PHOTOGRAPHS.....xiv**

**LIST OF TABLES.....xv**

**NONMENCLATURE.....xviii**

**CHAPTER 1: INTRODUCTION.....1**

**1.1 Gas hydrates: An introductory overview.....1**

        1.1.1 *Hydrate description.....1*

        1.1.2 *Technological aspects.....2*

        1.1.2 *Gas hydrate formation as a separation technology.....3*

**1.2 South African sugar mill overview.....7**

        1.2.1 *Overview of the South African sugar milling process.....7*

        1.2.2 *Current separation process in South African sugar mills.....9*

        1.2.3 *The need for increased energy efficiency in South African sugar mills.....10*

**CHAPTER 2: HYDRATE STRUCTURE AND THERMODYNAMIC MODELING.....12**

**2.1 Gas hydrate theory.....12**

        2.1.1 *Structural theory.....12*

        2.1.2 *Phase diagrams.....15*

        2.1.3 *Hydrate kinetics.....25*

**2.2 Thermodynamic modeling for hydrate-vapour-liquid equilibria.....30**

        2.2.1 *Thermodynamic phase equilibria.....30*

        2.2.2 *Thermodynamic models for vapour and liquid phases.....32*

        2.2.3 *Inhibition effect of sucrose.....40*

        2.2.4 *Thermodynamic models for hydrate phase.....41*

<b>CHPATER 3: REVIEW OF EXPERIMENTAL METHODS AND EQUIPMENT.....</b>	<b>50</b>
<b>3.1 Review of experimental methods.....</b>	<b>50</b>
3.1.1 <i>Visual isobaric temperature search method.....</i>	52
3.1.2 <i>Visual isothermal pressure search method.....</i>	53
3.1.3 <i>Isochoric pressure search method.....</i>	54
<b>3.2 Review of experimental equipment.....</b>	<b>55</b>
3.2.1 <i>Quartz crystal microbalance (QCM).....</i>	56
3.2.2 <i>Cailletet.....</i>	57
3.2.3 <i>The rocking cell apparatus.....</i>	58
3.2.4 <i>High-pressure differential scanning calorimetry.....</i>	59
3.2.5 <i>High pressure autoclave cell.....</i>	61
<b>3.3 Extent of separation.....</b>	<b>67</b>
3.3.1 <i>Direct method.....</i>	67
3.3.2 <i>Indirect method.....</i>	67
3.3.3 <i>Flash calculation method.....</i>	67
<b>CHAPTER 4: DESCRIPTION OF EXPERIMENTAL APPARATUS AND PROCEDURE....</b>	<b>69</b>
<b>4.1 Experimental apparatus.....</b>	<b>69</b>
4.1.1 <i>Isochoric pressure cell.....</i>	71
4.1.2 <i>Agitation technique.....</i>	73
4.1.3 <i>Temperature and pressure sensors.....</i>	74
4.1.4 <i>Liquid temperature bath.....</i>	75
4.1.5 <i>Temperature controllers.....</i>	75
<b>4.2 Experimental procedure.....</b>	<b>76</b>
4.2.1 <i>Isochoric cell preparation.....</i>	76
4.2.2 <i>Calibration procedure.....</i>	77
4.2.3 <i>Sample preparation.....</i>	81
4.2.4 <i>Operating procedure for isochoric pressure cell.....</i>	82
<b>4.3 NIST uncertainty analysis for H-L-V equilibrium data and vapour pressure measurements.....</b>	<b>84</b>
4.3.1 <i>Estimating uncertainty.....</i>	84
4.3.2 <i>Reporting uncertainty.....</i>	85
<b>CHAPTER 5: RESULTS AND DISCUSSION.....</b>	<b>86</b>
<b>5.1 Chemicals used.....</b>	<b>86</b>

## TABLE OF CONTENTS

<b>5.2 Calibrations.....</b>	<b>87</b>
<b>5.3 Measurement uncertainties.....</b>	<b>92</b>
<b>5.4 Test systems.....</b>	<b>92</b>
5.4.1 <i>The CO<sub>2</sub>(1) + water (2) system.....</i>	93
5.4.2 <i>The CO<sub>2</sub>(1) + water (2) + sucrose (3) system.....</i>	95
<b>5.5. New systems.....</b>	<b>96</b>
5.5.1 <i>The 1,1,1,2-tetrafluoroethane (1) + water (2) + sucrose (3)system.....</i>	98
5.5.2 <i>The R410a (1) + water (2) + sucrose (3)system.....</i>	100
5.5.3 <i>The R507 (1) + water (2) + sucrose (3)system.....</i>	102
5.5.4. <i>Comparison of the data measured for the systems consisting of refrigerant formers.....</i>	104
<b>5.6 Data modeling.....</b>	<b>105</b>
5.6.1 <i>Modeling approach of Parrish and Prausnitz (1972).....</i>	105
5.6.2 <i>Modeling approach of Eslamimanesh et al. (2011).....</i>	109
<b>5.7 Industrial application.....</b>	<b>113</b>
5.7.1 <i>“SMRI” sample analysis.....</i>	113
5.7.2 <i>Energy comparison.....</i>	117
5.7.3 <i>Hydrate separation technology.....</i>	118
5.7.4 <i>Industrial cost analysis.....</i>	121
<b>CHAPTER 6: CONCLUSIONS.....</b>	<b>125</b>
<b>CHAPTER 7: RECOMMENDATIONS.....</b>	<b>127</b>
<b>REFERENCES.....</b>	<b>128</b>
<b>APPENDIX A: CRITERIA FOR POTENTIAL FLUORINATED HYDRATE FORMERS.....</b>	<b>140</b>
<b>APPENDIX B: MEASURED HLV EQUILIBRIUM DATA.....</b>	<b>143</b>
<b>APPENDIX C: UNIFAC METHOD.....</b>	<b>146</b>
<b>APPENDIX D: ECONOMIC COST ANALYSIS.....</b>	<b>148</b>
<b>D.1 Capital costs.....</b>	<b>148</b>
D.1.1 <i>Base cost.....</i>	148
D.1.2 <i>Size factor (Fs).....</i>	149
D.1.3 <i>Temperature factor (Ft).....</i>	149
D.1.4 <i>Viscosity factor (Fv).....</i>	149



## TABLE OF CONTENTS

<i>D.1.5 Latent heat factor (<math>F_{hf}</math>)</i> .....	150
<i>D.1.6 Material of construction factor (<math>F_{mat}</math>)</i> .....	150
<b>D.2 Operating and maintenance costs</b> .....	<b>150</b>
<i>D.2.1 Labour component (<math>L</math>)</i> .....	150
<i>D.2.2 Energy component (<math>E</math>)</i> .....	151
<i>D.2.3 Maintenance component (<math>M</math>)</i> .....	151
<i>D.2.4 Amortisation component (<math>A</math>)</i> .....	152
<b>APPENDIX E: FIGURES</b> .....	<b>153</b>

## LIST OF FIGURES

## CHAPTER 1

- Figure 1-1: Phase equilibria diagram of water (Barron and Wrobel, 1985).....4  
 Figure 1-2: Simplified block flow diagram of South African sugar milling process.....7

## CHAPTER 2

- Figure 2-1: Three types of hydrates structures and their cavity arrangement (Khokhar, 1998).....13  
 Figure 2-2: Pressure-temperature phase diagram for pure water (Mooijer-van den Heuvel, 2004).....16  
 Figure 2-3: Pressure-temperature phase diagram for a binary system at a specified composition (Sloan and Koh, 2008).....17  
 Figure 2-4: Temperature-composition phase diagram for a binary system at a specified pressure (Mooijer-van den Heuvel, 2004).....18  
 Figure 2-5: Pressure-composition phase diagram for a binary system at a specified temperature (Mooijer-van den Heuvel, 2004).....18  
 Figure 2-6: Pressure-temperature phase diagram for a type A ternary system exhibiting gas-like behaviour (Mooijer-van den Heuvel, 2004).....21  
 Figure 2-7: Pressure-temperature phase diagram for a type A ternary system exhibiting liquid-like behaviour (Mooijer-van den Heuvel, 2004).....21  
 Figure 2-8: Pressure-temperature phase diagram for a type B ternary system exhibiting gas-like behaviour (Mooijer-van den Heuvel, 2004).....23  
 Figure 2-9: Pressure-temperature phase diagram for a type B ternary system exhibiting liquid-like behaviour (Mooijer-van den Heuvel, 2004).....23  
 Figure 2-10: Pressure-temperature phase diagram for a type C ternary system (Mooijer-van den Heuvel, 2004).....24  
 Figure 2-11: Experimental pressure-temperature trace (Bishnoi and Natarajan, 1996).....26  
 Figure 2-12: Fugacity profile in the diffusion and absorption film surrounding a growing hydrate (Bishnoi and Natarajan, 1996).....27  
 Figure 2-13: Dissociation of hydrate particles (Bishnoi and Natarajan, 1996).....29  
 Figure 2-14: Flow diagram for the Gamma-Phi bubble-pressure method for an isothermal system (Prausnitz and Chueh, 1968).....33  
 Figure 2-15: Flow diagram for the Phi-Phi bubble-pressure method for an isothermal system (Prausnitz and Chueh, 1968).....34

**CHAPTER 3**

Figure 3-1: Isobaric temperature search method (Tumba, 2010).....53

Figure 3-2: Isothermal pressure search method (Tumba, 2010).....54

Figure 3-3: Temperature and pressure trace for formation of simple hydrates (Sloan and Koh, 2008).....55

Figure 3-4: (a) Schematic illustration of the QCM crystal mounting and electrical connection configuration. ....57

(b) Schematic illustration of the QCM mounted with the high-pressure equilibrium cell (Tohidi et al., 2002).....57

Figure 3-5: Schematic illustration of Cailletet apparatus (Sabil and Bin, 2009).....58

Figure 3-6: Schematic illustration of rocking cell apparatus (Najibi et al., 2009).....59

Figure 3-7: Schematic illustration of high pressure DSC apparatus (Delahaye et al., 2006).....60

Figure 3-8: Thermal cycles of hydrate formation and dissociation for high pressure differential scanning calorimetry (Delahaye et al., 2006).....61

Figure 3-9: Schematic diagram of the experimental apparatus of Chun and Lee (1998).....62

Figure 3-10: Schematic diagram of the Jefri-DBR experimental apparatus of Carbone et al. (2012).....63

**CHAPTER 4**

Figure 4-1: Schematic diagram of the experimental setup.....70

Figure 4-2: Schematic of the equilibrium cell.....72

Figure 4-3: Calibration of the bottom temperature sensor. First order relation between standard and sensor temperatures.....78

Figure 4-4: Deviations from the standard temperature due to first order relation for the bottom temperature sensor.....78

Figure 4-5: Calibration of the top temperature sensor. First order relation between standard and sensor temperatures.....79

Figure 4-6: Deviations from the standard temperature due to first order relation for the top temperature sensor.....79

Figure 4-7: Calibration of the WIKA pressure transducer used in this apparatus. First order relation between standard and transducer pressure.....80

Figure 4-8: Deviations from the standard pressure due to first order relation.....81

CHAPTER 5

Figure 5-1: Vapour pressure measurements for the components 1,1,1,2-tetrafluoroethane, R410a and R507.....88

Figure 5-2: Hydrate dissociation conditions for the system CO<sub>2</sub>(1) + water (2).....94

Figure 5-3: Hydrate dissociation conditions for the system CO<sub>2</sub>(1) + water (2) + 20 wt.% sucrose (3).....95

Figure 5-4: Hydrate dissociation conditions for the system 1,1,1,2-tetrafluoroethane (1) + water (2) + sucrose (3).....99

Figure 5-5: Ln P versus 1/T plot for the system 1,1,1,2-tetrafluoroethane (1) + water (2) + sucrose (3). ....99

Figure 5-6: Hydrate dissociation conditions for the system R410a (1) + water (2) + sucrose (3).....101

Figure 5-7: Ln P versus 1/T plot for the system R410a (1) + water (2) + sucrose (3).....101

Figure 5-8: Hydrate dissociation conditions for the system R507 (1) + water (2) + sucrose (3).....103

Figure 5-9: Ln P versus 1/T plot for the system R507 (1) + water (2) + sucrose (3).....103

Figure 5-10: Hydrate dissociation conditions for the systems 1,1,1,2-tetrafluoroethane (1) + water (2) + sucrose (3), R410a (1) + water (2) + sucrose (3) and R507 (1) + water (2) + sucrose (3).....104

Figure 5-11: Computation flow chart for the predictive model for CO<sub>2</sub> (1) + water (2).....106

Figure 5-12: Figure 2.16: Computation flow chart for the predictive model for CO<sub>2</sub> (1) + water (2) + 20 wt.% sucrose (3).....107

Figure 5-13: H-V-L equilibrium data for the system CO<sub>2</sub> (1) + water (2).....108

Figure 5-14: H-V-L equilibrium data for the system CO<sub>2</sub> (1) + water (2) + 20 wt.% sucrose (3).....108

Figure 5-15: Computation flow chart for the predictive model for the hydrate formers R134a, R410a and R507 (1) + water (2) + various concentrations of sucrose (3).....110

Figure 5-16: H-V-L equilibrium data for the system 1,1,1,2-tetrafluoroethane (1) + water (2) + sucrose (3).....111

Figure 5.17: H-V-L equilibrium data for the system R410a (1) + water (2) + sucrose (3).....111

Figure 5.18: H-V-L equilibrium data for the system R507 (1) + water (2) + sucrose (3).....112

Figure 5-19: Hydrate dissociation conditions for the system R410a (1) + water (2) + “SMRI sample” (3).....115

Figure 5-20: Hydrate dissociation conditions for the system former (1) + water (2) + sucrose (3)...116

Figure 5-21: Hydrate dissociation conditions for the system former (1) + water (2) + glucose (3)...116

Figure 5-22: Hydrate dissociation conditions for the system former (1) + water (2) + fructose (3)...117

## LIST OF FIGURES

Figure 5-23: Hydrate separation process diagram (Werezak, 1969).....119

### APPENDIX E

Figure E-1: Capital cost factor – size (Barron and Wrobel, 1985).....153

Figure E-2: Capital cost factor – temperature (Barron and Wrobel, 1985).....153

Figure E-3: Capital cost factor – viscosity (Barron and Wrobel, 1985).....154

Figure E-4: Capital cost factor – latent heat (Barron and Wrobel, 1985).....154

Figure E-5: Labour cost factor – size (Barron and Wrobel, 1985).....155

**LIST OF PHOTOGRAPHS**

**CHAPTER 4**

Photograph 4-1: Experimental setup.....71  
Photograph 4-2a: Cell without magnetic stirring device.....73  
Photograph 4-2b: Cell with magnetic stirring device.....73  
Photograph 4-3: Magnetic stirrer device.....74

## LIST OF TABLES

**CHAPTER 1**

Table 1-1: Criteria used to determine suitable fluorinated clathrate former (McCormack and Andersen, 1995).....	6
---	---

**CHAPTER 2**

Table 2-1 Properties of Type I, Type II and Type H gas hydrates.....	14
Table 2-2: Application of Gibbs phase rule to single-component system (Mooijer-van den Heuvel, 2004).....	16
Table 2-3: Application of Gibbs phase rule to binary system (Mooijer-van den Heuvel, 2004).....	19
Table 2-4: Application of Gibbs phase rule to ternary system (Mooijer-van den Heuvel, 2004).....	20
Table 2-5: Commonly used EOS in hydrate modeling.....	35
Table 2-6: Pure component properties for PR EOS.....	37
Table 2-7: UNIFAC subgroup parameters.....	40
Table 2-8: Ratio of number of cavities to the number of water molecules present in hydrate lattice (van der Waals and Platteeuw, 1959).....	42
Table 2-9: Fitted Langmuir parameters for various formers used in this study.....	44
Table 2-10: Hydrate model developments.....	45
Table 2-11: Thermodynamic properties for sI and sII hydrates for liquid or ice and an empty hydrate lattice (Parrish & Prausnitz, 1972).....	48

**CHAPTER 3**

Table 3-1: Commonly used experimental methods for the determination of hydrate dissociation conditions (Sloan and Koh, 2008).....	52
Table 3-2: Review of high-pressure autoclave apparatus.....	64

**CHAPTER 5**

Table 5-1: Purity and supplier of the gases used in vapour-liquid equilibrium and hydrate measurements.....	87
Table 5-2: Vapour pressure data measured in this study.....	88
Table 5-3: Vapour pressure data for 1,1,1,2-tetrafluoroethane.....	89
Table 5-4: Vapour pressure data for R410a.....	90
Table 5-5: Vapour pressure data for R507.....	90
Table 5-6: Wagner-equation used to determine vapour pressures of R507.....	91

## LIST OF TABLES

Table 5-7: Measurement uncertainty applicable to this study.....	92
Table 5-8: Test systems measured for HLV equilibrium.....	93
Table 5-9: Hydrate dissociation measurements for the system CO <sub>2</sub> (1) + water (2).....	93
Table 5-10: Hydrate dissociation measurements for the system CO <sub>2</sub> (1) + water (2) + 20 wt.% sucrose (3).....	95
Table 5-11: New HLV equilibrium data measured for systems of interest.....	97
Table 5-12: Hydrate dissociation measurements for the system 1,1,1,2-tetrafluoroethane (1) + water (2) + sucrose (3).....	98
Table 5-13: Hydrate dissociation measurements for the system R410a (1) + water (2) + sucrose (3).....	100
Table 5-14: Hydrate dissociation measurements for the system R507 (1) + water (2) + sucrose (3).....	102
Table 5-15: Percent absolute average deviation for measured systems using the predictive model approach of Eslamimanesh et al. (2012).....	113
Table 5-16: SMRI systems measured for HVL equilibrium.....	114
Table 5-17: Hydrate dissociation measurements for the system R410a (1) + water (2) + “SMRI” sample (3).....	114
Table 5-18: Simple energy comparison between evaporation and fusion.....	118
Table 5-19: Characteristics of vaporization process versus fusion process (Barron and Wrobel, 1985).....	120
Table 5-20: Cost analysis assumptions (Barron and Wrobel, 1985).....	121
Table 5-21: Cost analysis scope (Barron and Wrobel, 1985).....	122

## APPENDIX A

Table A-1: Detailed analysis of specific criteria used to determine potential fluorinated hydrate formers.....	141
---	-----

## APPENDIX B

Table B-1: Measured HLV equilibrium data for the system CO <sub>2</sub> (1) + water (2) cited in literature...143	143
Table B-2: Measured HLV equilibrium data for the system 1,1,1,2-tetrafluoroethane (1) + water (2) cited in literature.....	143
Table B-3: Measured HLV equilibrium data for the system R410a (1) + water (2) cited in literature.....	143
Table B-4: Measured HLV equilibrium data for the system R507 (1) + water (2) cited in literature.....	144



## LIST OF TABLES

Table B-5: Measured HLV equilibrium data for the system Former (1) + water (2) + sucrose (3) cited in literature.....	144
Table B-6: Measured HLV equilibrium data for the system Former (1) + water (2) + glucose (3) cited in literature.....	144
Table B-7: Measured HLV equilibrium data for the system Former (1) + water (2) + fructose (3) cited in literature.....	145

### APPENDIX C

Table C-1: UNIFAC interactions parameters, $a_{mk}$ , in Kelvins (Fredenslund et al., 1993).....	147
--	-----

### APPENDIX D

Table D-1: Material of construction cost factors (Barron and Wrobel, 1985).....	150
---	-----

NOMENCLATURE

a	Attractive volume parameter
$a_w$	Activity of water
A	Reduced variable of a
Å	Angström unit
$A_{ml}$	Fitted constant for component l in cavity m (K)
$A_p$	Hydrate surface area per particle
b	Excluded volume parameter
B	Reduced variable of b
$B_{ml}$	Fitted constant for component l in cavity m (K)
°Brix	Sugar content by mass expressed as a percentage
C	Celsius
$C_{ml}$	Langmuir constant for component l in cavity m
$C_p$	Heat capacity (J/mol.K)
f	Fugacity
F	Degrees of freedom
G	Gibbs free energy
J	Joule
$k_d$	Mass transfer coefficient for hydrate desorption (m/s)
$k_r$	Mass transfer coefficient for hydrate reaction (m/s)
$k_{ij}$	Binary interaction coefficient
K	Kelvin
$K^*$	Mass transfer coefficient of diffusion and reaction (m/s)
$K_d$	Mass transfer dissociation rate constant
m	Meter
M	Molecular weight (kg/kgmol or g/gmol)
n	Adjustable parameter
N	Number of species
pm	Picometers
P	Pressure (MPa)
$Q_t$	Quintuple point
r	Core radius (m)
R	Universal Gas Constant (MPa.m <sup>3</sup> /kgmol.K)
t	Time
T	Absolute temperature (K)

## NOMENCLATURE

$v$	Molar volume
$V$	Molar volume ( $\text{m}^3/\text{mol}$ )
$w(r)$	Spherically symmetric cell potential (J)
$x$	Liquid mole fraction
$y$	Gas mole fraction

### Greek Letters

$\alpha$	Numerical parameter / core radius ( $\text{\AA}$ )
$\beta$	Interaction energy parameter
$\gamma_i$	Species Activity coefficient
$\mu$	Chemical potential (J/mol)
$\pi$	Number of phases
$\phi$	Fugacity coefficient
$\theta_{ml}$	Probability function
$v_m$	Number of cages per water molecule in a unit hydrate cell
$\omega$	Acentric factor

### Subscripts

a	Additive
b	Bulk
c	Critical
eq	Equilibrium
F	Former
g	Gas
HC	Hydrocarbon
i	component
s	Sucrose
w	Water

### Superscripts

-	Average
$\alpha$	Pure water
$\beta$	Empty hydrate
C	Combinatorial

H	Hydrate
i	adjustable parameter
L	Liquid
MT	Hypothetical empty hydrate
R	Residual
sat	Saturated
o	Reference point

### Abbreviations

%AAD	Percent absolute average deviation
atm	Atmospheres
EOS	Equation of state
H	Hydrate
H-V-L	Hydrate-Vapour-Liquid
I	Ice
L	Liquid
MW	Megawatts ( $J/s \cdot 10^{-3}$ )
PR	Peng-Robinson
PRSV	Peng-Robinson-Stryjek-Vera
PT	Patel and Teja
sI	Structure I
sII	Structure II
sH	Structure H
SRK	Soave-Redlich-Kwong
V	Vapour
VHP	Very high purity
wt.	Weight

## CHAPTER 1

### INTRODUCTION

Currently, one of the major challenges within process engineering is the execution of more economical and sustainable technologies to meet the ever-increasing human needs. One such industry where these challenges are faced is the South African sugar milling industry. This industry endures to experience diminished returns and suffers from the disorder of distorted world sugar market conditions (Parker, 2009). The South African sugar industry has the potential to be one of the largest suppliers of renewable energy into the national energy grid, and in doing so, not only increase the industry's profitability, but also assists in meeting government's renewable energy targets (Phillips, 2011). One such area of the sugar milling process where excess energy could be cultivated is the highly energy-intensive aqueous sucrose separation process.

This dissertation deals with experimental thermodynamic aspects in the context of an alternative sucrose separation technology, through gas hydrate formation.

#### **1.1 Gas hydrates: An introductory overview**

The 19<sup>th</sup> century marked the first discovery of hydrates. The discovery was made by Sir Humphry Davy when he found that a solid compound was formed when an aqueous solution of chlorine was cooled to temperatures below 9.0 °C (Englezos, 1993). This discovery was later confirmed by Michael Faraday in 1823, who made the suggestion that the solid compound was composed of 1 part chlorine and 10 parts water (Englezos, 1993). These solid compounds are referred to as hydrates. Currently there are over 130 known species capable of forming such nonstoichiometric compounds when combined with water (Sloan and Koh, 2008).

##### *1.1.1 Hydrate description*

Gas hydrates are a type of clathrate compound, which falls under the class of a solid inclusion compound (Huang et al., 1965). An inclusion compound consists of two species of molecules arranged in such a manner that one molecular species physically entraps the other. The molecular species, which forms the entrapping framework, is known as the 'host', whereas the entrapped molecular species is known as the 'guest' or 'hydrate former'.

Clathrate structures, which involve an aqueous host, are referred to as gas hydrates. Therefore, in such cases, the solid inclusion compound is formed of water and one or more hydrate formers. No covalent chemical bonds exist between the hydrate former and water molecule framework. The water molecules are attached only to each other by hydrogen bonds; the same type of bonds found in ice (Werezak, 1969). To ensure that the hydrate crystal remains stable, van der Waals forces are present between the host and former molecules.

Hydrate formers are generally low molecular weight gases or liquids, and their molecular size and geometry are important in determining their fit within the gas hydrate cavities. Formers are found to stabilize the hydrate crystal, allowing it to exist at temperatures higher than those where pure water crystals would have melted (Werezak, 1969; Barron and Wrobel, 1985). Due to the selection of the former, these higher crystallization temperatures have the advantage of increasing crystal growth rates, as well as decreasing the viscosity of the solution. Common hydrate formers (such as carbon dioxide, methane, ethane and propane) tend to form hydrates at high pressures (>1 MPa) and low temperatures (0 - 5°C); therefore the use of refrigerants to form hydrates is appealing as formation may occur at near ambient conditions (Heist, 1981; Eslamimanesh et al., 2012). In addition to the use of refrigerants, hydrate promoters can also be employed to either increase the hydrate formation temperature, or decrease the hydrate formation pressure. On the other hand, in areas where hydrate formation is a nuisance, inhibitors are used to produce the opposite effect to promoters.

### *1.1.2 Technological aspects*

In the early 1930s, the topic of gas hydrates entered the field of engineers (Englezos, 1993). This was due to the realisation that natural gas hydrates could form and block pipelines at temperatures greater than that at which water freezes. Thus, the prevention of hydrate formation became a great concern, particularly in the natural gas and crude petroleum industries.

However, gas hydrate formation is believed to be a promising novel separation technology (Huang et al., 1966; Englezos, 1993; Eslamimanesh et al., 2012). There exist a range of aqueous solutions that can be separated via gas hydrate formation in an approach similar to, but more economical than conventional freeze technologies (Heist, 1979; Barron and Wrobel, 1985; Chun et al., 1998). Water desalination is another process where the use of gas hydrates has been investigated (Englezos, 1993; McCormack and Andersen, 1995; Eslamimanesh et al., 2012; Peticrew, 2012). Various studies have been conducted in an attempt to design an efficient and economical desalination processes via gas hydrate formation. The formation of gas hydrates also presents a promising technology for gas separation (Guo et al., 2004; Eslamimanesh et al., 2012). Such gases include: greenhouse gases (carbon dioxide, methane, hydrogen sulfide and sulfur hexafluoride), hydrogen and nitrogen. Hydrate

formation can prove to be a more economically viable option for gas separation over conventional methods due to the use of promoters, which decrease energy requirements, and subsequently decrease operating costs (Eslamimanesh et al., 2012).

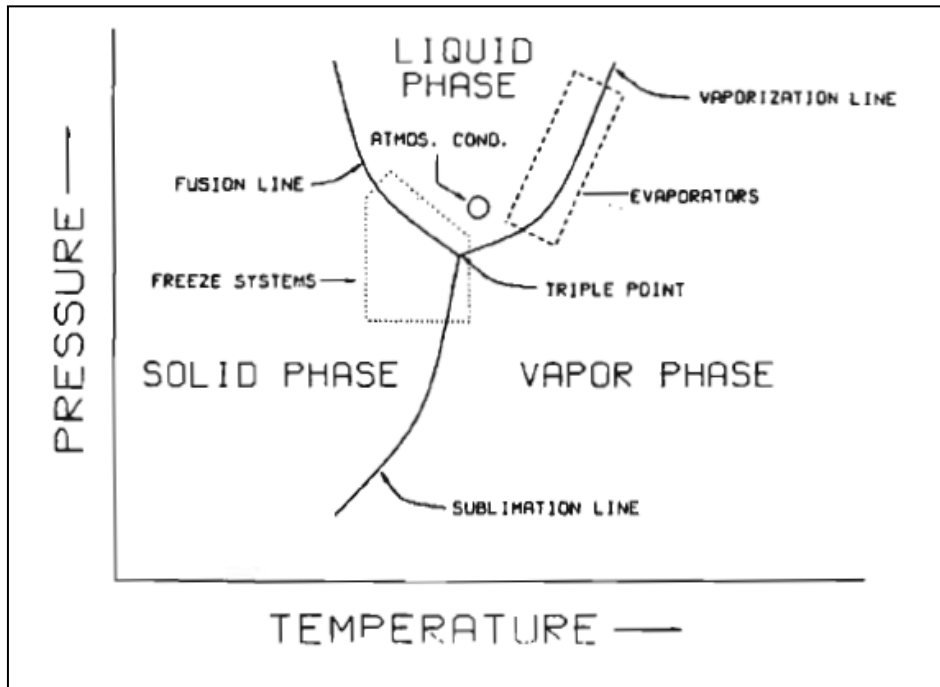
Additionally, if extracted in an economically viable manner, naturally occurring gas hydrates present in the earth's crust could prove to be a promising source of energy (Englezos, 1993). It is believed that approximately  $10^{16}$  m<sup>3</sup> of methane exists in hydrate form under the earth's surface (Eslamimanesh et al., 2012). This trapped methane is commonly harvested by reducing the pressure of the reservoir, increasing the reservoir temperature to conditions outside of the hydrate stability zone, or by the addition of inhibitors.

### *1.1.2 Gas hydrate formation as a separation technology*

#### *1.1.2.1 Emerging aqueous solution separation applications*

The majority of food industries, such as the South African sugar industry, are concerned with separations involving the removal of water. In most cases this separation is performed by either multiple-effect evaporation or freeze concentration (Deshpande et al., 1984; Englezos, 1994; Tongaat Hulett Sugar, 2012). According to Heist and Barron (1983), this is an ideal area for application of hydrate separation processes. It has been found that the energy consumption in the separation of aqueous solutions via evaporation can be reduced by 70 to 90% by using hydrate formation technologies (Heist and Barron, 1983). The thermodynamic basis for this substantially lowered energy requirement is due to the fact that the latent heat of fusion is less than that of evaporation, and since the process operates at lower temperatures, the entropy of separation is also less than that compared to evaporation processes. In studies conducted by Heist and Barron (1983), it was found that the crystallizing temperatures of aqueous solutions could be raised up to 30°C by the use of refrigerant hydrate systems.

A simplified comparison between the energy usage in evaporation techniques and hydrate formation techniques is shown below in Figure 1-1. This figure is a pressure-temperature diagram of the phase equilibria for a one-component solution of pure water. Shown in the diagram are the general phase regions in which vaporization and freeze or hydrate systems operate. The amount of energy needed by these processes is the sum of two parts: the amount of work or heat transfer needed to change the pressure and temperature to reach the process operating point, which can be either mechanical work or sensible heat transfer, plus the heat transfer needed to cause the phase change, known as latent heat transfer. For most applications the sum of these two energy components, i.e., the total separation energy, is less for a freeze or hydrate process than a vaporization process.



**Figure 1-1: Phase equilibria diagram of water (Barron and Wrobel, 1985).**

In addition to being less energy intensive, separation of aqueous solutions via gas hydrate formation has many other advantages. Since this is a low temperature operation and it can be designed to be totally sealed, it is especially suitable for volatile or heat sensitive foods, such as sucrose. The low temperature operation also reduces microbiological activity, resulting in longer periods between equipment cleaning and thus better equipment utilization (Barron and Wrobel, 1985). Lower temperatures also reduce corrosion effects; therefore less expensive materials of construction are required (Heist, 1979). The beet sugar industry is already a field where hydrate formation is being investigated as a separation method in place of the highly energy-intensive evaporation methods (Heist Engineering Corp, 1988).

#### 1.1.2.2 Previous studies in food engineering

Previous studies on the separation of aqueous solutions by use of gas hydrate formation (Huang et al., 1965; Huang et al., 1966) reported the characteristics of methyl bromide, trichlorofluoromethane (R11) and 1,1-difluoroethane (R152a) hydrates formed in a range of aqueous solutions containing carbohydrates, proteins and lipids, as well as the concentration of apple, orange, and tomato juices. These formers were chosen on the basis that they form hydrates which are stable under conditions of relatively high temperatures and low pressures (Huang et al., 1966). In these studies, sucrose concentrations of 20 and 60 wt.% were investigated. It was reported that the hydrates formed easily in the 20 wt.% solutions, however hydrate formation in the 60 wt.% solutions was not possible. Werezak (1969) also examined the separation of aqueous solutions by gas hydrate formation in an attempt to



establish a technology for the separation of temperature sensitive and/or viscous aqueous mixtures. The solutions used consisted of 25 wt.% of coffee extract, sucrose and sodium chloride. The hydrate formers used included ethyl oxide, trichlorofluoromethane, propylene oxide, sulfur dioxide and methyl chloride. The separation of aqueous coffee solutions by use of xenon gas hydrates has also been investigated by Purwanto et al. (2001) with positive results.

The phase equilibrium behaviour of various formers in the presence of carbohydrate systems has rarely been investigated in the literature, however three such investigations were performed by Chun and Lee (1998, 1999) and Carbone et al. (2012). Common hydrate formers, carbon dioxide and methane, as well as a refrigerant gas, chlorodifluoromethane (R22), were investigated in these studies in order to establish how the former properties affected hydrate formation, as well as the effect sugar systems exerted on hydrate formation.

Since no investigations into the effects of using fluorinated hydrate formers in the food industry have yet been conducted, in order to determine a suitable commercial fluorinated hydrate former for the concentration of aqueous sucrose solutions, several criteria were considered. Initially, commercially available fluorinated compounds were compared to the Montreal Protocol. Only those refrigerants that were not banned, or would not be banned in the near future, were considered for investigation. These refrigerants included R32, R125, R134a, R290, R407c, R410a and R507. The commercially available fluorinated clathrate formers that were not banned the Montreal Protocol were further investigated using the criteria in Table 1-1 below. A detailed analysis of each property and criteria for each potential fluorinated hydrate former is available in *Appendix A, Criteria for potential fluorinated hydrate formers*.

**Table 1-1: Criteria used to determine suitable fluorinated clathrate former (McCormack and Andersen, 1995).**

Property	Criteria
Environmentally friendly	Former approved by the Montreal protocol, has low ozone depletion potential and greenhouse warming potential.
Non-toxic	Former has low toxicity, non-carcinogenic and non-mutagenic.
Non-flammable	Former has high flash point, reduce fire risk.
Stable	Former reacts slowly with chemicals.
Low cost	Lower operating costs.
Transition temperature (in the range of 5.6° to 39.4°C)	Formers with operating conditions close to ambient conditions result in lower operating costs.
Operating pressure (in the range of 1 – 7 atm)	Formers with operating conditions close to ambient conditions result in lower operating costs.
Compatible with standard materials	Former has low chemical activity.
Availability (commercial quantities)	Former available in commercial quantities.
Water solubility	A former with low water solubility enhances the degree of recovery of the former from the water.
Quadruple point	Operation usually occurs near upper quadruple point.
Critical point	The upper quadruple point should be far away from the critical point in order to obtain a large heat of vaporization.

From the analysis performed, it was found that the most suitable fluorinated clathrate formers were R134a, R410 and R507. However, since the potential outcome of this study is the application of gas hydrate separation technologies in the food industry, further investigation into these refrigerants needs to take place. Although the chosen refrigerants have relatively low toxicity effects, this issue still presents a threat to the use of these formers in the sugar industry. In addition, while the chosen refrigerants are relatively non-soluble in water, further investigation into the concentrated solution is advised in order to determine the degree by which the fluorinated component is present in the final solution.

Although gas hydrate formation has not been investigated thoroughly with regards to aqueous carbohydrate solution separation, in order to improve the separation of a range of dilute aqueous solutions through the formation of gas hydrates, it is essential to know the phase equilibrium data and predictive methods for hydrate formation conditions (Barron and Wrobel, 1985; Chun and Lee, 1998).

## 1.2 South African sugar mill overview

### 1.2.1 Overview of the South African sugar milling process

In South Africa, all sugar is first produced as raw sugar (brown sugar). A portion of this raw sugar then undergoes further processing and de-colourisation to produce refined sugar (white sugar) (SMRI, 2012). The process of raw sugar manufacture from sugarcane can be divided into a number of distinct unit operations. A basic diagram of sugarcane processing is shown in Figure 1-2 below.

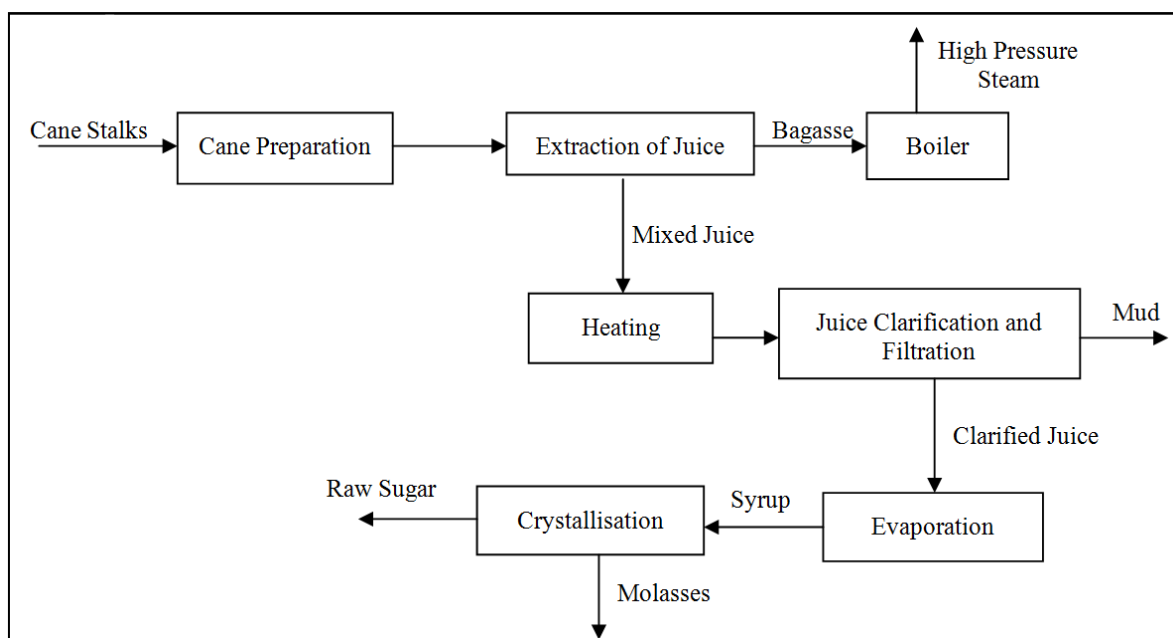


Figure 1-2: Simplified block flow diagram of South African sugar milling process.

After the sugarcane has been harvested, the first step in the manufacture of raw sugar is cane preparation. In cane preparation, the cane stalks are shredded and cut in order to disintegrate the cane material (SMRI, 2012). Cane preparation is an important operation since enhanced sucrose extraction is obtained by crushing finely shredded cane instead of intact sugarcane stalks (Tongaat Hulett Sugar, 2012).

Sugarcane juice is extracted from the prepared cane by either milling or diffusion. Milling involves the extraction of juice by repeated crushing and washing. Diffusion involves the extraction of juice by washing only, where a final squeezing is used to dry the spent fibre (SMRI, 2012). In an average sugarcane mill, the shredded sugarcane is squeezed between grooved rollers, which force the cane juice out of the fibre. However, fibre has the natural tendency to retain its own weight in juice irrespective of the pressure applied to it. To overcome this problem, water is poured over the sugarcane before crushing in a process known as imbibition. Typically, six sugar mills are operated in tandem, due to the low extraction of a single milling unit (Tongaat Hulett Sugar, 2012). In the diffusion process, the prepared cane is washed with large amounts of water. This prepared cane is slowly dragged through the diffuser where the water permeates through the bed in order to wash out the sucrose-containing juice. The fibre that leaves the diffuser is saturated with liquid and therefore has to be dewatered in a mill before being sent to the boilers (Tongaat Hulett Sugar, 2012).

The fibre (called bagasse) from the juice extraction process is sent to the boilers to produce high-pressure steam. This steam is used for later processing operations, production of electricity and turbine operation (Tongaat Hulett Sugar, 2013).

Extracted juice (called mixed juice) from the milling process contains a large amount of cane fibre. This fibre is removed by either pouring the juice over a wire-mesh screen or it is cascaded over an inclined wedge-wire screen. Juice exiting the diffuser process is usually not screened due to the screening effect of the cane bed itself (Tongaat Hulett Sugar, 2012). The mixed juice is then purified. In the purification process, the juice is heated, limed, and finally clarified to remove the solid materials present. The precipitate that settles (called mud) is removed from the bottom of the clarifier and filtered to extract the remaining juice. This filtrate is then returned to the process (SMRI, 2012). The overflow from the clarifier (called clarified juice) is sent to the evaporators.

Multiple-effect evaporators concentrate the clarified juice to approximately 60° to 65°Brix (SMRI, 2012), where °Brix is the sugar content by mass expressed as a percentage. The evaporated juice (called syrup) is then sent to vacuum pans for further concentration and crystallization.

In the crystallization process, vacuum pans are used to heat the syrup. As the concentration of the syrup increases, crystal growth is achieved within several pans in a series of steps. This is done in order to maximize the amount of sucrose recovered in the raw sugar. This is generally performed in three boiling steps. The first boiling step produces an A- massecuite mixture. The mixture is centrifuged to produce A-sugar (brown sugar), which is dried and dispatched or kept for refining into white sugar, and A-molasses. A-molasses still contains 80° to 85°Brix and is therefore boiled again in the vacuum pans to produce a B-massecuite. The process is repeated to finally produce C-sugar and C-molasses. All B and C sugars are remelted and returned to the syrup to produce more high quality A-sugar (called VHP sugar-very high purity sugar), the final raw sugar product. C-molasses is the final molasses product. It still contains considerable amounts of sucrose (32°- 42°Brix), which to date, has not been recovered by an economically viable method. In an average South African mill, for every 100 tons of sugarcane processed, approximately 12 tons of VHP sugar is produced and 14 tons of final molasses is produced (C-molasses) (SMRI, 2012).

The sugar and molasses harvests are warehoused and sold. A portion of the raw sugar is sent to refineries to produce refined sugar. Molasses is usually sold as an additive for animal feed, while some mills use the molasses to produce other products, such as anhydrous ethanol.

### *1.2.2 Current separation process in South African sugar mills*

In a typical South African raw sugar mill, the clarified juice is concentrated via multi-effect evaporation. In this process, water is removed from the mixture by vaporisation. The juice is boiled in series using multiple vessels, with steam fed to the first vessel only. The vapour produced in the first vessel boils the juice in the second vessel. The vapour produced in the second vessel is then used to heat/boil the juice in the third vessel and so on, until the vapour from the final vessel goes to waste (Tongaat Hulett Sugar, 2012). The juice typically enters the evaporator series at approximately 12°Brix (Chung, 2000) and is concentrated to roughly 60° to 65°Brix in the final evaporator (SMRI, 2012).

The main purpose of the evaporation process is to separate the water from the aqueous sucrose solution to produce a thick syrup. Sucrose is temperature sensitive, therefore the evaporation process needs to be performed as quickly as possible, and at temperatures that will reduce sucrose losses, colour formation and sucrose decomposition (Lewis et al., 2010). Since the latent heat of evaporation of water is comparatively high (2257 kJ/kg), this vaporisation process is highly energy intensive (Lewis et al., 2010).

In the proposed study, the evaporation step, shown in Figure 1-2, would be replaced by a hydrate separation technology step. This process is described in *Chapter 5.7.3, Hydrate separation technology*.

### *1.2.3 The need for increased energy efficiency in South African sugar mills*

Over the past few years, a noticeable decline in sugar production has been observed in South Africa (Parker, 2009; Phillips, 2011). The main reason for this decline is the less than optimal returns on investment for sugar cane and sugar production, as well as bad weather conditions. Even though South Africa continues to be one of the world's principal producers of high quality sugar, the South African sugar industry is harshly affected by world sugar market conditions which stem from unbalanced subsidy and tariff agreements between the major sugar producing countries (Parker, 2009; Phillips, 2011).

Globally, sugar cane-based industries are progressively turning towards energy production to sustain profitability (Phillips, 2011). Countries, which are currently implementing this process of energy production, include Brazil, India, Australia and Mauritius. Brazil has already seen a 60% growth in electricity production from sugarcane in the past ten years and have set their sights on an energy production capacity target of 15 000 MW by 2015. In 1995, India decided to follow the trend of Brazil and by 2010 had an energy production capacity of 3000 MW. Their 2015 target is 10 500 MW (SASA, 2012). In a similar manner, the South African sugar industry needs access to the electricity and fuel markets in order to be viable and competitive in the worldwide sector.

Currently, the 14 sugar mills in South Africa obtain their fuel requirements by burning the final bagasse produced during sugarcane processing. The steam produced by burning bagasse under steam boilers is then used for mechanical uses and heating (SASA, 2012). Some of these 14 sugar mills already have the capacity to produce electricity beyond their own power needs and already export around 5 MW into the national energy grid at a marginal income (Phillips, 2011).

As one of the highest carbon emitting countries in the world (ranked number 14), South Africa urgently needs to reduce its non-renewable energy consumption (Cambray, 2007). By supplying renewable energy into the national grid, the South African sugar industry would not only be increasing its appeal as an investment destination, it would also contribute significantly to the national energy grid and to government's renewable energy targets (Phillips, 2011; SASA, 2012). In addition, a transformed sugarcane agro-processing industry that commercially produces sugar and supplies renewable energy, would assist in reducing power losses, as well as add to the national grid capacity and stability.

An area where surplus power could possibly be harvested is the energy-intensive evaporation process. If this process could be modified to decrease energy intensity, such as the utilization of gas hydrate technologies, significant quantities of renewable energy would be available for supplementation into the national energy grid.

## CHAPTER 2

### HYDRATE STRUCTURE AND THERMODYNAMIC MODELING

Phase equilibrium data for systems containing mixtures are important for the design and operation of separation processes. However, it is not possible to measure all phase equilibrium data for all systems over an entire pressure or temperature range. As a result, thermodynamic methods are applied to available phase equilibrium experimental data in order to predict system properties. Nonetheless, before this can be achieved, knowledge pertaining to the classification and structure of such systems must be known.

Chapter Two introduces the reader to the manner in which hydrates are classified as well as the process of hydrate formation and dissociation. Thermodynamic fundamentals and principles are also outlined in this chapter. This is comprised of an overall description of thermodynamic chemical phase equilibrium, including fugacity and activity coefficients for vapour and liquid phases. Furthermore, the  $\gamma - \phi$  (combined method) and  $\phi - \phi$  (direct method) are described for the regression of vapour-liquid equilibrium data.

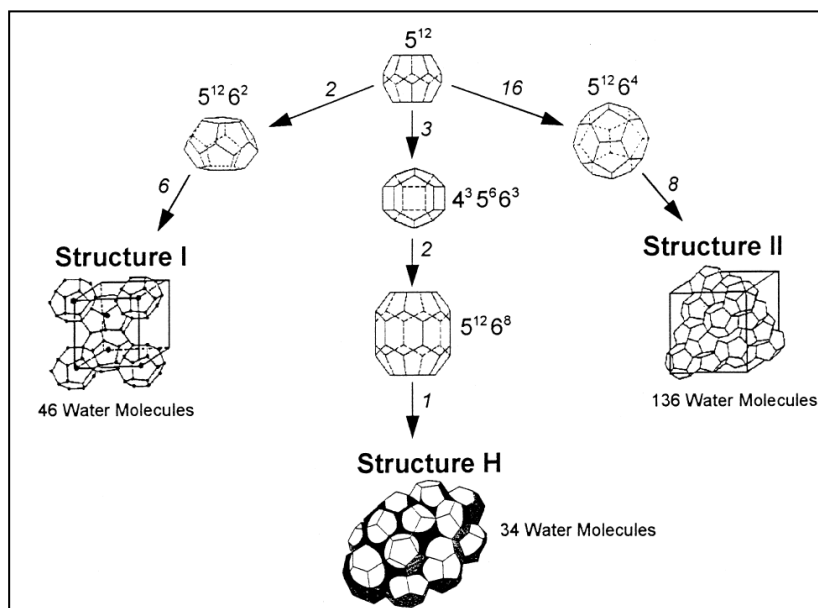
The chapter then extends vapour-liquid equilibrium modeling to hydrate-vapour-liquid (H-V-L) equilibrium modeling. The method used to determine H-V-L equilibrium data employs prediction techniques based on computer-based methods formulated from statistical thermodynamic techniques.

#### 2.1 Gas hydrate theory

##### 2.1.1 Structural theory

The majority of gas hydrates are known to form one of three structures, namely: structure I (sI), structure II (sII) or structure H (sH), where each structure is comprised of small and large cavities formed by the water molecules (Mohammadi and Richon, 2009). Figure 2-1 below provides a summary of crystal structures for sI, sII and sH hydrates.





**Figure 2-1: Three types of hydrates structures and their cavity arrangement (Khokhar, 1998).**

The basic cavity structure formed by water molecules bonded by hydrogen bonds is the pentagonal dodecahedron. This cavity is a polyhedron with twelve pentagonal faces. It can only accommodate one guest molecule. When these cavities arrange themselves in space and link through their vertices, they form sI gas hydrates. This results in a tetrakaidecahedron; a polyhedron with twelve pentagonal and two hexagonal faces (Carroll, 2003). The unit cell structure of sI hydrates is a cube with a side length of 1200 pm. It contains 46 water molecules. The oxygen atoms of the water molecules arrange in a manner to form two pentagonal dodecahedra and six tetrakaidecahedra (Englezos, 1993). The tetrakaidecahedron cavities are bigger than the dodecahedron cavities and are therefore often referred to as “large” cavities, while the dodecahedra are referred to as “small” cavities. Common sI hydrate formers include methane, ethane, hydrogen sulphide and carbon dioxide. Ethane molecules can only occupy large cavities, whereas the guest molecules of methane, hydrogen sulphide and carbon dioxide hydrates can occupy both small and large cavities (Carroll, 2003).

Through face sharing of the pentagonal dodecahedron cavities, sII gas hydrates are formed (Englezos, 1993). The result of this spacial arrangement produces a structure with twelve pentagonal and 4 hexagonal faces, known as a hexakaidecahedron (Carroll, 2003). The unit cell structure of sII hydrates is a cube with an approximate side length of 1730 pm. It contains 136 water molecules and is comprised of sixteen pentagonal dodecahedron (small) and eight hexakaidecahedron (large) cavities (Englezos, 1993). Common sII hydrate formers include nitrogen, propane and isobutane. Propane and isobutane can only occupy large cavities, whereas nitrogen can occupy both small and large cavities (Carroll, 2003).

Structure H (sH) gas hydrates are a relatively new discovery (Carroll, 2003). They are much less common than sI and sII, and their formation requires two formers to be present; a small molecule, such as methane, and a sH former. sH hydrates are composed of three types of cavities: a dodecahedron, a polyhedron with twelve regular pentagon faces; an irregular dodecahedron, a polyhedron with three square faces, six pentagonal faces, and three hexagonal faces; and an irregular icosahedron, a polyhedron with twelve pentagonal faces and eight hexagonal faces. The unit cell structure of sH hydrates contains 34 water molecules and is comprised of three dodecahedral (small), two irregular dodecahedral (medium), and one icosahedral (large) cavities (Carroll, 2003). Typical sH hydrate formers include methylcyclopentane, ethylcyclopentane, methylcyclohexane, cycloheptane, cyclooctane, 2-methylbutane, 2,2-dimethylbutane, 2,3-dimethylbutane, 2,2,3-trimethylbutane, 2,2-dimethylpentane, and 3,3-dimethylpentane. These components are not commonly found in nature (Carroll, 2003). For additional information on hydrate structures I, II and H, the reviews by Carroll (2003) and Sloan and Koh (2008) should be consulted.

Gas hydrate structures are described using the suggested nomenclature of  $n_i^{m_i}$ ; where “ $n_i$ ” is the number of edges in the face type “ $i$ ”, and “ $m_i$ ” is the number of faces with “ $n_i$ ” edges (Sloan and Koh, 2008). For a guest molecule to enter a crystal cavity, it must meet the dimensional, morphological and physiochemical criteria of that cavity. This criterion is explained by the ratios of molecular diameter to cavity diameter. Cavity diameters for sI, sII and sH are listed in Table 2-1 below. As a rule, for simple hydrate formers, stable structures occur within the diameter ratio’s upper and lower limits of approximately 1.0 and 0.76 respectively (Sloan and Koh, 2008).

**Table 2-1: Properties of Type I, Type II and Type H gas hydrates.**

Hydrate crystal type	I		II		H		
	Small	Large	Small	Large	Small	Medium	Large
Cavity size	Small	Large	Small	Large	Small	Medium	Large
Spacial arrangement <sup>a</sup>	5 <sup>12</sup>	5 <sup>12</sup> 6 <sup>2</sup>	5 <sup>12</sup>	5 <sup>12</sup> 6 <sup>4</sup>	5 <sup>12</sup>	4 <sup>3</sup> 5 <sup>6</sup> 6 <sup>3</sup>	5 <sup>12</sup> 6 <sup>8</sup>
Number of cavities per unit cell <sup>b</sup>	2	6	16	8	3	2	1
Average cavity radius (Å) <sup>a</sup>	3.95	4.33	3.91	4.73	3.94	4.04	5.79
Number of water molecules per unit cell <sup>a,b</sup>	46		136		34		

<sup>a</sup> (Sloan and Koh, 2008)

<sup>b</sup> (Carroll, 2003)

### 2.1.2 Phase diagrams

Subject to the size and chemical nature of guest molecules, the phase behaviour of gas hydrates changes considerably. Through the study of phase diagrams, the relationship between the microscopic structure, just described, and the macroscopic hydrate phase properties can be better understood.

#### 2.1.2.1 Gibbs phase rule

According to Smith et al. (2005), a *phase* is a homogenous state of matter. When the state of a pure homogenous liquid is fixed, two intensive thermodynamic properties are set at definite values. On the other hand, when two phases are in equilibrium, only a single property needs to be specified for the state of the system to be fixed. For multi-phase systems at equilibrium, the phase rule of J. Willard Gibbs provides the number of independent variables that must be arbitrarily fixed to establish its intensive state (Smith et al., 2005):

$$F = 2 - \pi + N \quad (2.1)$$

where  $\pi$  is the number of phases,  $N$  is the number of species, and  $F$  is the degrees of freedom of the system.

The degrees of freedom represent the number of fixed independent intensive variables. Such variables include pressure, temperature, concentration, volume, density and phase amounts. Since volume, density, phase amounts and certain concentrations are difficult to measure, hydrate phase equilibria are determined from pressure, temperature and composition data. These are phase rule variables, but they are not all independent. The phase rule provides the number of variables from this set, which must be arbitrarily specified to fix all remaining phase rule variables, and thus the intensive state of the system (Smith et al., 2005). Therefore, the intensive state of hydrate phase equilibria is established when the system pressure, temperature, water free former phase composition and water free phase composition are fixed. The remaining properties may then be calculated (Sloan and Koh, 2008).

The maximum number of degrees of freedom is represented by:

$$F_{max} = N + 1 \quad (2.2)$$

where  $F_{max}$  represents the dimension of space required to characterize the complete phase behaviour of the system (Mooijer-van den Heuvel, 2004).

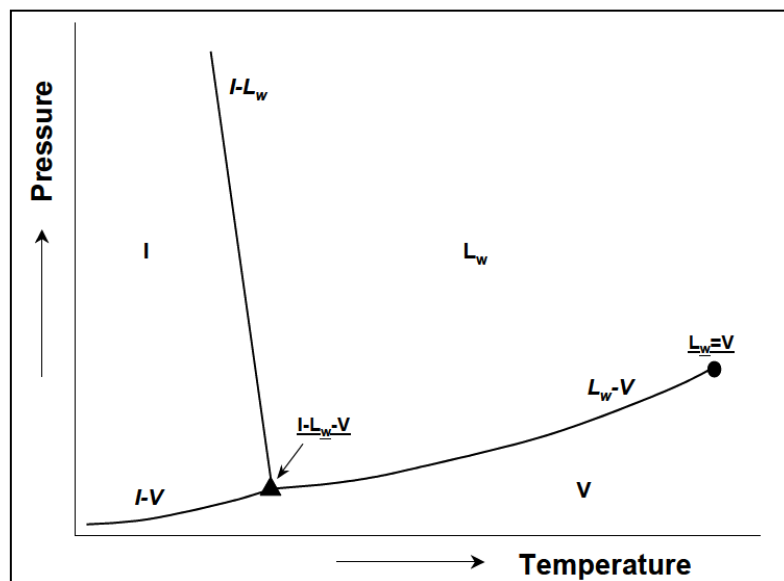
## 2.1.2.2 Single-component systems

Water is a crucial component for gas hydrate formation. The phases that may occur in a single-component system of pure water are ice, I, liquid water,  $L_w$ , and vapour, V. Equilibrium lines bound each phase region. These are represented as I- $L_w$ , I-V and  $L_w$ -V. The triple point, I- $L_w$ -V, is the locus of the three equilibrium lines. At this point, all three phases can occur simultaneously. The critical point marks the end of the  $L_w$ -V equilibrium line; thereafter the phases become indistinguishable (Mooijer-van den Heuvel, 2004). The application of Gibbs phase rule for a single-component system is represented in Table 2-2 below.

**Table 2-2: Application of Gibbs phase rule to single-component system (Mooijer-van den Heuvel, 2004).**

F	N	$\Pi$	Phase	Representation in Figure 2.2
2	1	1	$L_w$	Region
1	1	2	I- $L_w$	Curve
0	1	3	I- $L_w$ -V	Point

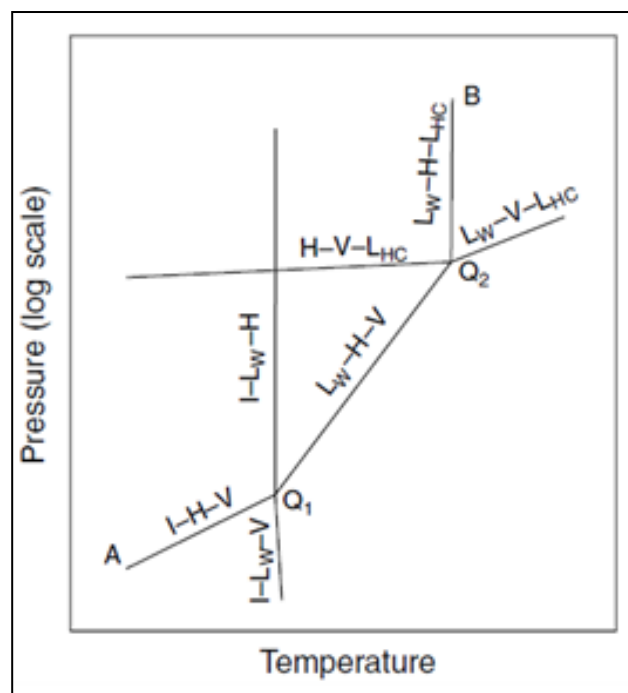
For a single-component system,  $F_{max} = 2$ . Therefore, temperature and pressure, temperature and composition, or composition and pressure provide sufficient information for the construction of the phase diagram.



**Figure 2-2: Pressure-temperature phase diagram for pure water (Mooijer-van den Heuvel, 2004).**

## 2.1.2.3 Binary systems

Hydrates existing in a binary system are comprised of water and one guest molecule. According to the Gibbs phase rule, a binary system may be represented as a function of temperature, pressure and composition. According to relation 2.2,  $F_{\max}$  for a binary system is 3. Therefore, the phase behaviour of a binary system may be represented on a three-dimensional plane, which now incorporates the dependence of composition on the equilibrium conditions. Cross-sections of the temperature-pressure-composition diagram are more commonly used than the former as they provide insight into the equilibrium conditions for coexisting phases (P,T-cross-section), as well as provide a visual means of understanding the dependence of composition on the equilibrium conditions (P, x- and T, x-cross-sections) (Mooijer-van den Heuvel, 2004). Figures 2-3 to 2-5 demonstrate the effect of composition on the phase behaviour, and give insight into systems comprising of water and a gas hydrate forming component.



**Figure 2-3: Pressure-temperature phase diagram for a binary system at a specified composition (Sloan and Koh, 2008).**

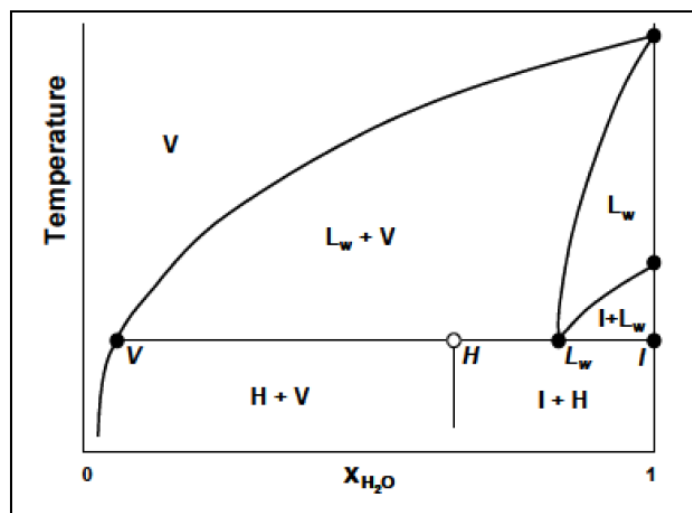


Figure 2-4: Temperature-composition phase diagram for a binary system at a specified pressure (Mooijer-van den Heuvel, 2004).

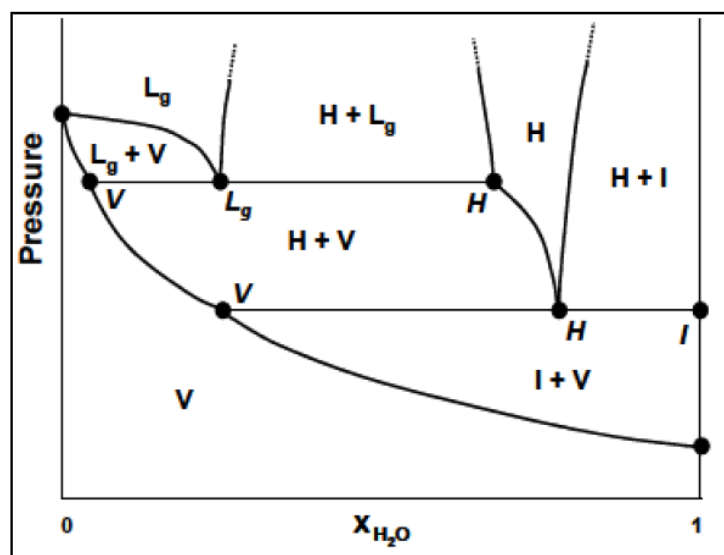


Figure 2-5: Pressure-composition phase diagram for a binary system at a specified temperature (Mooijer-van den Heuvel, 2004).

The phases that may occur in a binary system of water and a guest molecule are ice, I, liquid water,  $L_w$ , vapour, V, hydrate, H, and liquid guest molecule,  $L_g$ . Equilibrium lines bound each phase region. These are represented as I-H-V, vapour pressure of the guest molecule in the presence of ice, I- $L_w$ -V, freezing point of water depression, I- $L_w$ -H, H-V- $L_g$  and  $L_w$ -H-V, vapour pressure of the guest molecule and water,  $L_w$ -H- $L_g$ , hydrate melting point variation, and  $L_w$ -V- $L_g$ , saturation vapour pressure of the guest molecule equilibrium lines. The lower quadruple point,  $Q_1$  (I- $L_w$ -H-V) is the locus of equilibrium lines I- $L_w$ -H,  $L_w$ -H-V, I-H-V and I- $L_w$ -V. This point is approximately 273 K for

all hydrate formers, although quadruple point pressures vary significantly between different hydrate formers due to the different bonds present between particles (Sloan and Koh, 2008). The upper quadruple point,  $Q_2$  ( $L_w$ -H-V- $L_g$ ) is formed at the locus of  $L_w$ -H-V,  $L_w$ -V- $L_g$ ,  $L_w$ -H- $L_g$  and H-V- $L_g$ . Due to the fact that the slope of the equilibrium curve,  $L_w$ -H- $L_g$ , is so steep, the temperature of  $Q_2$  is often taken as the maximum temperature for gas hydrate existence (Mooijer-van den Heuvel, 2004). The application of the Gibbs phase rule for a binary system is represented in Table 2-3 below.

**Table 2-3: Application of Gibbs phase rule to binary system (Mooijer-van den Heuvel, 2004).**

F	N	$\Pi$	Phase	Representation in Figure 2.3
2	2	2	$L_w$ +V, H+ $L_w$ , H+I	Region
1	2	3	H- $L_w$ -V, H- $L_w$ - $L_g$ , I-H-V	Curve
0	2	4	I-H- $L_w$ -V, H- $L_w$ - $L_g$ -V	Point

The region below the I-H-V and  $L_w$ -H-V equilibrium curves is known as the hydrate instability region. No hydrates are able to form in this region. To ensure that the hydrate instability region is not reached, it is important to experimentally obtain points on the  $L_w$ -H-V equilibrium curve and to model these results to obtain a continuous  $L_w$ -H-V equilibrium curve. According to the Gibbs phase rule, to obtain this curve, the degree of freedom is 1. Therefore an independent intensive property must be specified. According to the isochoric method, this property is temperature (Sloan and Koh, 2008).

#### 2.1.2.4 Ternary systems

Hydrates existing in a ternary system are comprised of water, one guest molecule and an additive. The additive may be a second guest molecule or a solute. However, for the purposes of this study it will be considered as a solute. Since  $F_{max} = 4$  for a ternary system, the representation of the phase behaviour requires four dimensions. This is often difficult to work with; therefore, by keeping one or two free variables constant, clearer depictions of the phase diagrams may be obtained. The most common diagram used to represent ternary systems is the triangular diagram at constant temperature and pressure, or prisms at constant temperature or pressure.

The phases that may occur in a ternary system of water, one guest component and an additive are ice, I, liquid water,  $L_w$ , vapour, V, hydrate, H, liquid guest molecule,  $L_g$  and liquid additive component,  $L_a$ . The equilibrium points where five phases are coexisting is known as the quintuple point,  $Q_t$  (Mooijer-van den Heuvel, 2004). These points are formed from the intersection of five four-phase

equilibrium curves. The application of the Gibbs phase rule for a ternary system is represented in Table 2-4 below.

**Table 2-4: Application of Gibbs phase rule to ternary system (Mooijer-van den Heuvel, 2004).**

<b>F</b>	<b>N</b>	<b>Π</b>	<b>Phase</b>	<b>Representation in Figure 2.6</b>
3	3	2	$L_w+V, H+L_w, H+I$	Region
2	3	3	$H+L_w+L_g, H-L_w-L_a$	Surface
1	3	2	$L_w+L_g=V$	Curve
0	3	3	$L_w+L_a+L_g=V$	Point

Phase diagrams of ternary systems containing hydrates depend on three features (Mooijer-van den Heuvel, 2004):

- Hydrate formation in the binary system with water.
- Phase diagrams of the binary systems with water and the guest component.
- Size and presence of regions where liquid phases are immiscible.

Based on the above features, phase diagrams for ternary systems comprising of water + guest component + additive, where no structural transitions occur may be classified as follows (Mooijer-van den Heuvel, 2004):

- Type A: One of the guest components cannot form gas hydrates on its own.
- Type B: Both guest components can form gas hydrates in binary systems with water, where the phase behaviour in both binary systems is the same. Both exhibit gas-like or liquid-like phase behaviour.
- Type C: Both guest components can form gas hydrates in binary systems with water, where the phase behaviour in the binary systems is different; one exhibits gas-like phase behaviour while the other exhibits liquid-like phase behaviour.

*Type A system:*

Type A ternary systems are classified by one of the guest components being unable to form hydrates in a binary system containing water. This is represented by the phase diagrams in Figures 2-6 and 2-7.



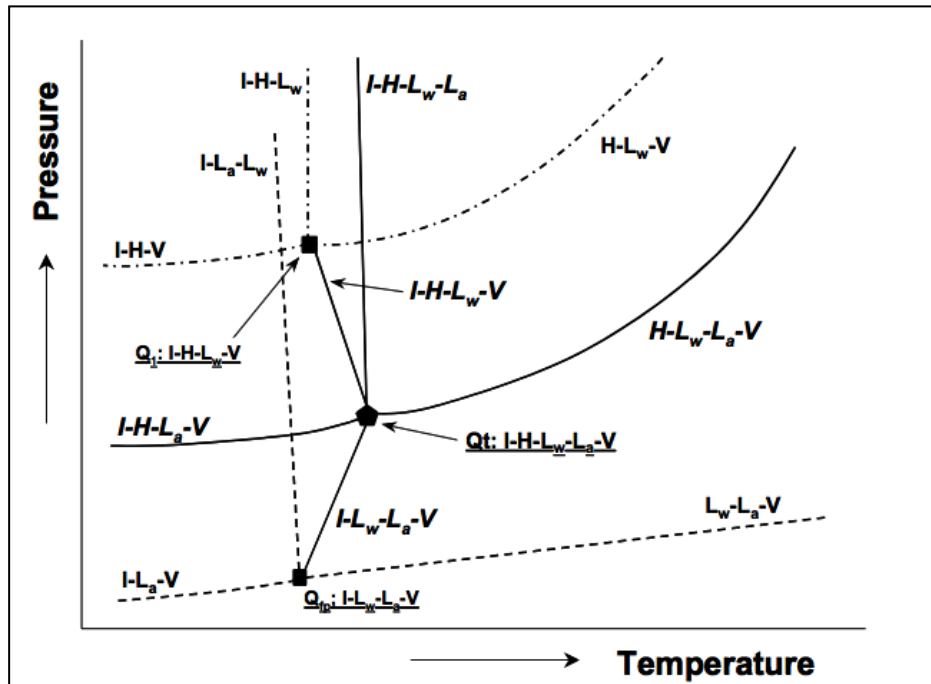


Figure 2-6: Pressure-temperature phase diagram for a type A ternary system exhibiting gas-like behaviour. The gaseous component forms clathrate hydrate in the binary system and shows gas-like behaviour (---). No clathrate hydrate is formed in the system H<sub>2</sub>O + additive (-.-.) (Mooijer-van den Heuvel, 2004).

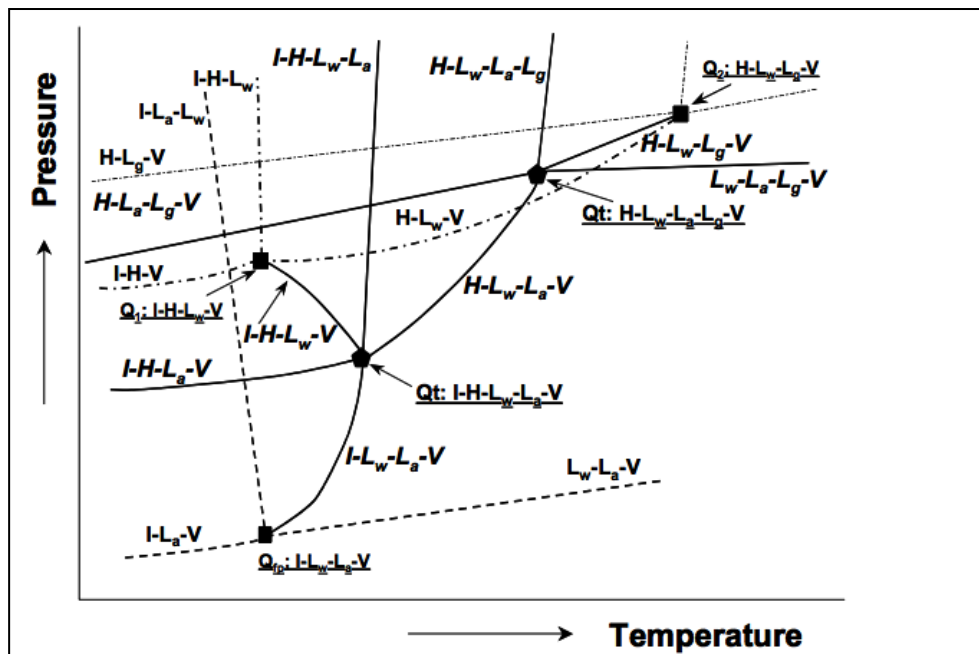


Figure 2-7: Pressure-temperature phase diagram for a type A ternary system exhibiting liquid-like behaviour. The additive does not form clathrate hydrate in the binary system with H<sub>2</sub>O (---), the gaseous component forms clathrate hydrate in the binary system and shows liquid-like behaviour (---). The gaseous and additive components are immiscible. (Mooijer-van den Heuvel, 2004).

Various assumptions are made for the construction of ternary type A phase diagrams (Mooijer-van den Heuvel, 2004). They are as follows:

- Water and guest component have immiscible  $L_w$  and  $L_g$  phases.
- Water and additive component have immiscible  $L_w$  and  $L_a$  phases.
- Guest component and additive component have immiscible  $L_g$  and  $L_a$  phases.

One quintuple point,  $Q_t$ , is represented in Figure 2-6. This is shown by I-H- $L_w$ - $L_a$ -V. The hydrate instability region of Figure 2-6 is bounded by I-H- $L_a$ -V and H- $L_w$ - $L_a$ -V equilibrium curves. Two quintuple points,  $Q_t$ , are represented in Figure 2-7. These are shown by I- $L_w$ - $L_a$ - $L_g$ -V and I-H- $L_w$ - $L_a$ -V. The hydrate instability region in Figure 2-7 is bounded by I-H- $L_a$ -V, H- $L_w$ - $L_a$ -V and H- $L_w$ - $L_g$ -V equilibrium curves.

If the assumption pertaining to  $L_a$  and  $L_g$ 's immiscibility does not apply, then the number of quintuple points decreases (Mooijer-van den Heuvel, 2004).

*Type B system:*

Type B ternary systems are classified by both of the guest components being able to form hydrates in a binary system containing water, where both of the phase diagrams are similar. This is represented by the phase diagrams in Figures 2-8 and 2-9 below.

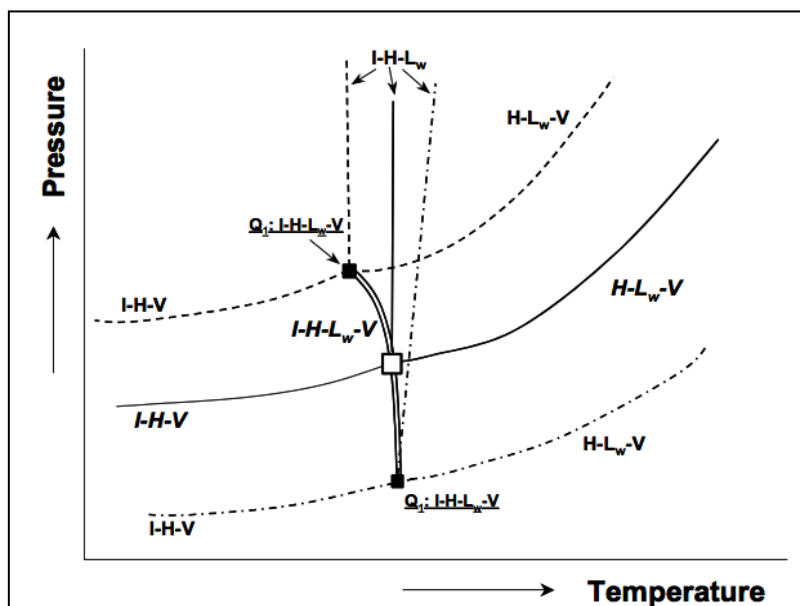


Figure 2-8: Pressure-temperature phase diagram for a type B ternary system exhibiting gas-like behaviour. —, phase boundaries for one overall-composition (isopleth); ■, the quadruple point locus I-H-Lw-V; □, point of intersection of the phase boundaries on the quadruple point locus.

In both the binary systems with water, clathrate hydrate is formed and the components show gas-like behaviour (-.-.- and ---). An example of a system exhibiting this behaviour is  $\text{H}_2\text{O} + \text{CH}_4 + \text{CF}_4$  (Mooijer-van den Heuvel, 2004).

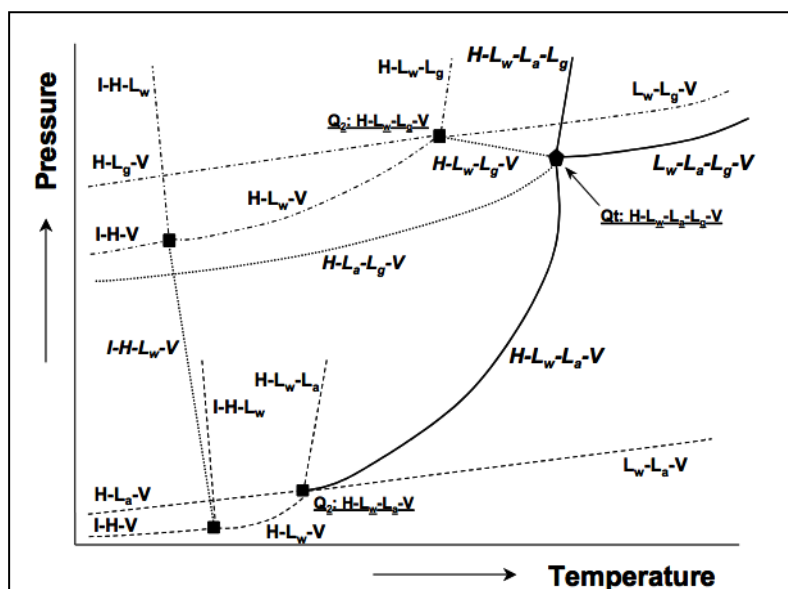


Figure 2-9: Pressure-temperature phase diagram for a type B ternary system exhibiting liquid-like behaviour. —, phase boundaries for one overall-composition (isopleth). In both the binary systems with water, gas hydrates are formed and the components show liquid-like behaviour (-.-.- and ---). An example of a ternary system showing this behaviour is  $\text{H}_2\text{O} + \text{C}_3\text{H}_8 + \text{cyclobutanone}$ . Some of the indicated equilibria (····) may be difficult to determine experimentally (Mooijer-van den Heuvel, 2004).



Various assumptions are made for the construction of ternary type C phase diagrams (Mooijer-van den Heuvel, 2004). They are as follows:

- Water and guest component have immiscible  $L_w$  and  $L_g$  phases.
- Water and additive component have immiscible  $L_w$  and  $L_a$  phases.
- Guest component and additive component have immiscible  $L_g$  and  $L_a$  phases.
- Water, guest component and additive component have immiscible  $L_w$ ,  $L_a$  and  $L_g$  phases.

### 2.1.3 Hydrate kinetics

The process that governs the formation of hydrates is analogous to the crystallization process (Bishnoi and Natarajan, 1996; Sloan and Koh, 2008; He et al., 2011). As in crystallization, this formation process can be sub-divided into nucleation and growth processes (Bishnoi and Natarajan, 1996). In the nucleation process, microscopic nuclei are formed at the vapour-liquid interface of supersaturated solutions. Thereafter, in the growth process, stable nuclei increase in size to form stable hydrate crystals (He et al., 2011). Thus, the hydrate formation induction time is the time between the creation of the supersaturated solution and the appearance of the first hydrate crystals (He et al., 2011). When the three phase (H- $L_w$ -V) equilibrium is disturbed, such as a decrease in pressure, or an increase in temperature, the hydrate crystals decompose in a sequence of lattice destruction and gas desorption steps (Bishnoi and Natarajan, 1996).

#### 2.1.3.1 Hydrate nucleation

The hydrate nucleation process is a microscopic stochastic occurrence wherein gas-water clusters (nuclei) grow and disperse in the solution until the nuclei have reached critical size (Bishnoi and Natarajan, 1996). If the growing nuclei size is smaller than the critical size, the nuclei are unstable and may breakdown in the aqueous solution (Bishnoi and Natarajan, 1996). However, if a growing hydrate nucleus achieves critical size, it is stable and instantly leads to the formation of a hydrate crystal. Experimental and calculated results show that a stable hydrate nucleus should have a radius between 25-170 Å (Englezos et al., 1987).

The nucleation of gas hydrates is a phase transformation that occurs in a supersaturated environment. Dissolved gas molecules in the aqueous solution form this supersaturated environment. The water molecules position themselves around the former (guest) molecules, and the precursors to the hydrate phase, nuclei, are formed. If sufficient former gas is present in the solution, the nuclei subsequently grow.

Based on a series of measurements performed on natural gas and carbon dioxide hydrates, Long and Sloan (1996) proposed that in non-stirred systems, the hydrate nucleation site is located at the gas-liquid interface. This proposal was reinforced by a number of other researchers based on their observations made on methane hydrate (Huo et al., 2001; Ostergaard et al., 2001) and carbon dioxide hydrate (Kimuro et al., 1993; Hirai et al., 1995) nucleation. According to Sloan and Koh (2007), the vapour-liquid interface is preferred for hydrate formation due to lower Gibbs free energy of nucleation, as well as the high concentration of water and former (guest) molecules. For systems where stirring occurs, the nuclei may form anywhere in the solution, depending on where the highest concentration of the dissolved former gas is present (Bishnoi and Natarajan, 1996).

Referring to Figure 2-11 below, for an isochoric system, nucleation occurs between points A and B. The induction time is dependent on the time required for the nucleation process to occur. For systems in which hydrates have previously been formed, the induction time is reduced. This is known as the memory effect (Vysniauskas and Bishnoi, 1983). Therefore, the induction time is also dependent on water history and agitation, and consequently surface area.

Three models have been developed to describe the nucleation process. More information on these models can be found in the book of Sloan and Koh (2007), *Natural Gas Hydrates: A Guide for Engineers*.

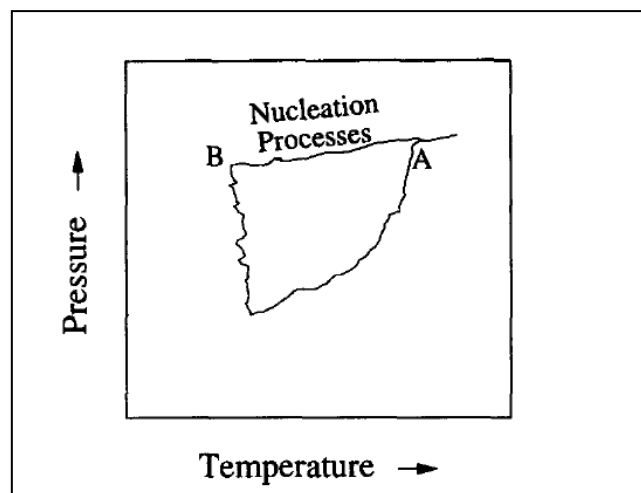


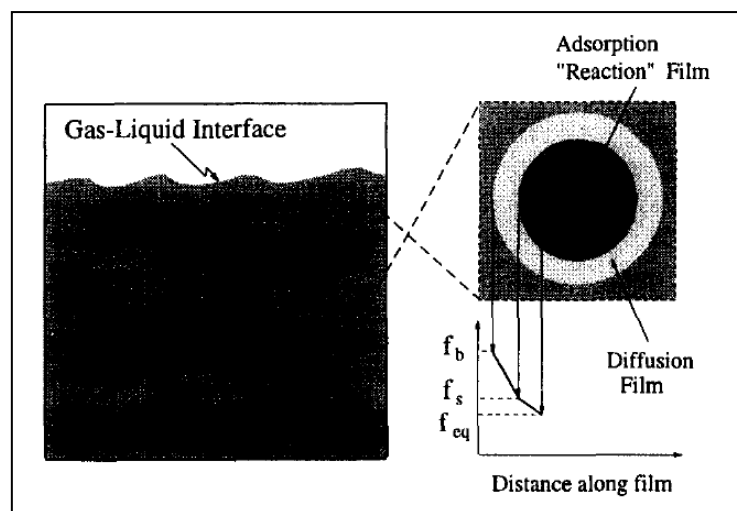
Figure 2-11: Experimental pressure-temperature trace (Bishnoi and Natarajan, 1996).

## 2.1.3.2 Crystal growth

The hydrate crystal growth process applies to the growth of stable hydrate nuclei to form solid hydrate crystals. The transfer of heat and mass play a paramount role in the growth process; however, most of the nucleation parameters such as surface area, agitation, and gas composition continue to be significant during this process (Bishnoi and Natarajan, 1996).

Once the hydrate nuclei have reached critical size, they continue to grow to form gas hydrate crystals. During the crystal growth phase, a large pressure drop is observed in the system. This is due to diffusion and absorption of the former gas into the crystal cavities. Consequently, stable gas hydrates are formed.

Numerous models for hydrate growth have been developed (Sloan and Koh, 2008). One such model is that of Englezos et al. (1987). This model is a mechanical model based on mass transfer and crystallization theories. It visualises the solid hydrate particle as being surrounded by an adsorption “reaction” layer followed by a stagnant liquid diffusion layer. This is schematically represented in Figure 2-12 below.



**Figure 2-12: Fugacity profile in the diffusion and adsorption film surrounding a growing hydrate (Bishnoi and Natarajan, 1996).**

The authors proposed two consecutive steps for the hydrate growth process; step one involves diffusion of the gas phase from the bulk of the solution (point  $f_b$ ) to the crystal-liquid interface through the laminar diffusion layer around the particle (point  $f_s$ ), while step two involves the “reaction” at this interface, where the gas is absorbed into the hydrate structure, which is assumed to be spherical.

The reaction rates of the growth process are based on system fugacity instead of dissolved gas concentration. At equilibrium, the growth rate per particle can be expressed as (Bishnoi and Natarajan, 1996):

$$\left(\frac{dn}{dt}\right)_p = K^* A_p (f_b - f_{eq}) \quad (2.3)$$

where  $A_p$  is the hydrate surface area per particle,  $(f_b - f_{eq})$  is the difference in fugacity of the dissolved gas and its fugacity at the three phase equilibrium and  $K^*$  is expressed in terms of the coefficients for diffusion ( $k_d$ ) and reaction ( $k_r$ ) as (Bishnoi and Natarajan, 1996):

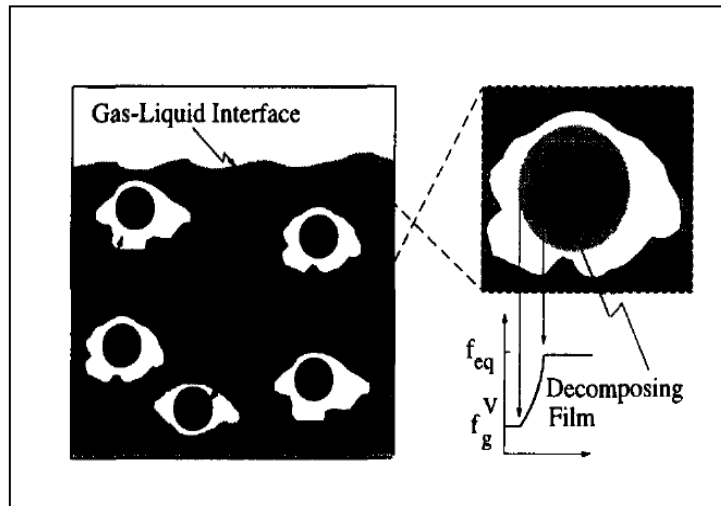
$$\frac{1}{K^*} = \frac{1}{k_r} + \frac{1}{k_d} \quad (2.4)$$

### 2.1.3.3 Hydrate dissociation

The dissociation of hydrate crystals is an endothermic process. For such a process to occur, heat of some form must be provided by an external source in order to break the hydrogen bonds that are present between water molecules, as well as the van der Waals interaction forces present between the former (guest) molecules and the water molecules of the hydrate lattice. Thereafter, the hydrate dissociates into water and gas. The heat transfer that occurs during the hydrate dissociation process has been studied by Kamath et al. (1984). It was observed that the dissociation process is analogous to that of the nucleate boiling phenomena. Later, Kamath and Holder (1987) generalized this relationship and applied it to methane hydrate dissociation.

Kim et al. (1987) proposed two consecutive steps for the hydrate dissociation process: step one involves the destruction of the hydrate host lattice at the particle surface, while step two involves the desorption of the former (guest) molecule from the surface of the particle. Based on these ideas, an intrinsic kinetic model for hydrate dissociation was developed. This is represented schematically in Figure 2-13 below.





**Figure 2-13: Dissociation of hydrate particles (Bishnoi and Natarajan, 1996).**

At very low temperatures, the molecular motion within the hydrate lattice stops. Consequently the hydrate lattice becomes rigid. As temperature increases, the motion due to water molecule reorientation and diffusion causes the hydrate to dissociate. The trapped gas in the hydrate is then released which increases the system pressure.

At equilibrium, the dissociation rate for a hydrate particle is given as (Bishnoi and Natarajan, 1996):

$$-\left(\frac{dn_H}{dt}\right)_p = K_d A_p (f_{eq} - f_g^v) \quad (2.5)$$

where  $K_d$  is the dissociation rate constant and  $f_g^v$  is the fugacity of the gas obtained at the particle surface temperature and the experimental pressure.

## 2.2 Thermodynamic modeling for hydrate-vapour-liquid equilibria

### 2.2.1 Thermodynamic phase equilibria

A system at equilibrium exists such that no change in state can occur (Smith et al., 2005). Therefore, a system is in thermodynamic equilibrium when it is in chemical, thermal and mechanical equilibrium. For such a state to occur, the following specific criteria need to be satisfied for a transfer of  $dn_i$  moles of a substance between two phases,  $\alpha$  and  $\beta$ :

1. Equivalent temperature and pressure between phases.
2. Minimum global Gibbs free energy.
3. Equivalent chemical potential ( $\mu$ ) for a specific component between each phase.

In equilibrium at constant temperature and pressure, the change in the Gibbs free energy ( $G$ ) is represented as:

$$\overline{dG} = (\mu_i^\beta - \mu_i^\alpha)dn_i \quad (2.6)$$

where  $\mu_i$  is the chemical potential of substance  $i$  and  $n_i$  is the number of moles of  $i$ .

At equilibrium, the Gibbs free energy of a system is at a minimum, therefore:

$$\left(\frac{\partial \overline{G}}{\partial n_i}\right)_{T,P,n_j} = 0 \quad (2.7)$$

Therefore:

$$\mu_i^\alpha = \mu_i^\beta \quad (2.8)$$

For a multi-phase-multicomponent equilibrium condition, equation (2.8) can be extended to:

$$\mu_i^\alpha = \mu_i^\beta = \dots = \mu_i^k, \text{ for } i = 1, 2, \dots, N \quad (2.9)$$

where  $k$  is the number of coexisting phases and  $N$  is the number of coexisting components.

The chemical potential of a system can be expressed in terms of the fugacity ( $f$ ) of a component by the following expression:

$$\mu = \mu^0 + RT \ln \left( \frac{f(P)}{P^0} \right) \quad (2.10)$$

where  $\mu^0$  is the reference state chemical potential,  $T$  is the temperature,  $R$  is the Universal Gas Constant,  $P^0$  is the reference state pressure and  $f(P)$  is the fugacity as a function of pressure.

By combining equations (2.9) and (2.10), the equality of fugacities at thermodynamic equilibrium is represented as:

$$\hat{f}_1^\alpha = \hat{f}_1^\beta, \hat{f}_2^\alpha = \hat{f}_2^\beta \quad (2.11)$$

where  $\hat{f}$  is the fugacity of component 1 or 2 in phase  $\alpha$  or  $\beta$ .

In this study, the hydrate phase equilibrium is modeled using the approach of Parrish and Prausnitz (1972). The proposed method is based on solving the condition of equal fugacities of water in the hydrate phase and the fluid phase:

$$\hat{f}_w^H(T, P) = \hat{f}_w^L(T, P, x) \quad (2.12)$$

To solve these conditions, the fugacity of water in the liquid phase is calculated using the UNIFAC group-contribution model, while the fugacity of water in the hydrate phase is calculated using the solid solution theory of van der Waals and Platteeuw (1959) statistical thermodynamic theory.

### 2.2.2 *Thermodynamic models for the vapour and liquid phases*

#### 2.2.2.1 Vapour-liquid equilibrium data regression

There exist two common methods used to regress phase equilibrium data; the Gamma-Phi ( $\gamma - \phi$ ) or combined method, and the Phi-Phi ( $\phi - \phi$ ) or direct method. In the direct method, an EOS is used to calculate both the liquid and vapour phase non-idealities, whereas in the combined method, an EOS is used to describe the vapour phase non-ideality while an activity coefficient model is used to describe the liquid phase non-ideality.

##### 2.2.2.1.1 Gamma-Phi ( $\gamma - \phi$ ) method

The calculation procedure for the Gamma-Phi ( $\gamma - \phi$ ) method is shown in Figure 2-14. This is specifically for an isothermal system.

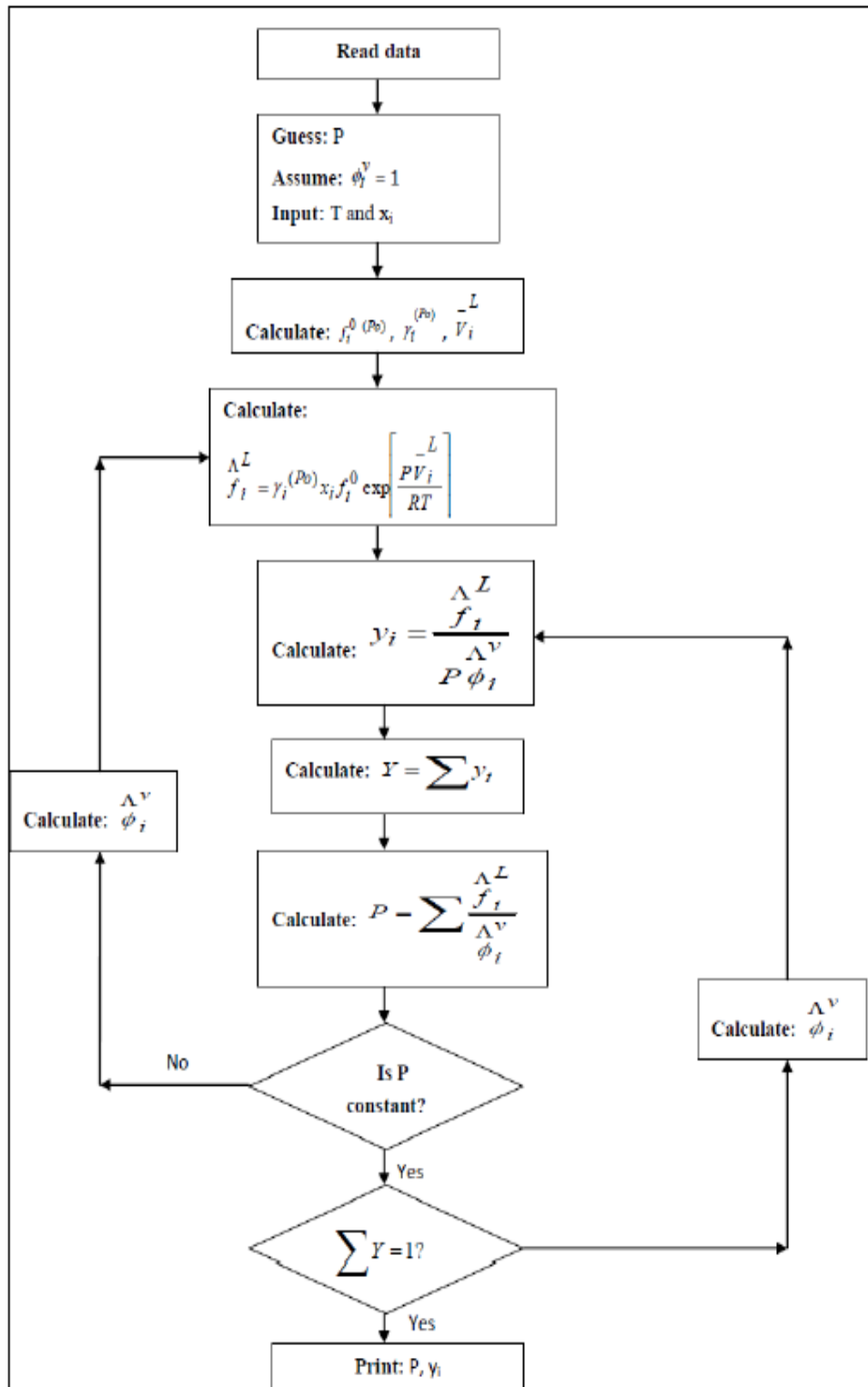


Figure 2-14: Flow diagram for the Gamma-Phi ( $\gamma - \phi$ ) bubble-pressure method for an isothermal system (Prausnitz and Chueh, 1968).

2.2.2.1.2 Phi-Phi method ( $\phi - \phi$ )

The calculation procedure for the Phi-Phi ( $\phi - \phi$ ) method is shown in Figure 2-15 below. As before, this is specifically for an isothermal system.

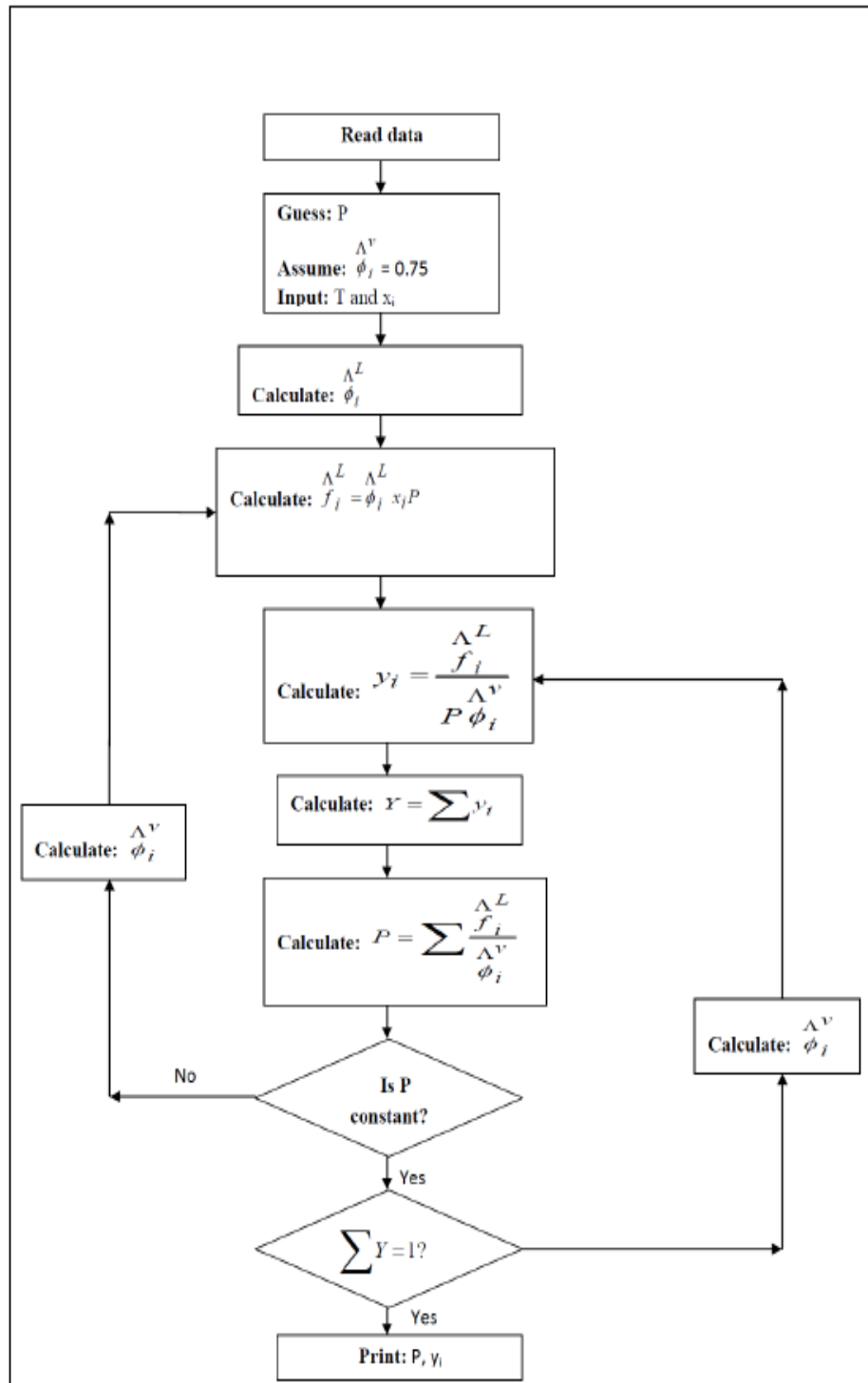


Figure 2-15: Flow diagram for the Phi-Phi ( $\phi - \phi$ ) bubble-pressure method for an isothermal system (Prausnitz and Chueh, 1968).

In order to calculate the fugacity of different components in various fluid phases, thermodynamic models are used. These models include Equations of State (EOS) with mixing rules, as well as liquid phase activity coefficients models. Conventional methods for hydrate phase equilibrium calculations (Chun and Lee, 1998; Cao, et al., 2001; Klauda and Sandler, 2003) use different thermodynamic models to calculate the fugacity of water in the fluid phases.

The following equations of state and mixing rules, represented in table form, are commonly used in hydrate modeling.

**Table 2-5: Commonly used EOS in hydrate modeling.**

<b>EOS</b>	<b>Reference</b>	<b>Mixing Rule</b>
<b>Soave-Redlich-Kwong (1948)</b>	Chun and Lee (1998)	Modified Huron-Vidal
	Sugahara et al. (2005)	van der Waals
	Delahaye et al. (2006)	Modified Huron-Vidal
	Mooijer-van den Heuvel et al. (2006)	N/S
<b>Peng-Robinson (1976)</b>	Tohidi et al. (1995)	van der Waals
	Javanmardi et al. (2004)	N/S
	Keshavarz et al. (2013)	N/S
<b>Peng-Robinson-Stryjek-Vera (1986)</b>	Klauda and Sandler (2000)	N/S
	Chen et al. (2001)	Modified Huron-Vidal
	Khosravani et al. (2013)	Non-density-dependent
<b>Patel and Teja (1982)</b>	Chen and Guo (1996)	N/S
	Ma et al. (2003)	Kurihara
<b>Trebble-Bishnoi (1988)</b>	Englezos et al. (1991)	N/S
	Englezos (1994)	Quadratic
<b>Valderrama (1990)</b>	Tohidi et al. (1995)	Non-density-dependent
	Mohammadi et al. (2003)	Non-density-dependent
	Javanmardi et al. (2012)	Non-density-dependent

N/S – Not specified

Tohidi et al. (1995) compares the results using the Valderrama EOS with non-density-dependent mixing rules to the Peng-Robinson EOS with van der Waals classical mixing rules. It was shown that both models can be used to determine the liquid and vapour phase fugacities for a non-electrolyte mixture where gas solubility is low.

Based on the above-mentioned factors, the Peng-Robinson EOS in combination with the van der Waals mixing rules was used to model the vapour phase in this study for the systems containing carbon dioxide. This EOS was chosen as it is commonly used in industry, requires little input information and is more accurate for gas system predictions compared to the Soave-Redlich-Kwong EOS (Smith et al., 2005). For systems containing refrigerant gases, the vapour phase is assumed to be and ideal gas ignoring its water content (Eslamimanesh et al., 2011). In order to model the liquid phase, the UNIFAC group-contribution model was chosen. The method was chosen based on the approach of Chun and Lee (1998).

#### 2.2.2.2 Vapour phase modelling

The fugacity in solution of the vapour phase, with respect to water, can be calculated as follows:

$$\hat{f}_w^V = \hat{\phi}_w^V y_w P \quad (2.13)$$

The Peng-Robinson (PR) EOS (1976) is used to determine the fugacity coefficient in solution,  $\hat{\phi}_w^V$ , and is represented as follows:

$$P = \frac{RT}{v-b} - \frac{a(T)}{v(v+b)+b(v-b)} \quad (2.14)$$

where  $R$  is the Universal Gas Constant,  $T$  is the temperature,  $P$  is the pressure,  $v$  is the molar volume,  $a$  is the attractive volume parameter and  $b$  is the excluded volume parameter.



The parameters  $a$  and  $b$  can be calculated as follows:

$$a(T) = 0.45724 \frac{(RT_c)^2}{P_c} a(T_c) \quad (2.15)$$

where

$$a(T_c) = \left\{ 1 + \alpha \left[ 1 - \left( \frac{T}{T_c} \right)^{0.5} \right] \right\}^2 \quad (2.16)$$

$$\alpha = 0.37464 + 1.54226\omega - 0.26992\omega^2 \quad (2.17)$$

$$b = 0.0778 \left( \frac{RT_c}{P_c} \right) \quad (2.18)$$

where  $T_c$  is the critical temperature,  $P_c$  is the critical pressure and  $\omega$  is the acentric factor.

The pure component parameters for the PR EOS used in this study are shown below in Table 2-6.

**Table 2-6: Pure component properties for PR EOS.**

Component	$P_c$ /MPa	$T_c$ /K	$\omega$	$k_{ij}^b$
water <sup>a</sup>	22.064	647.14	0.344	0.1896
CO <sub>2</sub> <sup>a</sup>	7.3830	304.21	0.224	

<sup>a</sup> (Poling et al., 2001)

<sup>b</sup> (Dhima et al., 1999)

The compressibility of the liquid and vapour phases are found by obtaining the smallest and largest real roots respectively of the following cubic equation:

$$Z^3 - (1 - B)Z^2 + (A - 3B^2 - 2B)Z - (AB - B^2 - B^3) = 0 \quad (2.19)$$

A and B are reduced variables of a and b respectively:

$$A = \frac{Pa(T)}{(RT)^2} \quad (2.20)$$

$$B = \frac{Pb}{RT} \quad (2.21)$$

For a multicomponent system, the classical mixing rules of van der Waals are used to incorporate all components present in the system into the  $a$  and  $b$  parameters. The  $a$  and  $b$  mixing parameters become:

$$a_{mix} = \sum_j^n \sum_j^n x_i x_j a_{ij} \quad (2.22)$$

$$b_{mix} = \sum_j^n x_i b_{ij} \quad (2.23)$$

where

$$a_{ij} = (1 - k_{ij})(a_{ii}a_{jj})^{0.5} \quad (2.24)$$

$$b_{ij} = \frac{(b_{ii}+b_{jj})}{2} \quad (2.25)$$

where  $k_{ij}$  is the binary interaction coefficient.

The fugacity coefficient ( $\hat{\phi}_i^{EOS}$ ) of component  $i$  can then be calculated as follows:

$$\hat{\phi}_i^{EOS} = \exp \left\{ (Z - 1) \frac{B}{b_{mix}} - \ln(Z - b_{mix}) - \frac{A_i}{2\sqrt{2}B_i} \left( \frac{2\sum_j a_{ij}}{a_{mix}} - \frac{b_i}{b_{mix}} \right) \ln \left[ \frac{Z+(1+\sqrt{2})b_{mix}}{Z+(1-\sqrt{2})b_{mix}} \right] \right\} \quad (2.26)$$

### 2.2.2.3 Liquid phase modeling

The fugacity in solution for the liquid phase may be expressed in terms of the fugacity coefficient in solution. This definition of fugacity in solution as used in the Phi-Phi method mentioned in Chapter 2.2.2.1.2, is

$$\hat{f}_w^L = \hat{\phi}_w^L x_w P \quad (2.27)$$

The fugacity in solution for a liquid phase may also be expressed in terms of the activity coefficient. This definition of fugacity in solution is used in the Gamma-Phi method of thermodynamic data regression (refer to section 2.2.2.1.1).

$$\hat{f}_w^L = \gamma_w^L x_w P_w^{sat} \quad (2.28)$$

where

$$\gamma_w^L x_w = a_w \quad (2.29)$$

For system temperatures above 273.15 K, the saturation pressure can be calculated as (Dharmawardhana et al., 1980):

$$P_w^{sat} = 10^{-6} \exp \left( 73.649 - \frac{7258.2}{T} - 7.3037 \ln(T) + 4.1653 \times 10^{-6} T^2 \right) \quad (2.30)$$

While, for system temperatures below 273.15 K, the saturation pressure can be calculated as (Dharmawardhana et al., 1980):

$$P_I^{sat} = \frac{10 \exp \left( \frac{-1032.558}{T} + 51.056 \log(T) - \frac{0.0977}{T} + 0.7.0357 \times 10^{-5} T^2 - 98.512 \right)}{7600} \quad (2.31)$$

The fugacity or activities coefficients represent the non-ideality of the liquid phase. This non-ideality may be due to high system pressures or instances where gas solubility cannot be ignored. The UNIFAC group-contribution method treats this non-ideality as being comprised of two additive parts: a combinatorial term,  $g^C$ , to account for molecular size and shape differences, and a residual term,  $g^R$ , to account for molecular interactions (refer to equation 2.31).

$$g = g^C + g^R \quad (2.32)$$

The UNIFAC method for the estimation of activity coefficients depends on the concept that a liquid mixture may be considered as a solution of the structural units from which the molecules are formed, rather than a solution of the molecules themselves. The UNIFAC method is based on the UNIQUAC method equation, for which the activity coefficients are given by (Smith et al., 2005):

$$\ln \gamma_i = \ln \gamma_i^C + \ln \gamma_i^R \quad (2.33)$$

where

$$\ln \gamma_i^C = 1 - J_i + \ln J_i - 5q_i \left( 1 - \frac{J_i}{L_i} + \ln \frac{J_i}{L_i} \right) \quad (2.34)$$

$$\ln \gamma_i^R = q_i \left[ 1 - \sum_k \left( \theta_k \frac{\beta_{ik}}{s_k} - e_{ki} \ln \frac{\beta_{ik}}{s_k} \right) \right] \quad (2.35)$$

In the calculation of the activity coefficients using the UNIFAC model, the basic subgroups were provided by Fredenslund et al. (1993). These are presented in Table 2-7.

Table 2-7: UNIFAC subgroup parameters.

Subgroup	k	R <sub>k</sub>	Q <sub>k</sub>	v <sub>k</sub> <sup>2</sup>	v <sub>k</sub> <sup>3</sup>
CH2	2	0.6744	0.54	0	3
CH	3	0.4469	0.228	0	7
OH	15	1	1.2	0	8
H2O	17	0.92	1.4	1	0
CHO	24	0.998	0.948	0	1
COO	50	1.38	1.2	0	1

For a detailed overview of the UNIFAC method calculation procedure, please refer to *Appendix D, UNIFAC Method*.

### 2.2.3 Inhibition effect of sucrose

The inhibition effect of sucrose is accounted for using a purely empirical correction method proposed by Englezos and Hall (1994). In their study, this correction method was used to account for the inhibition effect of polymers, however, Chun and Lee (1998, 1999) employed this approach to account for the inhibition effect of sucrose in their studies involving gas hydrates in the presence of sucrose. Therefore, due to the limited literature data regarding sucrose systems, the above-mentioned approach was chosen for this study.

In this approach, the activity of the water is taken to be equal to the product of the water mole fraction in the water-former liquid system without sucrose and the activity of water in the sucrose-water solution without the former gas present (Englezos and Hall, 1994). It is assumed that sucrose does not enter the crystal cavities during hydrate formation. Therefore, taking into account the inhibition effect of sucrose, the activity of water show in equation 2.29 may now be expressed as:

$$a_w = x_{wF} a_{wS} \quad (2.36)$$

where

$$a_{wS} = x_{wS} \gamma_{wS} \quad (2.37)$$

Therefore, the fugacity in solution represented in equation 2.28 is presented as:

$$\hat{f}_w^L = x_{wF} a_{wS} P_w^{sat} \quad (2.38)$$

## 2.2.4 Thermodynamic models for hydrate phase

Hydrates maintain a regular structure; therefore statistical thermodynamics can be used to calculate thermodynamic hydrate properties. From this viewpoint, the hydrate formation process can be thermodynamically modeled by considering two steps. The first step considers the transformation of pure water to an empty hydrate cage, while the second step, which is hypothetical, considers the filling of the hydrate lattice with a guest molecule. The change in chemical potential for this process is represented as follows:

$$\mu_w^H - \mu_w^L = (\mu_w^H - \mu_w^{MT}) - (\mu_w^{MT} - \mu_w^L) = 0 \quad (2.39)$$

where  $\mu_w^H$  is the chemical potential of water in the hydrate phase,  $\mu_w^L$  is the chemical potential of water in the liquid phase and  $\mu_w^{MT}$  is the chemical potential of water in the empty hydrate lattice.

The term on the left-hand side,  $\mu_w^H - \mu_w^L$ , represents the stabilization of the hydrate lattice, while the term on the right-hand side,  $(\mu_w^H - \mu_w^{MT}) - (\mu_w^{MT} - \mu_w^L)$ , represents the phase change which water undergoes. Sucrose is known to be excluded from the hydrate crystal lattice, as well as the vapour phase (Chun & Lee, 1998), therefore the van der Waals and Platteeuw (1959) solid solution theory can be used to describe the hydrate phase. As a result, the following relationship is valid due to the incorporation of vapour-liquid equilibria into the model:

$$f_w^H(T, P) = f_w^L(T, P, x) \quad (2.40)$$

## 2.2.4.1 Model development

The first model for calculating gas hydrate formation was developed by van der Waals and Platteeuw (1959). This model made use of fundamental statistical thermodynamic equations for gas hydrates in conjunction with the concept of Langmuir gas absorption. The following assumptions were made for the development of this theory:

- Classical thermodynamic statistics is valid
- Ideal gas phase behaviour
- Single gas hydrate former present in gas phase
- Maximum of one gas molecule present in each spherical cavity
- Gas molecules small enough to not distort hydrate lattice
- No interactions between encaged gas molecules and hydrate lattice

van der Waals and Platteeuw (1959) derived an equation by means of the Gibbs Free Energy which incorporates the internal and extensive properties, volume and entropy (Sloan & Koh, 2008). This is represented as:

$$\frac{\mu_w^{MT} - \mu_w^H}{RT} = - \sum_m v_m \ln(1 - \theta_{ml}) \quad (2.41)$$

where  $v_m$  is the number of cavities of type  $m$  and  $\theta_{ml}$  is the probability function.

The ratio of the number cavities to the number of water molecules present in the hydrate lattice are reported in Table 2-8 below. As stated previously (Section 2.1.1), gas hydrate cavities are categorized by either small or large sizes.

**Table 2-8: Ratio of number of cavities to the number of water molecules present in hydrate lattice (van der Waals and Platteeuw, 1959).**

Property	Value	
	Structure I	Structure II
$v_{small}$	1/23	2/17
$v_{large}$	3/23	1/17

The probability function,  $\theta_{ml}$ , represents the probability of a cavity of type  $ml$  to be occupied by a guest molecule. This is given by:

$$\theta_{ml} = \frac{C_{ml}P}{(1+C_{ml}P)} \quad (2.42)$$

The gas-water interactions of the system are accounted for by the Langmuir constant,  $C_{ml}$ , by making use of the Lennard-Jones-Devonshire cell theory (van der Waals and Platteeuw, 1959).

The original van der Waals and Platteeuw (1959) model provided an approach that was sufficient for performing hydrate calculations, but was not adequate for accurate engineering calculations. Therefore, the van der Waals and Platteeuw (1959) model was extended by Parrish and Prausnitz (1972). These extensions included:

- Non-ideal gas phase; therefore can account for higher pressures
- Multicomponent gas phase (includes hydrate formers and non-hydrate formers)
- London forces to account for interactions between gas and water molecules
- Polar forces to account for bonding in hydrate lattice
- Kihara potential parameters used to determine Langmuir parameters

Since multiple hydrate formers may be present in the gas phase, the potential for a specific gas former to occupy the cavity decreases. This is represented by:

$$\frac{\mu_w^{MT} - \mu_w^H}{RT} = -\sum_m v_m \ln(1 - \sum_j \theta_{mj}) \quad (2.43)$$

The probability function for the parameter  $ml$  then becomes:

$$\theta_{ml} = \frac{C_{ml}f_l}{(1+\sum_j C_{mj}f_l)} \quad (2.44)$$

where

$$f_l = \Phi_l y_l P \quad (2.45)$$

$$C_{ml} = \frac{4\pi}{kT} \int_0^\infty \exp\left[\frac{-w(r)}{kT}\right] r^2 dr \quad (2.46)$$

where

$$w(r) = 2z\varepsilon \left[ \frac{\sigma^{12}}{R^{11}r} \left( \delta^{10} + \frac{a}{R} \delta^{11} \right) - \frac{\sigma}{R^5 r} \left( \delta^4 + \frac{a}{R} \delta^5 \right) \right] \quad (2.47)$$

$$\delta^N = \frac{\left[ \left( 1 - \frac{r}{R} \frac{a}{R} \right)^{-N} - \left( 1 + \frac{r}{R} \frac{a}{R} \right)^{-N} \right]}{N} \quad (2.48)$$

Equations 2.45 and 2.46 above are functions of the core radius ( $a$ ), the radial coordinate ( $r$ ), and the depth of intermolecular potential ( $\varepsilon$ ). The reader is referred to Parrish and Prausnitz (1972) for these parameter values. For systems where the temperature range is between 260 and 300 K, Equation 2.44 can be simplified to:

$$C_{ml} = \frac{A_{ml}}{T} \exp\left(\frac{B_{ml}}{T}\right) \quad (2.49)$$

**Table 2-9: Fitted Langmuir parameters for various formers used in this study.**

Former	Value (K)							
	Structure I				Structure II			
	Small		Large		Small		Large	
	$A_{ml}$	$B_{ml}$	$A_{ml}$	$B_{ml}$	$A_{ml}$	$B_{ml}$	$A_{ml}$	$B_{ml}$
<b>CO<sub>2</sub></b>	1.20x10 <sup>-3</sup>	2860.50	0.8507 x10 <sup>-2</sup>	3277.90	0.0	0.0	0.0	0.0
<b>R134a<sup>b</sup></b>	0.0	0.0	0.0	0.0	0.0	0.0	5.70x10 <sup>-3</sup>	4908.71
<b>R410a<sup>b</sup></b>	0.0	0.0	0.0	0.0	0.0	0.0	4.75x10 <sup>-3</sup>	5969.68
<b>R507<sup>b</sup></b>	0.0	0.0	0.0	0.0	0.0	0.0	4.50x10 <sup>-4</sup>	6233.08

<sup>a</sup> (Parrish and Prausnitz, 1972)

<sup>b</sup> (Ngema et al., 2012)

Recent expansions have been made to the model developed by Parrish and Prausnitz (1972). These are reported in Table 2-10 below:



Table 2-10: Hydrate model developments.

Model	Development on	Development description
<b>Sloan, Khoury and Kobayashi model (1976)</b>	van der Waals and Platteeuw model (1959)	Fugacity of water in the filled hydrate is related to the difference in chemical potential in the filled and empty hydrate by: $f_w^H = f_w^{MT} \exp\left(\frac{\mu_w^H - \mu_w^{MT}}{RT}\right) \quad (2.50)$
<b>Ng and Robinson model (1980)</b>	Parrish and Prausnitz model (1972) <sup>a</sup> and Sloan et al. (1976) <sup>b</sup>	<sup>a</sup> Model extended for the incorporation of a hydrocarbon liquid former <sup>b</sup> Model extended to determine $f_w^{MT}$ term. This is demonstrated by using correlative methods from vapour-hydrate data for a range of components. Since an empirical fit is employed, $f_w^{MT}$ becomes negative for temperatures below 285 K for sI and 287 K for sII.
<b>Sloan, Sparks and Johnson model (1987)</b>	Ng and Robinson (1980)	Model modified by fitting vapour pressure data for various components obtained from H-L-V equilibrium data. $f_w^{MT} = P_w^{MT} \phi_w^{MT} \exp\int_{P_w^{MT}}^P \frac{V_H^{MT}}{RT} dp \quad (2.51)$ $\phi_w^{MT}$ is determined using the second virial coefficient. This value becomes significant at high pressures. This modification can be simplified by assuming that the hydrate partial molar volume is equal to the molar volume and is pressure independent. $P_w^{MT}$ is in the order of $10^{-3}$ MPa, therefore $\phi_w^{MT} = 1$ . Therefore: $f_w^{MT} = P_w^{MT} \exp\frac{V_H^{MT}(P - P_w^{MT})}{RT} \quad (2.52)$

Table 2-10 (continued): Hydrate model expansions.

Model	Development on	Development description
<b>Chen and Guo model (1998)</b>	Van der Waals and Platteeuw (1959) two step hydrate formation mechanism	Developed a model based on a two-step hydrate formation mechanism, as in van der Waals and Platteeuw (1959). The first step considers the formation of a basic hydrate structure from a quasi-chemical reaction process. This step is based on the assumption that the gas molecules dissolve in the liquid phase, and each guest molecule will be surrounded by a cluster of dissolved gas molecules with water molecules. The second step considers the adsorption of the dissolved gas molecules into the empty hydrate cavity. This step can only occur for small gas molecules such as N <sub>2</sub> , Ar, CH <sub>4</sub> and O <sub>2</sub> . The Langmuir adsorption theory is used to calculate this step.
<b>Mohammadi and Richon model (2008)</b>	Sloan et al. (1987)	<p>The following assumption was made to simplify the equation of Sloan et al. (1987):</p> $\exp \frac{V_H^{MT}(P-P_w^{MT})}{RT} = 1 \text{ for } P \leq 2MPa \quad (2.53)$ <p>Therefore, the model of Sloan et al. (1987) becomes:</p> $f_w^{MT} = P_w^{MT} \exp \frac{\mu_w^H - \mu_w^{MT}}{RT} \quad (2.54)$
<b>Eslamimanesh, Mohammadi and Richon model (2011)</b>	Parrish and Prausnitz (1972)	<p>By assuming that for systems where the dissociation pressure of the hydrate is low, the vapour phase consisting of pure guest molecules is assumed ideal, therefore:</p> $f_l = P$ <p>The model of Parrish and Prausnitz therefore becomes:</p> $\frac{\mu_w^H - \mu_w^{MT}}{RT} = \sum_m \ln (1 + \sum_j C_{mj}P)^{-v_m} \quad (2.55)$

## 2.2.4.2 Hydrate model used in this study

The model published by Parrish and Prausnitz (1972) and modified by Holder and Grigoriou (1980) is used as a general approach to model the H-L-V equilibrium data of a pure hydrate former. It accounts for the gas solubility in the liquid phase as well as the liquid solubility in the gas phase. Systems which are modelled by Parrish and Prausnitz (1972) include CO<sub>2</sub> (1) + water (2) and CO<sub>2</sub> (1) + water (2) + sucrose (3) systems. The gas has a high water solubility and therefore was chosen to verify the model programmed in this study. For the system CO<sub>2</sub> (1) + water (2) the direct ( $\emptyset - \emptyset$ ) method was used to account for gas solubility, whereas for the system CO<sub>2</sub> (1) + water (2) + sucrose (3), the combined ( $\gamma - \emptyset$ ) method was used. The flow diagrams for these predictive models are shown in Figures 5-11 and 5-12 respectively.

The fugacity of water in the hydrate phase,  $f_w^H(T, P)$ , shown in Equation 2.38, is given by the model developed by Sloan, Khoury and Kobayashi (1976):

$$f_w^H = f_w^{MT} \exp\left(\frac{\mu_w^H - \mu_w^{MT}}{RT}\right) \quad (2.56)$$

Here,  $f_w^{MT}(T, P)$ , represents the fugacity of water in the hypothetical empty hydrate cavity and  $\mu_w^H - \mu_w^{MT}$  is the chemical difference of water in the empty hydrate lattice and the hydrate phase. The fugacity of water in the empty hydrate cage,  $f_w^{MT}(T, P)$ , is calculated according to the following equation (Englezos, 1992):

$$f_w^{MT} = f_w^L \exp\left(\frac{\mu_w^{MT} - \mu_w^L}{RT}\right) \quad (2.57)$$

The quantity inside the parenthesis is calculated by a correlation proposed by Holder and Grigoriou (1980).

$$\frac{\mu_w^{MT} - \mu_w^L}{RT} = \frac{\Delta\mu_w^0(T^0, P)}{RT^0} - \int_{T^0}^T \left[\frac{\Delta h_w^{MT-L}}{RT^0}\right]_P dT + \int_{P^0}^P \left[\frac{\Delta v_w^{MT-L}}{RT}\right]_T dp \quad (2.58)$$

where

$$\Delta h_w^{MT-L} = \Delta h_w^{MT-L^0}(T^0) + \int_{T^0}^T \Delta C p_w^{MT-L} dT \quad (2.59)$$

$$\Delta C p_w^{MT-L} = \Delta C p_w^{MT-L^0}(T^0) + \beta_w^{MT-L}(T - T^0) \quad (2.60)$$

**Table 2-11: Thermodynamic properties for sI and sII hydrates for liquid or ice and an empty hydrate lattice (Parrish & Prausnitz, 1972).**

Property	Value		Unit
	sI	sII	
$\Delta\mu_w^{MT-I^0}$	1264	883	J/mol
$\Delta h_w^{MT-L^0}(T^0)$	-4858	-5201	J/mol
$\Delta h_w^{MT-I^0}(T^0)$	1151	808	J/mol
$\Delta Cp_w^{MT-L^0}(T^0)$		-38.13	J/(mol.K)
$\beta^{MT-L}$		0.141	J/(molK <sup>2</sup> )
$\Delta V_w^{MT-L^0}(T^0)$	$4.6 \times 10^{-6}$	$5.0 \times 10^{-6}$	m <sup>3</sup> /mol
$\Delta V_w^{MT-I^0}(T^0)$	$3.0 \times 10^{-6}$	$3.4 \times 10^{-6}$	m <sup>3</sup> /mol

The model proposed by Parrish and Prausnitz (1972) later modified by Holder and Grigoriou (1980), is simplified specifically for refrigerants by Eslamimanesh et al. (2011). Systems modeled using the following approach include R134a (1) + water (2) + sucrose (3), R410a (1) + water (2) + sucrose (3) and R507 (1) + water (2) + sucrose (3). The following simplifications are assumed:

*Liquid phase assumptions:*

1. Negligible gas solubility,  $\gamma_w^L = 1$
2. Pure water liquid phase,  $x_w = 1$ .

*Vapour phase assumptions:*

1. Low dissociation pressure, below 2 MPa,  $\hat{\phi}_w^V = 1$ .
2. No water in the vapour phase,  $y_w = 0$ .

This model contains many of the simplifications and assumptions made by Parrish and Prausnitz (1972). This results in a simpler approach to modelling hydrate systems containing refrigerants with a low water solubility. However, in this study, the liquid phase assumptions made by Eslamimanesh et al. (2011) cannot be used as they do not take into account the effect of sucrose. Therefore, as stated previously, only the vapour phase assumptions are used and the liquid phase is modeled based on the approach of Chun and Lee (1998). Therefore the resulting model is expressed as follows:

$$x_w F a_{wS} P_w^{sat} = P_w^{MT} \left[ (1 + C_{small} P)^{-v'_{small}} + (1 + C_{large} P)^{-v'_{large}} \right] \quad (2.61)$$

The pressure of water in the empty hydrate lattice,  $P_w^{MT}$ , is calculated based on the model of Dharmawardhana et al. (1980).

For sI hydrates:

$$\ln P_w^{MT} = 0.1x \left( 17.440 - \frac{6003.925}{T} \right) \quad (2.62)$$

For sII hydrates:

$$\ln P_w^{MT} = 0.1x \left( 17.332 - \frac{6017.635}{T} \right) \quad (2.63)$$

The flow diagram for this predictive model is shown in Figure 5-15.

## CHAPTER 3

### REVIEW OF EXPERIMENTAL METHODS AND EQUIPMENT

Advances in any scientific research field have fundamental dependence on the apparatus available. In the case of gas hydrates, the measurement of hydrate-liquid-vapour equilibrium data has been performed using various apparatus over the past few decades. The most common experimental set-up encountered is comprised of a batch reactor cell, with a stirrer and heating/cooling mechanisms. Gas sampling and visual observation systems are also common (Lee, et al., 2005; Sloan & Koh, 2008).

In the following chapter, a variety of methods developed for high-pressure phase equilibrium measurement are investigated. These methods include isothermal, isobaric and isochoric search techniques. In addition, several apparatus used in literature for the measurement of hydrate phase equilibria are assessed. These apparatus include the quartz crystal microbalance, Cailletet, rocking cell, high-pressure differential scanning calorimetry, and high-pressure autoclave cell.

In this study, a modified version of the high-pressure autoclave cell, known as the isochoric pressure autoclave cell, is used for hydrate measurements. This apparatus is relatively simple to operate and boasts numerous advantages over other hydrate apparatus. This is discussed further in *Chapter 4, Description of Equipment and Experimental Procedure*.

#### 3.1 Review of experimental methods

Richon (1996) and Dorhn et al. (2010) suggest different classifications of experimental methods for the determination of high-pressure phase equilibria. Although both classifications share various similarities, the core determinants between the classifications differ greatly. Richon's (1996) classification of the experimental method is based on the method of equilibration between phases in equilibrium. Dorhn et al. (2010) however, classifies the different experimental methods according to the manner in which the compositions of the equilibrium phases are measured and whether the investigated mixture is prepared with accurately known compositions or not. These are known as analytical and synthetic methods respectively.

Returning to the classification proposed by Richon (1996), essentially two main categories are distinguished: dynamic (open circuit) methods involve forced circulation of one or more phases, whereas in static methods (closed circuits) equilibrium can be achieved with or without recirculation of fluid phases. Static methods generally make use of an internal stirring mechanism to reduce the

time required for reaching equilibrium (Raal and Mühlbauer, 1998). More information on these classifications can be found in the book of Raal and Mühlbauer (1998), *Phase Equilibria: Measurement and Computation*.

In the following section, the static method for hydrate phase equilibrium measurements is discussed. For such measurements, the static method is commonly preferred over the dynamic method (Oellrich, 2004), as dynamic methods are usually associated with increased time and costs for maintenance and construction.

A further distinction among the most frequently used experimental methods for determining hydrate equilibrium conditions can be made between those based on visual and non-visual manners of hydrate detection. As constant pressure and constant temperature methods commonly require visual observation of hydrate crystals, they may only be used at temperatures above the freezing point of water to avoid confusion with ice crystals (Schroeter et al., 1983). As an alternative, hydrate phase equilibrium measurement at high and low pressures can be performed in a constant volume (isochoric) cell without the need of visual observation. In this method, the hydrate dissociation conditions are determined from the intersection point of the cooling and heating isochors. These conditions are typically reported over hydrate formation conditions as they present a more accurate representation of the true hydrate equilibrium temperature and pressure. This is due to the effect of hysteresis that occurs during hydrate growth (Sun and Duan, 2007).

Three experimental techniques have thus been established for operating a hydrate formation apparatus: isobaric, isothermal and isochoric (Sloan and Koh, 2008). Table 3-1 summarizes the fundamentals of each method.

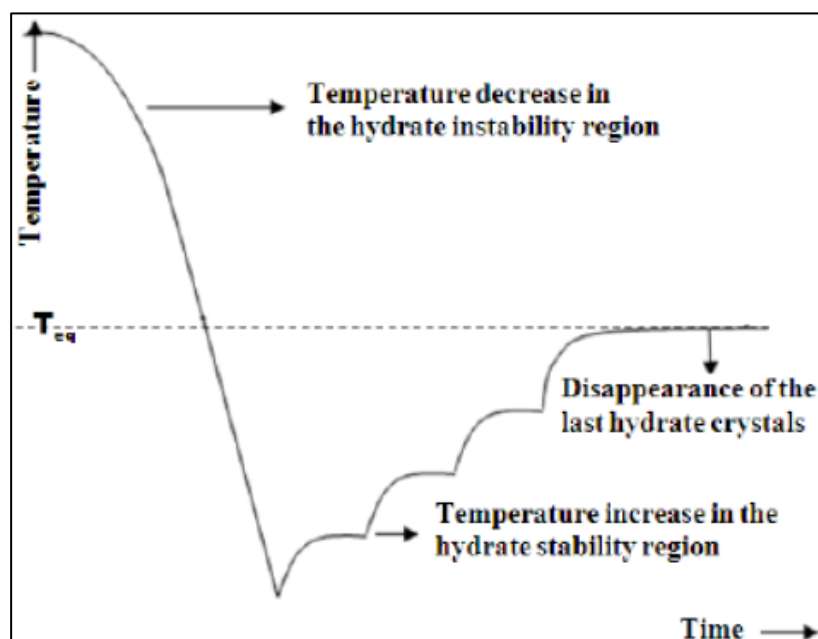
**Table 3-1: Commonly used experimental methods for the determination of hydrate dissociation conditions (Sloan and Koh, 2008).**

Method	Principle	Hydrate formation	Hydrate dissociation
<b>Isothermal</b>	Constant temperature	Temperature increase	Visual observation of hydrate crystal disappearance
<b>Isobaric</b>	Constant pressure	Exchange of gas or liquid from an external reservoir	
<b>Isochoric</b>	Constant volume	Pressure decrease	Intersection point of cooling and heating isochors

### *3.1.1 Visual isobaric temperature search method*

In isobaric operation, the system pressure is generally maintained constant by the exchange of a gas or liquid from an external reservoir (Sloan and Koh, 2008). Once the cell has been charged and pressurised to the desired pressure with the hydrate former, the system is cooled to approximately 5 K below the anticipated hydrate forming temperature. When the system temperature is constant, hydrate nucleation is induced by use of a stirring technique. After hydrate formation, and once the system pressure has reached steady-state, the cell temperature is increased until the hydrate phase is in coexistence with liquid and vapour phases. The system temperature is then slowly increased further until the last hydrate crystal dissociates (Sloan and Koh, 2008). This point, which is considered to be the equilibrium temperature of hydrate dissociation at constant pressure, may be established by visual observation of hydrate dissociation (Sloan and Koh, 2008). In order to reduce the hysteresis effect, the nucleation and dissociation procedures are usually carried out at least two times (Chun and Lee, 1999).





**Figure 3-1: Isobaric temperature search method (Tumba, 2010).**

### 3.1.2 Visual isothermal pressure search method

In the isothermal approach, the cell is loaded with the required system and pressurised with the former gas to a value higher than the expected hydrate forming region (Sloan and Koh, 2008). Meanwhile, the temperature is set to a value that corresponds to the highest experimental hydrate formation pressure (Englezos and Bishnoi, 1991). The system is then maintained for a period of time to ensure equilibrium is achieved. As hydrate formation occurs, the temperature at the hydrate interface increases due to the release of translational energy during solidification of the fluid molecules. This energy however, must be dissipated through convection/agitation or conduction to the surrounding phases and bath (Sloan and Koh, 2008). Absorption of the gas into the fluid phase decreases the pressure to the three phase ( $L_w$ -H-V) point. The system pressure may be controlled by an external reservoir for addition or withdrawal of gas, aqueous liquid, or some other fluid such as mercury (Sloan and Koh, 2008).

After hydrate formation, the pressure is slowly reduced. The equilibrium pressure is then determined by the visual observation of hydrate crystal disappearance (Sloan and Koh, 2008). The equilibrium temperature and pressure conditions may also be taken as the mean of the conditions at which the final hydrate crystal was observed and the conditions at which it disappeared (Beltran and Servio, 2008).

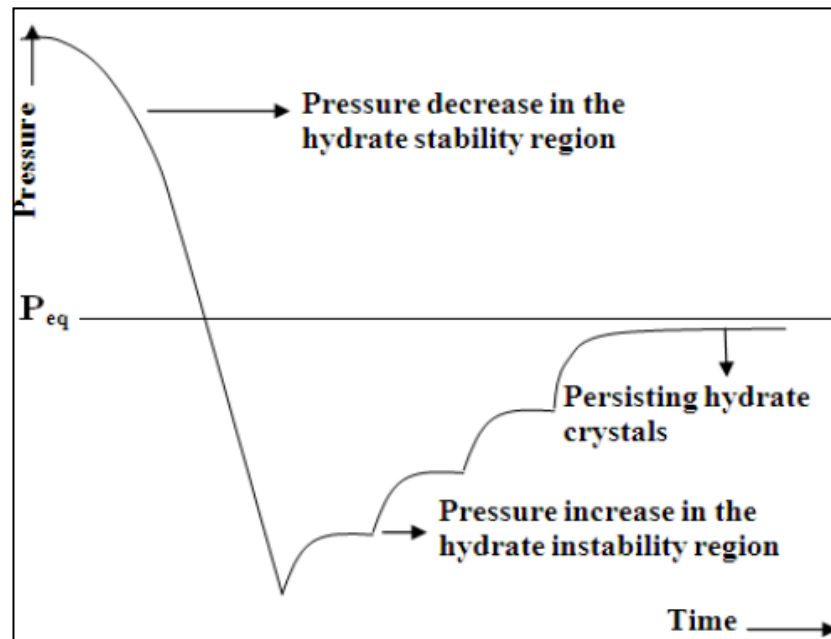
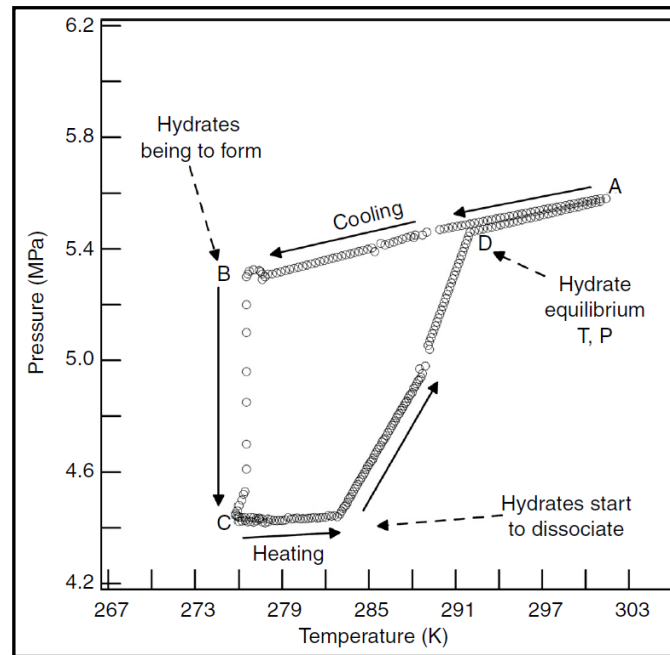


Figure 3-2: Isothermal pressure search method (Tumba, 2010).

### 3.1.3 Isochoric pressure search method

The isochoric operation of the hydrate formation cell is shown in Figure 3-3. The preliminary system temperature and pressure is set in the hydrate instability region, point A. Initially, the cell temperature is lowered, causing the cell pressure to decrease to point B. At this point, hydrate crystals begin to form and the pressure immediately decreases further (point C). Thereafter, the temperature is slowly increased, resulting in a pressure increase as the hydrate crystals dissociate. Once the hydrates are fully dissociated, all the gas is released from the crystals and the temperature and pressure are recorded as the dissociation conditions (point D). This method is independent of visual observation and since the setup is a closed system, it is safer to operate at higher pressures (Sloan and Koh, 2008).



**Figure 3-3: Temperature and pressure trace for formation of simple hydrates (Sloan and Koh, 2008).**

### 3.2 Review of experimental equipment

The features of the most commonly used apparatus employed for measuring hydrate phase equilibria are presented in this section. Examples from literature are used to illustrate their main advantages, while some of the experimental difficulties typically encountered by use of such apparatus are also presented.

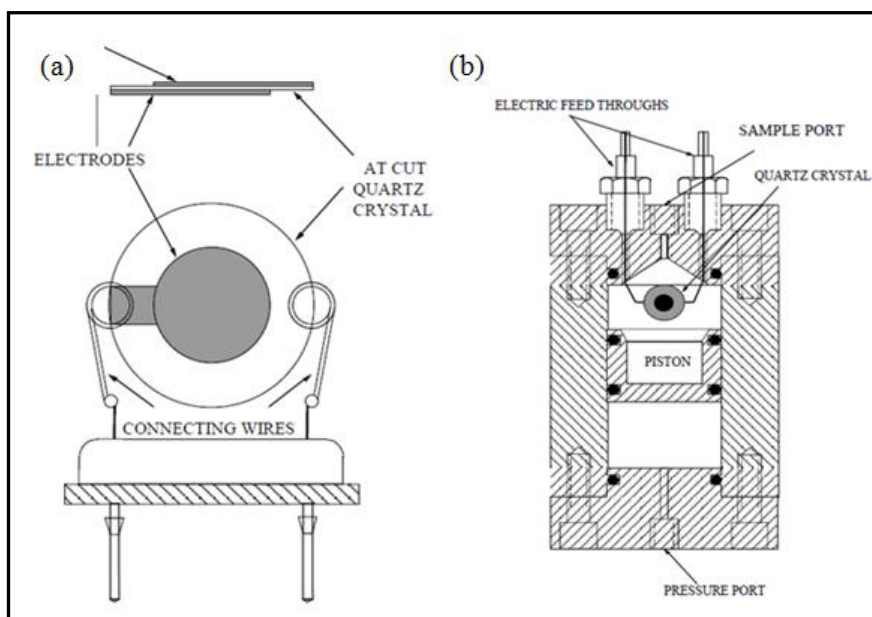
As previously mentioned, for the determination of phase equilibrium data, static methods are generally preferred over dynamic methods (Oellrich, 2004). Several of the main advantages of static devices include:

- Simple technique and experimental set-up
- Wide temperature and pressure ranges
- Suitable for single and multiple component systems, thereby permitting reliable evaluation of industrial systems
- Easy modification of fluid samples, including total compositions and quantities
- Small material quantities required
- Possible observation of high pressure phase behaviour

### 3.2.1 Quartz crystal microbalance (QCM)

The QCM, shown in Figure 3-4, became widely used as a mass balance after the work relating frequency change to mass absorption was demonstrated by Sauerbrey in 1959 (Dixon, 2008). More recently, an innovative method for measuring gas hydrate phase behaviour based on the QCM was derived by Tohidi et al. (2002) (Mohammadi et al., 2003; Sloan and Koh, 2008). The QCM consists of two electrodes, with a thin disk of quartz sandwiched in between them. Upon application of an electric current through the electrodes, the crystal oscillates at a specific frequency, known as the resonant frequency. The high-pressure cell is jacketed and the equilibrium cell temperature is controlled by circulation of coolant through the cell jacket. The cell pressure is controlled by gas injection behind a mobile piston. Initially, a drop of distilled water is added to the surface of the QCM before it is placed within the high-pressure cell. The temperature of the cell is then decreased to freeze the water drop. Thereafter, the cell is evacuated and the components are introduced into the cell. Once the cell is filled, the pressure is increased to the desired point. For hydrate formation, the temperature of the cell is lowered until a considerable extent of subcooling has occurred (Tohidi et al., 2002). Upon hydrate formation, a mass attaches itself to the surface of the crystal, resulting in a decrease in resonant frequency. After hydrate formation, the cell temperature is increased in a stepwise fashion. For each step, the pressure and resonant frequency is recorded. The point at which the resonant frequency significantly rises is taken as the hydrate dissociation point.

The advantages of using the QCM include shorter reaction times (15 min per temperature step versus numerous hours for conventional methods) and smaller experimental samples (~ one drop of water) (Sloan and Koh, 2008). Although the QCM method has been considered unfeasible (Sloan and Koh, 2008) due to good contact requirement between the surface of the quartz crystal and hydrates, Lee et al. (2012) have recently demonstrated that by modifying the droplet size, this method yields acceptable results, especially for rapid and practical gas hydrate application purposes.



**Figure 3-4: (a) Schematic illustration of the QCM crystal mounting and electrical connection configuration. (b) Schematic illustration of the QCM mounted with the high-pressure equilibrium cell (Tohidi et al., 2002).**

### 3.2.2 Cailletet

The Cailletet apparatus is commonly known for operating at high pressures (0.35-14.00 MPa) (Peters et al., 2000; Peters et al., 2006). It is comprised of a capillary glass tube, wherein mercury is used to seal the tube and transmit pressure. For phase behaviour measurements, the core working principle of the Cailletet apparatus is based on the visual observation of the quantity of the various phases present at a given temperature and pressure (Peters et al., 2006; Sabil and Bin, 2009). Initially, the experimental fluid is injected into the Cailletet tube and kept frozen by liquid nitrogen. Consequently, the air present in the tube is evacuated under high vacuum while the liquid sample is kept frozen. Thereafter, the liquid sample is degassed by consecutive freezing steps with liquid nitrogen. When degassing is complete, mercury is pressed on a known quantity of gas (either carbon dioxide or ethane) in order to seal the tube. After the sample is prepared, the Cailletet tube is transferred to the high pressure Cailletet apparatus. The tube pressure is applied by pushing hydraulic oil into the system, while a dead-weight pressure gauge controls this pressure. A thermostat jacket surrounds the tube and the temperature is controlled by circulating thermostat liquid through the jacket (Peters et al., 2000). The sample is then cooled, while stirring vigorously, and the cell volume is manipulated until hydrate formation occurs. Thereafter, the pressure is monitored until a constant pressure is obtained. The resulting pressure and temperature values are then recorded as the hydrate dissociation conditions.

Although the Cailletet apparatus boasts experimental work at elevated pressure, environmental concerns arise due to the use of highly toxic mercury. In addition, since the apparatus is subject to frequent volume manipulations, it is susceptible to mechanical degradation.

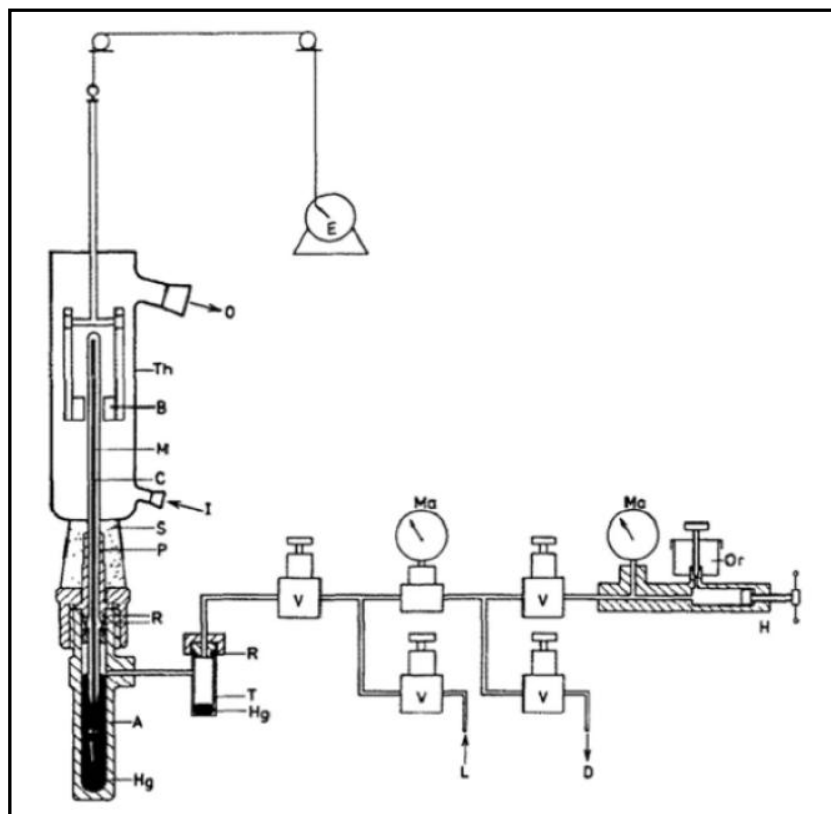


Figure 3-5: Schematic illustration of Cailletet apparatus (Sabil and Bin, 2009).

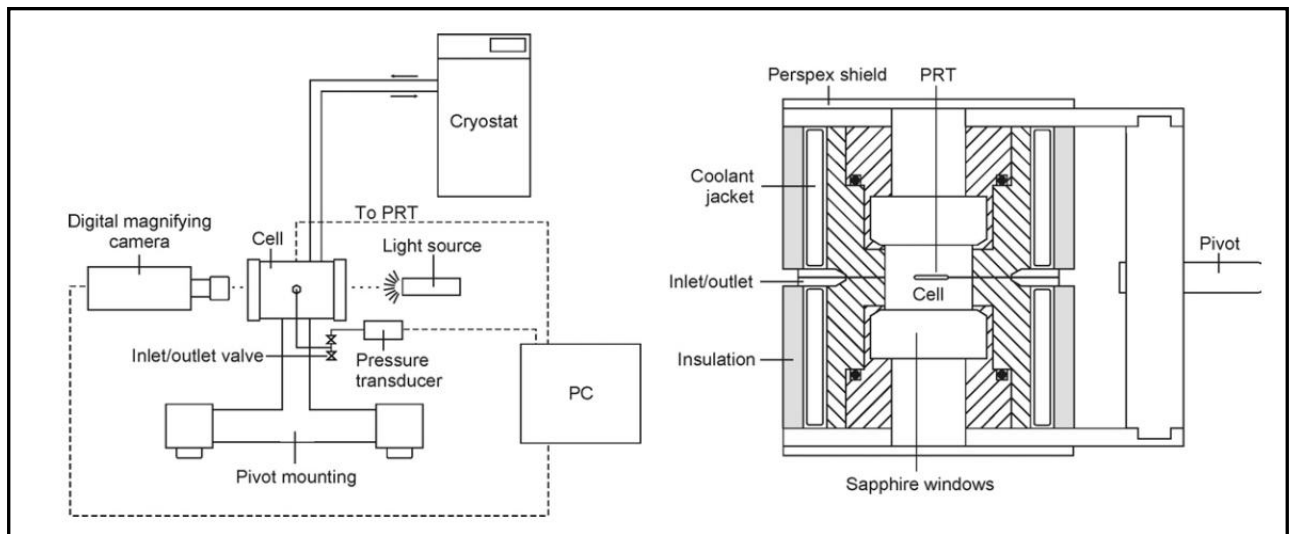
A, autoclave; B, magnets; C, Capillary glass tube; D, drain; E, motor; F, metal stirrer; Hg, mercury; I, thermostat liquid - in; L, line to dead weight pressure gauge; M, investigated mixer; Ma, manometers; O, I, thermostat liquid – out; Or, hydraulic oil reserve; P, closing plug; R, viton O rings; S, silicon rubber stopper; T, mercury trap; Th, glass thermostat; V, valve.

### 3.2.3 The rocking cell apparatus

In 1937, Deaton and Frost fabricated a static hydrate equilibrium apparatus that became the prototype of many others. The fundamental features of this apparatus included a basic cell with options for gas flow above, or sparged through the liquid, as well as the option for rocking the cell in a thermostatted bath (Sloan & Koh, 2008). Recent developments of the rocking cell apparatus consist of a high-pressure cell that is positioned on a horizontal pivot. The cell undergoes 180° pneumatic controlled rocking, causing displacement of mixing balls positioned inside the cell. The high-pressure cell can either be manufactured from sapphire or stainless steel. This allows apparatus of this kind to withstand temperatures in the range of 243.15 K to 323.15 K and pressures up to 50 MPa (Najibi et al., 2009).

The cell temperature is maintained by circulation of coolant through a cryostat jacket surrounding the cell. The isochoric step-heating method is commonly practiced with this apparatus, as it has been found to be the most reliable technique (Najibi et al., 2009).

One of the promising aspects of this apparatus is that it allows for direct observation of hydrate formation, however, due to the continuous rocking motion, the experimental setup is susceptible to mechanical deterioration.



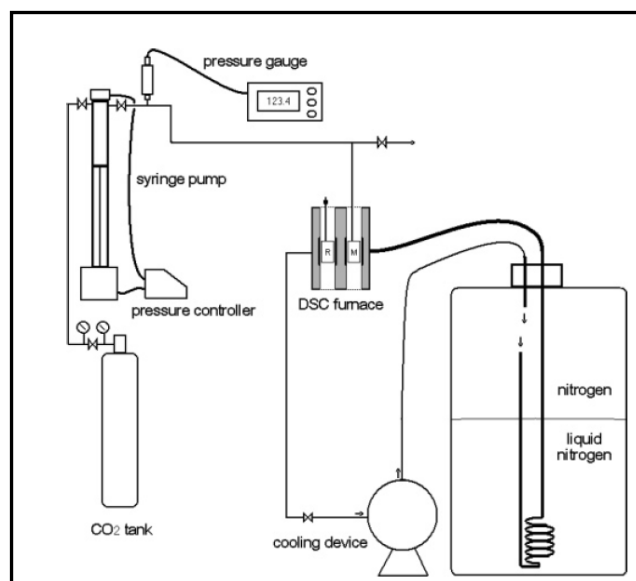
**Figure 3-6: Schematic illustration of rocking cell apparatus (Najibi et al., 2009).**

### 3.2.4 High-pressure differential scanning calorimetry

Recently, the use of high-pressure differential scanning calorimetry (DSC) has been used for the determination of hydrate phase equilibrium data, as well as gas hydrate thermal property data. Dalmazzone et al. (2002) introduced a micro-DSC analyser used in conjunction with special high-pressure vessels, namely High-Pressure Differential Scanning Calorimetry (HP-DSC), to illustrate the thermodynamic stability boundaries of natural gas and methane hydrates in the presence of various inhibitors. The apparatus, shown in Figure 3-7, is comprised of two pressure-controlled cells. The first cell, called the sample cell, houses the experimental fluid, while the second cell, called the reference cell, remains empty. Due to the nature of this apparatus, no stirring can be used (Martinez et al., 2008). The DSC technique is based on observing the heat exchange between the sample and reference cells. The experimental method commonly used to measure the hydrate dissociation conditions is the isochoric pressure search method (Martinez et al., 2008; Mayoufi et al., 2010). The sample cell is initially filled with the experimental fluid and placed in the furnace. The cell is then connected to the feed gas line where it is purged to evacuate any air present. The gas pressure is then set to a specified value and kept constant for each determination point. In order to measure the hydrate

equilibrium points, the cell temperature is first decreased (cooling sequence) in a step-wise fashion, left to remain constant for crystal growth to occur, and then increased (warming sequence) to melt the solids. From the thermograms produced, the hydrate dissociation temperature is found to be the crest of the hydrate progressive dissociation peak, as shown in Figure 3.8. This procedure is then repeated for a series of pressures. The DSC device is able to operate at temperatures in the range of 228.1 K to 393.15 K and a maximum pressure of 40 MPa (Martinez et al., 2008).

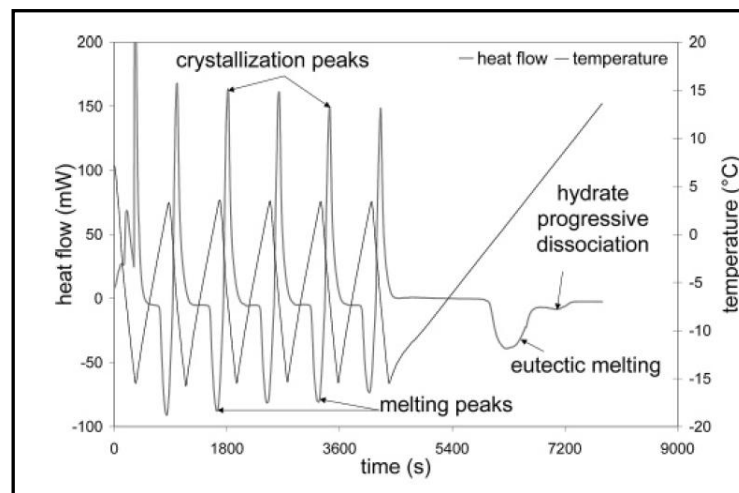
The main advantage of this apparatus is that results of the same precision as classical PVT techniques can be obtained in less time (Le Parlouer et al., 2004). However, the method of data interpretation that accompanies this apparatus is relatively complex and time consuming.



**Figure 3-7: Schematic illustration of high pressure DSC apparatus (Delahaye et al., 2006).**

**R, reference vessel; M, sampling vessel.**





**Figure 3-8: Thermal cycles of hydrate formation and dissociation for high-pressure differential scanning calorimetry (Delahaye et al., 2006).**

### 3.2.5 High-pressure autoclave cell

Hydrate phase equilibria measurements are commonly determined by use of stirred autoclave cells (Sloan and Koh, 2008). This apparatus is generally constructed of either sapphire or stainless steel. Hydrate formation may be determined by either visual or non-visual methods, whereas in the former case, sapphire or flexi glass windows are fitted to the cell for direct observation. Cell agitation is generally achieved by use of either a magnetic or mechanical stirrer. In cases where vortex formation is probable, baffles are used to reduce this effect (Lee et al., 2005). In the high-pressure autoclave cell, the hydrate dissociation points can be determined by either of three methods; isothermal pressure search, isobaric temperature search or isochoric pressure search, discussed in section 3.1.

Due to the limited literature regarding aqueous sucrose hydrate systems, an in-depth review of high-pressure autoclave cell apparatus used in the presence of carbohydrates was undertaken. In addition, a summarised review of various other high-pressure autoclave apparatus used for gas hydrate equilibrium measurements was also made.

## 3.2.5.1 High-pressure autoclave cell of Chun and Lee (1998)

The equilibrium cell shown in Figure 3-9 consists of two sight glasses fitted at the front and back of the cell for visual observation of phase transitions. The cell was manufactured from 316 stainless steel, with an internal volume of 50 cm<sup>3</sup>. Hydrate equilibrium conditions were determined by the isobaric temperature search method. A magnetic stirrer, with an external magnet immersed in the water bath was used to ensure vigorous agitation of the cell contents, while the water bath temperature was controlled by an externally circulating heater/refrigerator. A K-type thermocouple with digital thermometer, having a resolution of  $\pm 0.1$  K, was used to measure cell temperature. The calibration of the thermometer was performed with an ASTM 63C mercury thermometer. The ASTM 63C thermometer had a temperature range of 265.15 K to 305.15 K, with a resolution of  $\pm 0.1$  K. Pressure was supplied by means of a high pressure-metering pump and is measured by use of a Heise gauge. The pressure gauge had a range of 0 - 20 MPa, with a maximum difference of  $\pm 0.01$  MPa.

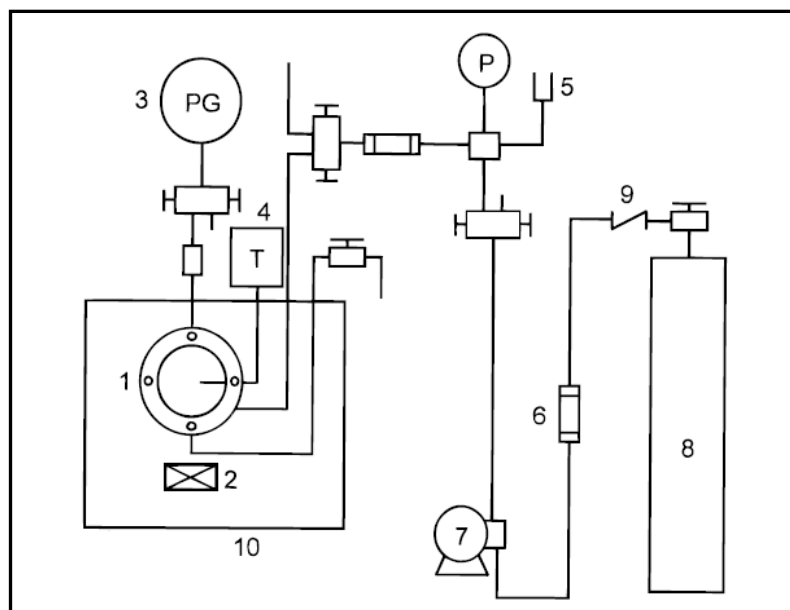


Figure 3-9: Schematic diagram of the experimental apparatus of Chun and Lee (1998).

1, equilibrium cell; 2, magnet; 3, pressure gauge; 4, thermometer; 5, rupture disk; 6, check valve; 7, high-pressure pump; 8, former cylinder; 9, line filter; 10, water bath.

## 3.2.5.2 High-pressure autoclave cell of Carbone et al. (2012)

The experimental setup shown in Figure 3-10 consists of a high-pressure pressure-volume-temperature (PVT) cell built with a glass cylinder secured between two full-length viewing windows. This is all contained within a stainless steel frame. The cylinder is 20 cm tall with a void volume of 150 cm<sup>3</sup>. The equilibrium conditions were determined by the isothermal pressure search method. Constant monitoring of the system was achieved by use of the viewing windows. A high pressure, positive displacement pump generated the experimental pressure required inside the reaction vessel. The fluid inside the pump contacts a floating stainless steel piston, therefore isolating the hydraulic fluid from the process side of the cell. This prevents contamination of the process side with the pump fluid when pressure is exerted on the experimental contents. The high-pressure PVT cell is mounted inside a temperature-regulated air bath by means of a bracket and horizontal shaft. The temperature and pressure ranges were 275.15 – 281.25 K and 3.4 to 8.0 MPa respectively. The shaft is attached to an electric motor. Cell agitation is produced by this motor which powers the shaft to allow the cell to oscillate through 60° about its centre of gravity, at a rate of 40 oscillations cycles per minute. The cell temperature and pressure were monitored by use of a platinum RTD probe and pressure transducer respectively, that were both supplied with the experimental setup. The temperature uncertainty was found to be 0.2 K, while the pressure uncertainty was found to be 0.014 MPa.

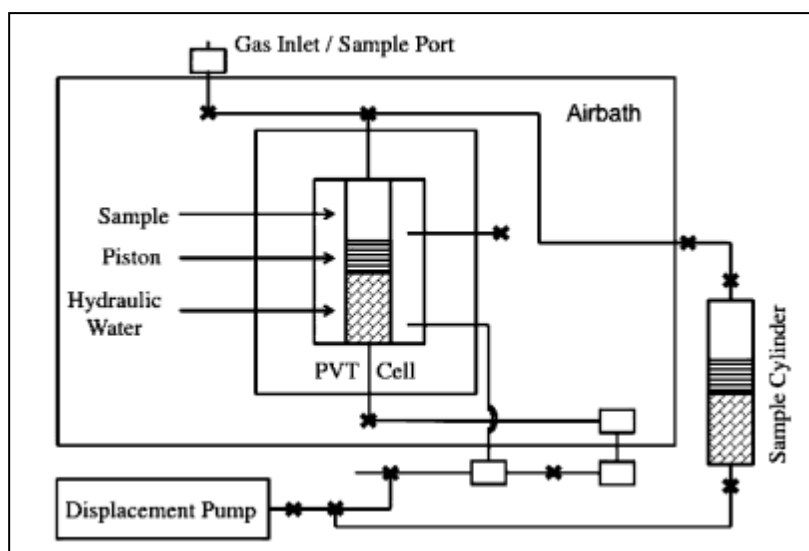


Figure 3-10: Schematic diagram of the Jefri-DBR experimental apparatus of Carbone et al. (2012).

Table 3-2: Review of high-pressure autoclave apparatus.

Reference	Experimental Method	Temperature a) Range b) Accuracy	Pressure a) Range b) Accuracy	Cooling/Heating Mechanism	Equilibrium cell a) Type b) Volume c) Agitation	Comments
Nixdorf and Oellrich (1997)	Non-visual isochoric pressure search	a) 243.15 - 423.15 K b) $\pm 0.02$ K	a) 0 - 25 MPa b) $\pm 0.06$ MPa	Pressureless heating sleeve filled with circulating water/glycol mixture	a) Acid and corrosion resistant stainless steel b) 500 cm <sup>3</sup> c) Permanent magnetic stirrer	Impeller used to ensure maximum distribution of gas in liquid.
Ivanic et al. (2004)	Non-visual isochoric pressure search	a) 274-300 K b) $\pm 0.05$ K	a) 0 - 35 MPa b) $\pm 5\%$	Water bath heated with two, 120W Vycor glass emersion heaters, and cooled with a Blue M constant-flow portable cooling unit	a) Stainless steel b) 300cm <sup>3</sup> c) Mechanic stirrer	
Ruffine et al. (2010)	Visual isobaric temperature search	a) 253 - 473 K b) $\pm 0.4$ K	a) 0- 60 MPa b) $\pm 0.01$ MPa	Welded metal jacket with circulating thermal fluid	a) 316-Ti stainless steel with sapphire windows b) Variable ( diameter = 25.5 mm) c) N/S	Cell volume manipulations by piston action.

N/S – Not specified

Table 3-2 (continued): Review of high-pressure autoclave apparatus.

Reference	Experimental Method	Temperature a) Range b) Accuracy	Pressure a) Range b) Accuracy	Cooling/Heating Mechanism	Equilibrium cell a) Type b) Volume c) Agitation	Comments
Herri et al. (2011)	Visual isochoric pressure search	a) 273-277 K b) 0.02 K	a) 0-10 MPa b) $\pm 0.05$ MPa	Double jacketed cell connected to an external cooler	a) Stainless steel b) 1 L c) Mechanical stirrer	Four vertical-blade turbine impeller ensure adequate mixing
Villano and Kelland (2011)	Isothermal pressure search ( <sup>a</sup> visual)	<sup>a</sup> a) 273-303 K b) $\pm 0.1$ K  <sup>b</sup> a) 273-303 K b) $\pm 0.1$ K	<sup>a</sup> a) 0-9 MPa b) $\pm 0.02$ MPa  <sup>b</sup> a) 0-9 MPa b) $\pm 0.02$ MPa	Cooling bath	<sup>a</sup> a) Sapphire b) 22.8 ml c) Magnetic stirrer (0-1700 rpm) <sup>b</sup> a) Stainless steel b) 200 ml c) Magnetic stirrer (600 rpm)	Shorter hold times obtained in the steel cell compared to that in the sapphire cell
He et al. (2011)	Visual isothermal pressure search	a) 276 K b) $\pm 0.1$ K	a) 0 - 10 MPa b) $\pm 1 \times 10^{-4}$ MPa	Thermostatted water bath	a) N/S b) N/S c) Mechanic stirrer	Impeller used to ensure maximum distribution of gas in liquid.

Table 3-2 (continued): Review of high-pressure autoclave apparatus.

Reference	Experimental Method	Temperature a) Range b) Accuracy	Pressure a) Range b) Accuracy	Cooling/Heating Mechanism	Equilibrium cell a) Type b) Volume c) Agitation	Comments
McNamee and Conrad (2011)	Visual isochoric pressure search	a) 263.15 - 333.15 K b) $\pm 0.1$ K	a) 20 MPa b) N/S	Cooling jacket and chiller	a) 316-Ti stainless steel with sapphire windows b) 450 cm <sup>3</sup> c) Overhead and magnetic stirrer	Overhead stirring found to be best stirring method, followed by magnetic wedge-stir bar, then cylindrical stir-bar.
Javanmardi et al. (2012)	Visual isochoric pressure search	a) 256.4 - 282.0 K b) $\pm 0.1$ K	a) 1.97 - 6.96 MPa b) $\pm 0.01$ MPa	Thermostatic bath	a) 316 stainless steel with double sight glasses b) 75 cm <sup>3</sup> c) N/S	Experimental results were consistent with previously reported data.
Maekawa (2013)	Non-visual isochoric pressure search	a) 273.6 - 295.7 K b) $\pm 0.2$ K	a) 0 - 1 MPa b) $\pm 0.004$ MPa	Thermostatic bath with water/glycol mixture	a) Stainless steel b) 700 cm <sup>3</sup> c) Magnetic stirrer	Experimental results were consistent with previously reported data.

### 3.3 Extent of separation

In separation technologies involving aqueous hydrate systems, such as food concentration and water desalination, the separation step appears to be the bottleneck in the process (Werezak, 1969). This is commonly attributed to poor crystal growth, in both size and geometry. Centrifugation appears to be the most promising method of separation (over filtration), although some crystal washing may still be necessary (Werezak, 1969).

The extent of solution separation is generally determined by using either mechanical or computational methods (Englezos, 1993). When the apparatus is available, mechanical methods usually provide more accurate results. The progress of hydrate formation, and thus the extent of solution separation, can be determined by the following methods.

#### 3.3.1 Direct method

In the direct method, the hydrate crystals formed are separated in a basket-type centrifuge. Centrifugation pressures either need to be above 1.14 MPa (Werezak, 1969) or the centrifugation process needs to be operated in a room maintained at 275 K to 277 K (Huang et al., 1965). After the appropriate centrifugation period, the filtrate is weighed and its solids content determined using refractive index. The hydrate crystals are also weighed, decomposed, and their solids content determined using refractive index. From the resulting refractive indices, the degree of separation may be determined. The resulting partially concentrated filtrate may then be remixed with a measured quantity of hydrate former and the process may be repeated until the desired solution concentration is achieved. In systems where the hydrate former is not highly soluble in the solution, vapour-tight centrifuges may be necessary for hydrate stability during centrifugation (Werezak, 1969).

#### 3.3.2 Indirect method

After hydrate formation has occurred, a sintered glass tube is used to remove a small portion of the fluid phase from the hydrated sample. The composition of the filtrate can then either be determined with a refractometer or by titration (Huang et al., 1965). From the resulting refractive indices, or titration results, the degree of separation may be determined.

#### 3.3.3 Flash calculation method

The amount of hydrate formed from a given solution can be calculated if the mass balance equations, along with the hydrate phase, are solved simultaneously with the phase equilibrium equations

(Englezos, 1993). Bishnoi et al. (1989) were the initial researchers to formulate and solve this problem in its general form. This was performed by including all possible liquid and solid phases. Cole and Goodwin (1990) also performed flash calculations with hydrates systems. These calculations were used to determine the amount of hydrate that will form under given circumstances, the compositions of all equilibrium phases in a rigorous manner, and the distribution of hydrate inhibitors throughout the equilibrium phases.



## CHAPTER 4

### DESCRIPTION OF EXPERIMENTAL APPARATUS AND PROCEDURE

Engineering design relies on accurate modeling, and modeling relies on accurate experimental data (Richon, 2009). Data collected from experimental studies is therefore an invaluable and timeless source of information, which is only as reliable as the methods and apparatus used to collect it.

The static, non-visual isochoric method using a constant volume isochoric pressure cell with magnetic stirring was chosen for this study. From the static methods available, the isochoric method is advantageous over the others as the entire process is automated, allowing for measurements to be undertaken overnight. In addition, this method does not depend on visual observation of hydrate formation and therefore eliminates this source of uncertainty (Oellrich, 2004).

This chapter describes the apparatus used in this study. The experimental set-up includes an isochoric pressure equilibrium cell, agitator, liquid bath, temperature controllers and temperature and pressure sensors. The measuring devices used, as well as their accuracies and limitations are also presented. In addition, the source and type of materials, including their purities, are discussed. This chapter also documents the experimental procedure used in this study. This includes leak testing, calibrations, cell preparation, and the operating method used to determine the hydrate dissociation conditions.

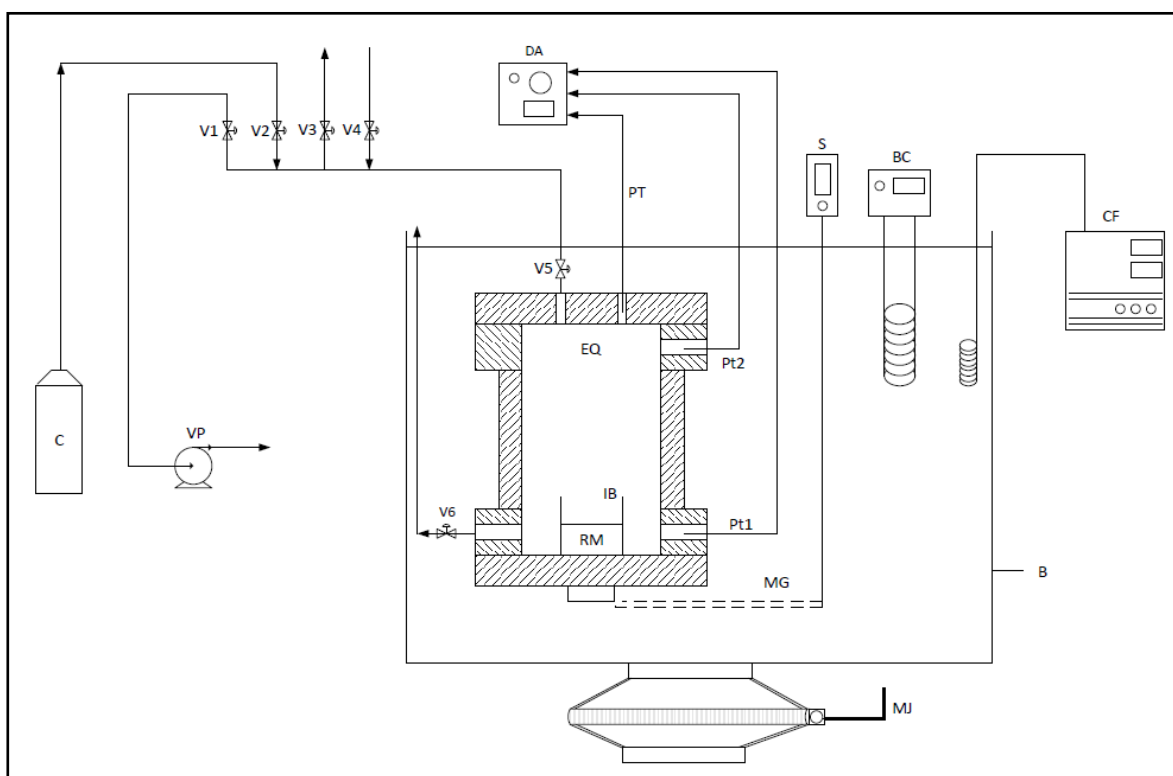
#### 4.1 Experimental apparatus

A newly developed high-pressure equilibrium cell, commissioned in this study, was used for the experimental hydrate measurements. The experimental setup consists of:

- A stainless-steel equilibrium cell (approximately 64 cm<sup>3</sup>)
- an agitation device
- a liquid temperature bath (43 cm x 35 cm x 26 cm)
- a programmable temperature controller
- two Pt100 temperature sensors
- a WIKA pressure sensor

- a 34972A LXI Agilent data acquisition unit
- a Variac
- temperature programmable circulator
- one Polyscience IP-35cold finger
- a mechanical jack
- an RV3 Edwards vacuum pump

The reader is referred to Figures 4-1 and 4-2 for the equipment layout.



**Figure 4-1: Schematic diagram of the experimental setup. B, liquid temperature bath; BC, liquid temperature bath controller; C, refrigerant gas cylinder; CF, cold finger; DA, data acquisition unit; EQ, isochoric pressure equilibrium cell; IB, impellor blades; MG, mechanical gears; MJ, mechanical jack; Pt1, temperature probe; Pt2, temperature probe; PT, pressure transducer; S, overhead mechanical stirrer; V1, vacuum valve; V2, gas valve; V3, vent valve; V4, loading valve; V5, inlet valve; V6, drain valve; VP, vacuum pump.**



**Photograph 4-1: Experimental setup.**

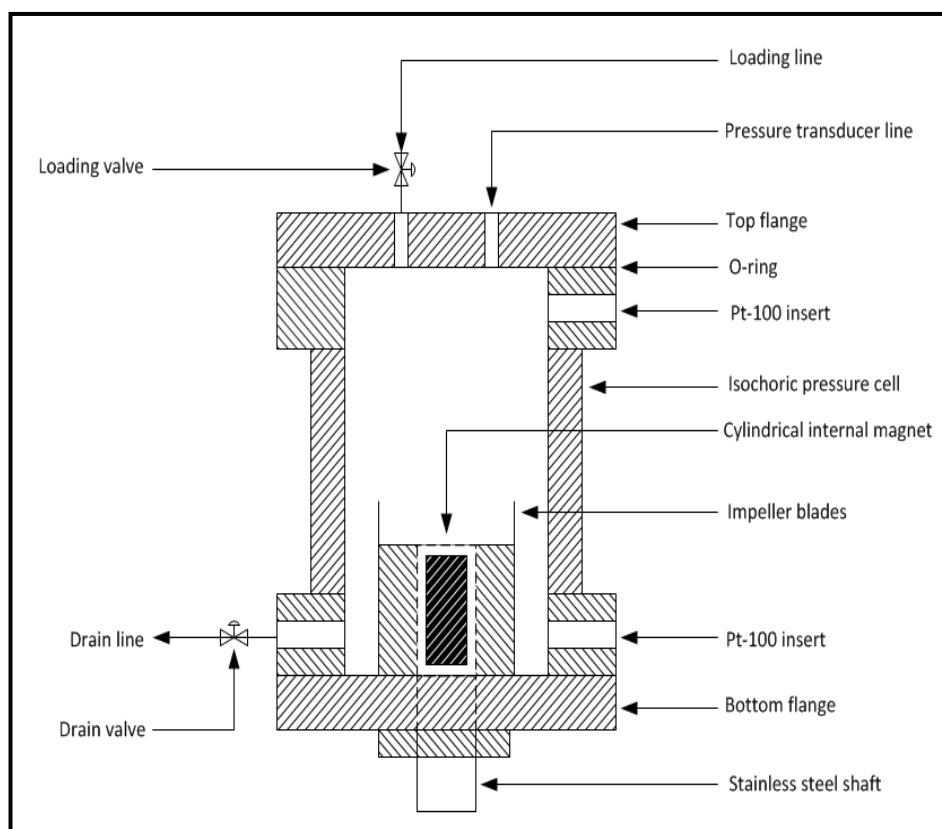
#### *4.1.1 Isochoric pressure cell*

The equilibrium cell was constructed using 316 stainless steel. This material was selected due to its resistance to corrosion and mechanical strength. In addition, one of the main advantages of 316 stainless steel is that it can perform well at both high and low temperatures, as well as withstand the high pressures required for hydrate measurements. The cell has a height of 40 mm and a diameter of 45 mm, resulting in an internal volume of approximately 64 cm<sup>3</sup>. A new stirring technique was designed by Richon (2013) (personal communication) to improve the stirring efficiency. Please refer to section 4.1.2 for more information. Therefore, due to the displacement of the magnetic stirrer inside the cell, the working volume resulted in a value of approximately 53 cm<sup>3</sup>.

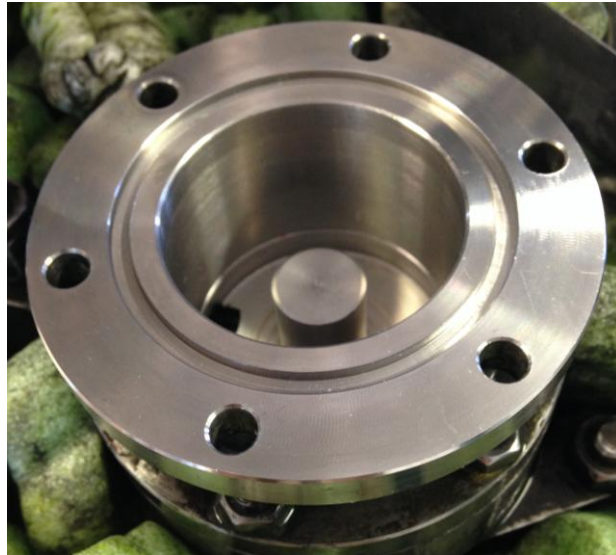
On the top of the cell, an O-ring was sandwiched into a groove between the top flange and the cylinder. For this study, a Viton O-ring was selected, as it is compatible with both sucrose and the refrigerant gases used. The top flange is fixed to the cell using 6 x 10 mm stainless steel bolts. The overall diameter of the top flange is 5 mm. Three holes, each with a diameter of 8 mm were drilled into the top flange. The first hole, situated on the top right of the cell, was used for the filling and evacuation of the cell contents. The second hole, situated on the top left of the cell, was used to connect a 1/16' inch 316 stainless steel tubing to the pressure transducer. The third hole, situated on

the side of the flange, was used to house a Pt-100 temperature probe, which measured temperature at the top of the equilibrium cell.

Two holes, each with a diameter of 8 mm were drilled into the bottom flange. The first hole, situated at the bottom right side of the flange, was used to house another Pt-100 used to measure the temperature at the bottom of the equilibrium cell. The second hole, situated at the bottom left side of the flange, was used to discharge the cell contents. All valves were bidirectional and were supplied by Swagelok.



**Figure 4-2: Schematic of the equilibrium cell.**



**Photograph 4-2a: Cell without magnetic stirring device.**



**Photograph 4-2b: Cell with magnetic stirring device.**

#### *4.1.2 Agitation technique*

Agitation within the cell was required to reduce the time in which equilibrium is achieved. The new stirring device design by Richon (2013) (personal communication) consisted of two external magnets and several small magnets situated inside the shaft. The magnets were manufactured from Neodymium. This material was chosen due to its strong magnetic field. The stirring device, situated at the bottom of the cell, made use of a Heidolph RZR 2041 overhead stirrer. The overhead stirrer drives a gear chain at the bottom of the cell, which subsequently drives the magnetic stirrer. The Heidolph RZR 2041 overhead stirrer consisted of two gear speeds; 40 to 400 rpm and 200 to 2000 rpm. The

new design of the stirring device consists of three impeller blades, each with a length of 5 mm, height of 33 mm, width of 1 mm, as well as two neodymium magnets. A Teflon® covering was made to fit the external magnet in order to reduce friction, caused by the high magnetic field, between the stainless steel shaft and neodymium magnet. The external magnet with the impeller blades is removable from the shaft as shown in Photograph 4-3.

The advantages of the new stirring device are:

- Improved stirring power and efficiency compared to magnetic bar stirring device
- Reduced gas hydrate dissociation time through fast homogenization
- Direct agitation in the cell promotes homogenous aqueous solution



**Photograph 4-3: Magnetic stirrer device.**

#### *4.1.3 Temperature and pressure sensors*

##### *Temperature*

Two platinum resistance thermometers (Pt-100) were used to measure temperature within the equilibrium cell. The Pt-100's are capable of sensing temperatures between 73.15 K and 1073.15 K with an accuracy of  $\pm 0.03$  K. The probes were fixed on the equilibrium cell; one at the top of the cell and one at the bottom. This was to monitor the temperature gradient within the cell, usually 0.05 K. As a result, the uniformity of the bath temperature could be checked. The temperature probes were

connected to the 34972A LXI Agilent data acquisition unit where the temperature readings were electronically displayed with respect to time and logged at two second intervals.

#### *Pressure*

One WIKA pressure transducer, with a stated accuracy of  $\pm 0.02$  kPa, was used to provide the cell pressure readings. The pressure transducer was situated on the top flange, where it was able to measure pressures in the range of 0-10 MPa. The total pressure exerted on the cell was the sum of the 0-10 MPa pressure transducer and the atmospheric pressure (taken as 1.03125 bar). The transducer was connected to the 34972A LXI Agilent data acquisition unit where the pressure readings were electronically displayed with respect to time.

#### *4.1.4 Liquid temperature bath*

The equilibrium cell was submerged in a liquid temperature bath to ensure an isothermal environment was maintained. The bath had a length, width and height of 43 cm, 35 cm and 26 cm respectively. The bath was constructed of 316 stainless steel. It contained a 30 L mixture of 80 wt.% ethylene glycol and 20 wt.% water antifreeze (supplied by MIDAS). This allowed for operation in the temperature range of 228 K (melting point at atmospheric pressure) to 397 K (boiling point at atmospheric pressure).

#### *4.1.5 Temperature controllers*

The bath temperature was controlled using a Model TX150 programmable controller supplied by Grant®. The controller temperature range was 243.15 K to 323.15 K. It contained an immersion circulator pump with an internal temperature probe. The programmable controller heated or cooled the antifreeze mixture in the bath which in turn heated or cooled the equilibrium cell contents to the required temperature. A programmable controller was used to control the temperature of the equilibrium cell contents at a specified rate to ensure that adequate separation between the hydrates and the sucrose was achieved. This controller was connected to the computer setup, where software supplied by Labwise® was used to program the heating and cooling steps.

An immersion cooler or cold finger, supplied by PolyScience®, was used to cool the bath contents. It operated at temperatures as low as 173.15 K. The refrigeration unit was composed of an evaporator, condenser, compressor and throttling valve.

One heating cartridge, with a diameter of 7 mm and a length of 40 mm, was situated in a heating block housing for the pressure transducer. This ensured the pressure transducer was maintained at a constant temperature due to its sensitivity to temperature fluctuations. The transducer was maintained at 313.15 K, which was the maximum temperature the experimental apparatus was expected to reach. The line connecting the pressure transducer to the equilibrium cell was heated with nichrome wire. This prevented condensation in the lines leading to the pressure transducer for pressure measurements.

## 4.2 Experimental procedure

In the isochoric method, the equilibrium condition is established through temperature and pressure measurement. No visual observation or complicated calculations are required, allowing for a reliable determination of hydrate equilibrium data. Additionally, the technique is suitable over the entire range of hydrate formation temperatures and pressures, and smaller volumes of fluids are used, as no volume changes are required. Furthermore, it is suited to automated control of experiments (Rivollet, 2005; Khalil, 2006). Thus, the isochoric method is considered rather advantageous to investigate the phase behavior of multicomponent mixtures, compared to isobaric and isothermal approaches with a visual observation requirement. For the above reasons, the isochoric method combined with stepwise heating and efficient mixing was applied in this investigation.

### 4.2.1 Isochoric cell preparation

#### 4.2.1.1 Cleaning of isochoric pressure equilibrium cell

In order to reduce any contamination of the cell contents, the equilibrium cell was cleaned prior to undertaking any experimental measurements. Initially, the cell was loaded with 50 ml of pure ethanol. This was then allowed to agitate inside the cell at a speed of 600 rpm for 1 hour in order to absorb any contaminant present on the cell wall. Thereafter, the ethanol was drained from the cell. Next, the cell was rinsed twice with acetone. Once the acetone was drained from the cell, nitrogen was used to flush any remaining acetone residue. This was performed in order to ensure that the cell was clean and dry. Thereafter, the Edwards vacuum pump was used to evacuate the cell to a pressure of 0.0002 kPa for 30 minutes to remove any air or volatile matter present in the cell. Once this cleaning process was completed, the cell was ready for leak testing.

Cleaning the cell between experiments required a less intensive procedure as all the systems only contained sucrose, ultrapure water and the refrigerant gas of choice. Initially, the cell was drained and the top flange was removed. The cell was loaded with 50 ml ultrapure water and allowed to agitate



inside the cell for 5 minutes. Thereafter, the water was drained from the cell and the agitation device/stirring mechanism was removed. The magnetic stirrer, top flange, and O-ring were then rinsed with water and dried. The cell was also wiped clean and dried before the O-ring and top flange were reattached. The cell was then evacuated to a pressure of 0.0002 kPa for 5 minutes. Finally the cell was flushed three times with the refrigerant gas of the next system in the investigation. This entire procedure was repeated before undertaking the next system of interest.

#### 4.2.1.2 Leak testing

Leak testing was conducted on the cell in order to reduce the risk of errors. During the initial leak test, the cell was filled to a pressure of 9 MPa with nitrogen and the inlet valve to the cell was closed. A leak detecting fluid (SNOOP®) was applied to all fittings and connections. A leak was detected at a fitting by observing the presence of foam or bubbles. All fittings, at which such leaks were observed, were tightened, or replaced. Thereafter, the equilibrium cell was immersed in the liquid bath at 298.15 K. The bath was maintained at a constant temperature to eliminate temperature and pressure fluctuations. The experimental set up was then left at these conditions (9 MPa, 298.15 K) for the same time period as the experiment (approximately 24 hours). This ensured no significant pressure loss was detected over this time frame. When no leaks were detected calibrations were conducted.

#### 4.2.2 Calibration procedure

##### 4.2.2.1 Temperature calibration

The two Pt-100 temperature probes used in this study were calibrated against a standard WIKA CTH6500 temperature standard. For a temperature range between 73.15 K and 873.15 K, the standard probe had stated full-scale uncertainty of  $\pm 0.03$  K. The two temperature probes were inserted together with the standard probe in the liquid silicon oil bath. All probes were immersed in the fluid and held together using a thin copper wire. This was done in order to reduce any temperature gradient that may occur. At specified stabilised temperatures, temperature readings from the two temperature probes and the standard probe were recorded. Initially, the liquid bath temperature was set to 268.15 K. Thereafter, increments of 5 K per point were used to reach a final temperature of 298.15 K. Subsequently, in order to account for the effect of hysteresis, the same procedure was used to decrease the temperature back to 268.15 K, followed by increasing the temperature back to 298.15 K. For each point, once the reading had stabilized, the temperature readings were collected for three minutes and then averaged. The temperature of the standard probe was plotted against the temperature readings of the two Pt-100s. The maximum calibrated uncertainty for both the bottom and top temperature probes were found to be  $\pm 0.021$  K. The overall temperature uncertainty was found to be  $\pm 0.140$  K.

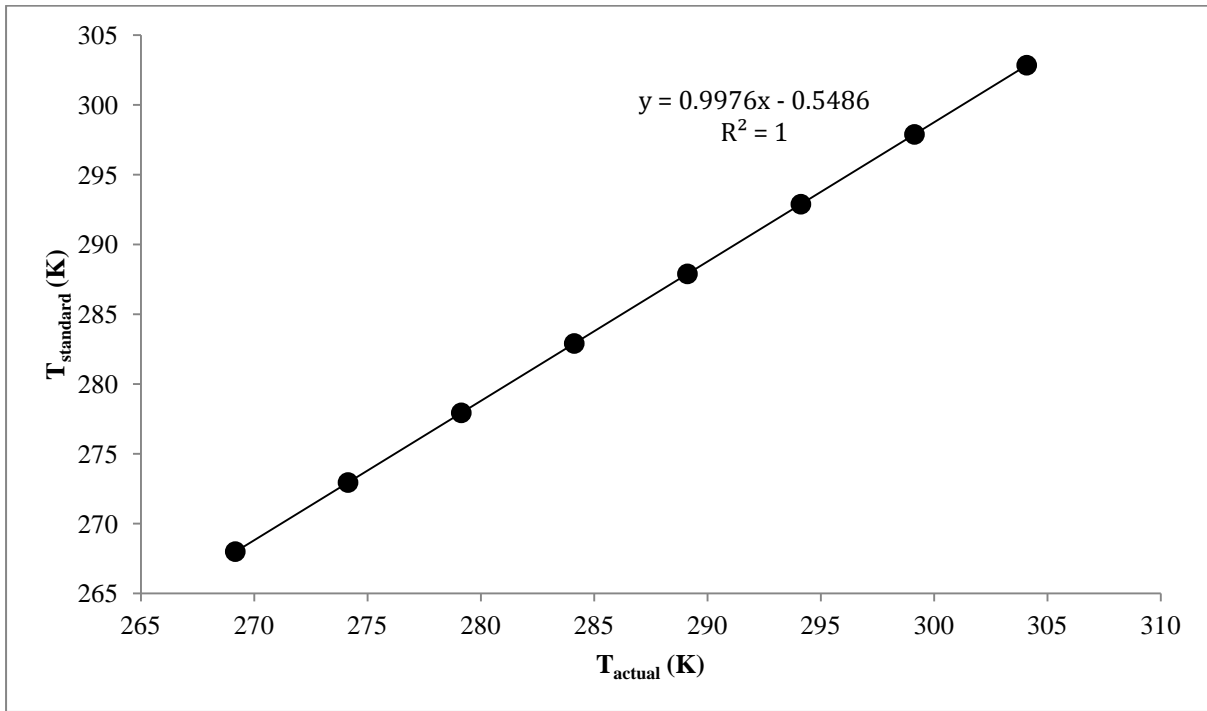


Figure 4-3: Calibration of the bottom temperature sensor. First order relation between standard and sensor temperatures.

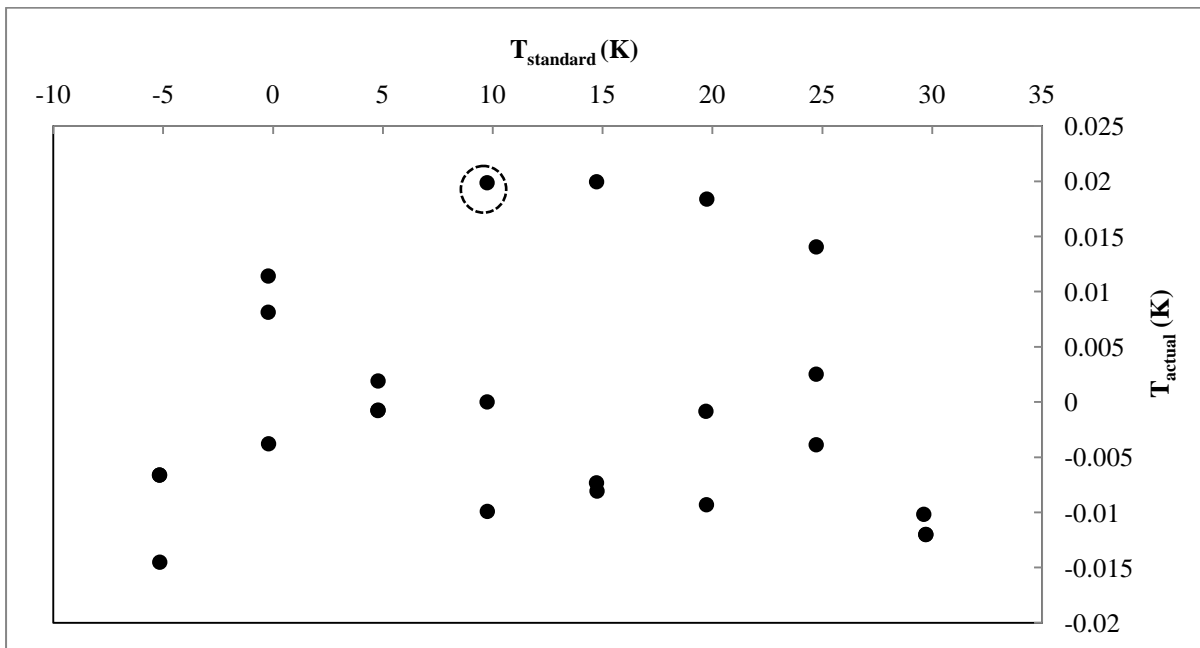



Figure 4-4: Deviations from the standard temperature due to first order relation for the bottom temperature sensor, where  indicates a maximum deviation of  $\pm 0.02 \text{ K}$ .

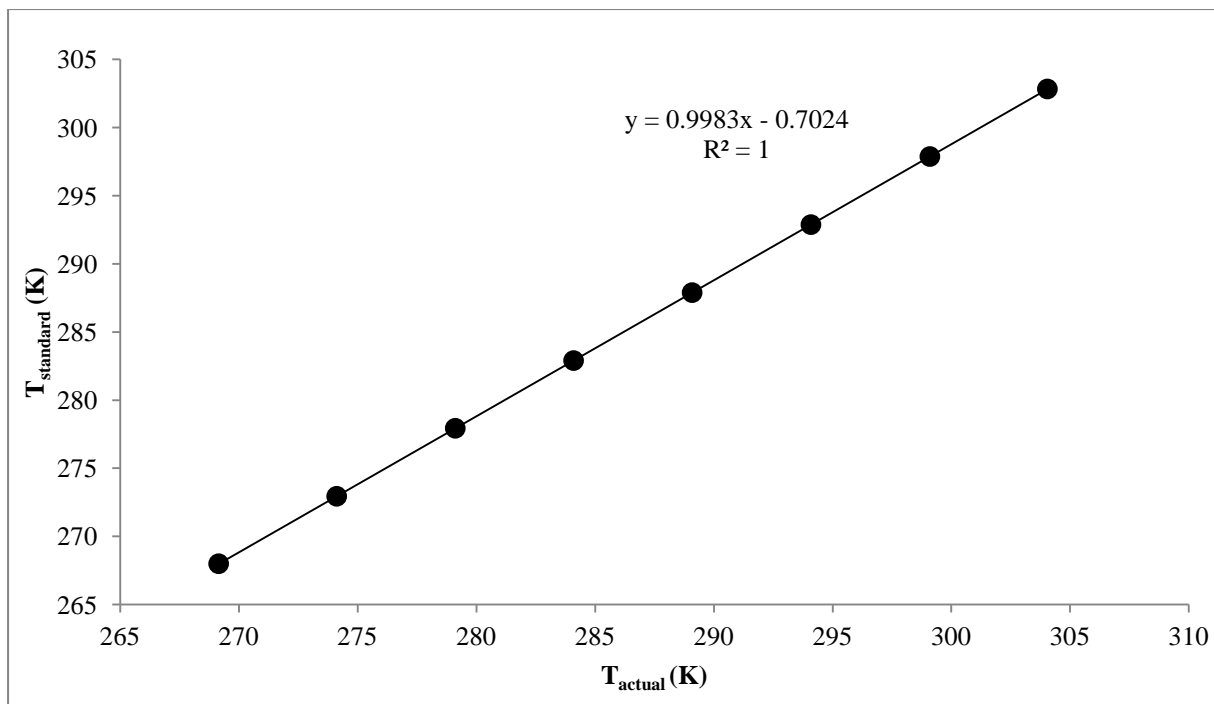


Figure 4-5: Calibration of the top temperature sensor. First order relation between standard and sensor temperatures.

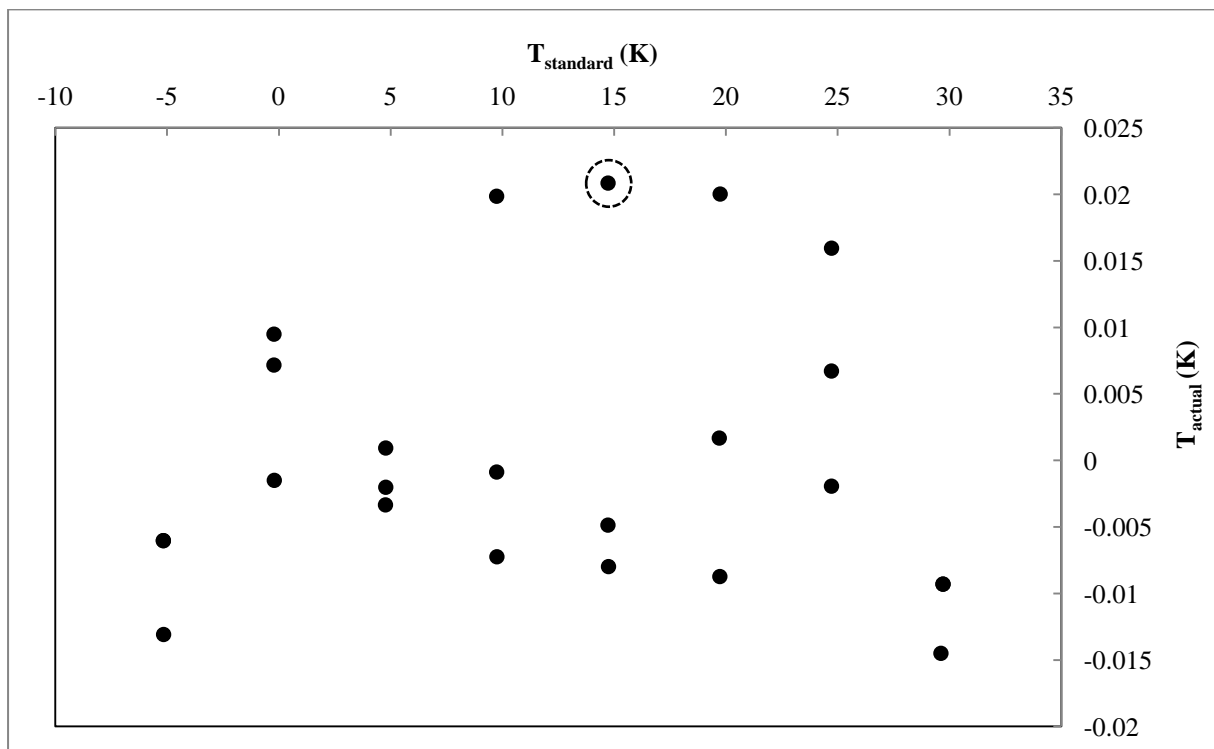

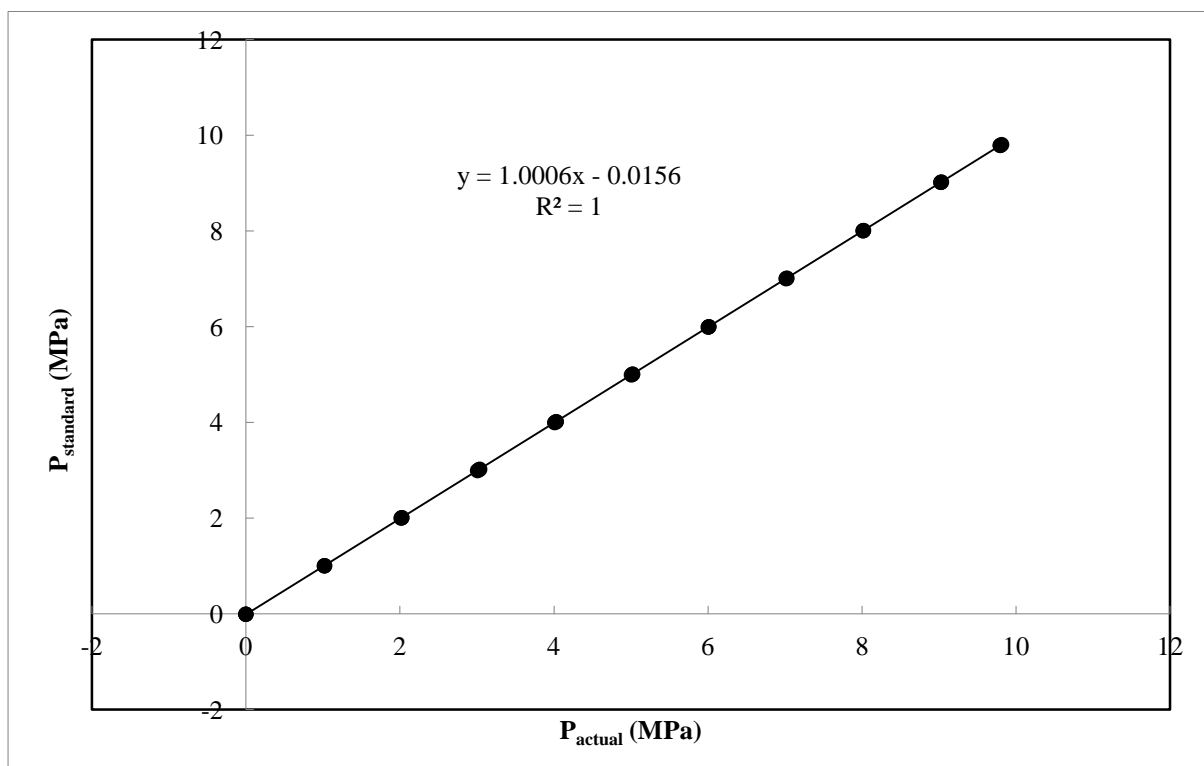


Figure 4-6: Deviations from the standard temperature due to first order relation for the top temperature sensor, where  indicates a maximum deviation of  $\pm 0.020$  K.

## 4.2.3.2 Pressure calibration

The WIKA pressure transducer used in this study was calibrated internally against a standard WIKA CPH6000. For the pressure range of 0 – 25 MPa, the standard transducer had a stated full-scale uncertainty of  $\pm 0.02$  kPa. The pressure transducer was connected to a common pressure manifold together with the standard. Since the standard transducer was calibrated for a temperature of 298.15 K, it was maintained at room temperature ( $\pm 25$  °C). The transducer housing was maintained at a constant temperature of 313.15 K during measurements to eliminate the effect of fluctuating temperature on the calibration. At specified stabilised pressures, pressure readings from the pressure transducer and the standard transducer were recorded. Initially, the equilibrium cell was loaded with nitrogen gas until a pressure of 1 MPa was achieved. Thereafter, increments of 1 MPa per point were used to reach a final pressure of 9.8 MPa. Subsequently, in order to account for the effect of hysteresis, the same procedure was used to decrease the pressure back down to 1 MPa, followed by increasing the pressure back to 9.8 MPa. For each point, data was collected for three minutes and then averaged. The standard transducer pressure was plotted against the transducer pressure readings. The maximum calibrated uncertainty for the pressure transducer was found to be  $\pm 0.980$  kPa. The overall temperature uncertainty was found to be  $\pm 0.566$  kPa.



**Figure 4-7: Calibration of the WIKA pressure transducer used in this apparatus. First order relation between standard and transducer pressure.**

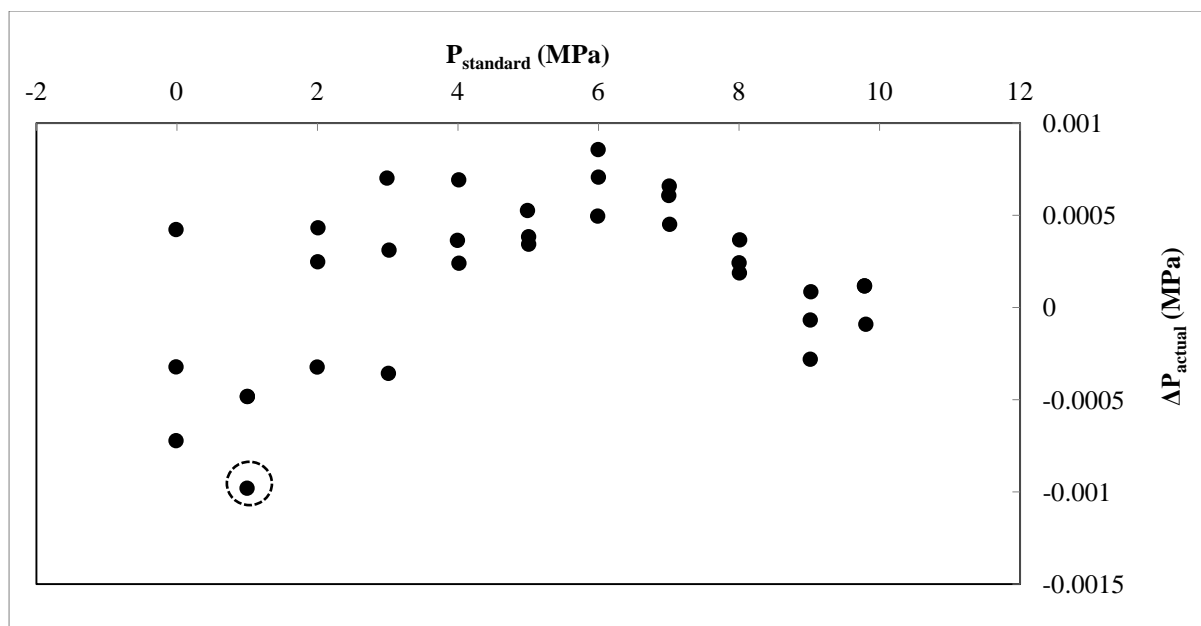



Figure 4-8: Deviations from the standard pressure due to first order relation, where

 indicates a maximum deviation of  $\pm 0.98$  kPa.

#### 4.2.3 Sample preparation

All sucrose samples were prepared in a 50 ml beaker using an OHAUS AV 114 digital mass balance in order to obtain the desired weight percent. The mass balance had a full-scale uncertainty of  $\pm 0.01$  mg. Before measurements took place, the required mass of sucrose and water for each desired composition was determined. Initially, the mass of the empty beaker was recorded. Thereafter, the sucrose mass was measured. The required amount of water required to obtain the final solution mass was then added slowly with a syringe. Once the sucrose had dissolved completely in the water solution, the sample purity was determined by use of an ATAGO Model RX-7000 $\alpha$  refractometer. The refractometer had a full-scale refractive index uncertainty of  $\pm 0.0001$ . The refractive indices of the various samples were measured at 293.15 K and compared with literature values. The resultant composition uncertainty was found to be  $\pm 0.018$ .

#### 4.2.4 Operating procedure for isochoric pressure cell

##### 4.2.4.1 Start-up procedure – Loading of equilibrium cell

Once the cell had been adequately cleaned, the Edwards vacuum pump was used to evacuate the cell to 0.0002 MPa for a period of  $\pm 5$  minutes. The inlet valve was closed to maintain the cell under vacuum, while the pressure transducer monitored the cell pressure. The prepared aqueous solution of interest was drawn into a 20 ml plastic syringe. Any air bubbles present in the syringe were removed by tapping the syringe lightly. The filled syringe was connected to the inlet valve of the cell and the valve was opened slightly to allow the solution to be fed into the equilibrium cell. Thereafter, the syringe was removed and the loading line was evacuated to remove any excess air present. The cell was then pressurized to its initial starting pressure with the gas of the system being investigated. For systems that had been measured previously ( $\text{CO}_2 + \text{water} + \text{sucrose}$ ), the system pressure was initially set to the expected hydrate dissociation value, while the system temperature was set to a value outside the expected hydrate stability region. For systems that had not been measured previously in literature ( $\text{R134a/R410a/R507} + \text{water} + \text{sucrose}$ ) the system temperature was set to 288.15 K while the pressure was set to a value below the vapour-liquid equilibrium curve at 288.15 K. This was therefore in the hydrate instability region.

##### 4.2.4.2 Hydrate measurements

Once the initial temperature and pressure had been set, the magnetic stirrer was switched on and set to 600 rpm. When the gas had been fully adsorbed into the solution and the system pressure stabilized, the programmable temperature controller was set to 10 K below the anticipated hydrate dissociation temperature. If the temperature was above 273.15 K, the water phase and hydrate phase were in equilibrium, whereas if the temperature was below 273.15, the hydrate phase was in equilibrium with ice. The temperature was slowly decreased at a rate of  $1 \text{ K}\cdot\text{h}^{-1}$  to ensure hydrate formation occurs with a good separation between the hydrate crystals and the sucrose molecules. This procedure is known as the cooling curve. Two distinct slopes are observed in the cooling curve. The first slope is characterized by a small decrease in pressure. This represented the occurrence of the nucleation process, whereby the pressure change is primarily a function of the change in temperature. This is represented by the vapour-liquid isochoric curve in Figure 3.3. A large decrease in pressure signified that hydrate growth had occurred, and therefore hydrates had formed (refer to Figure 3.3). If no large decrease in pressure was observed, the temperature was further decreased.

Once the system had stabilized after hydrate formation, the temperature was increased in a stepwise manner. This is known as the heating curve. Initially, large temperature steps were used ( $1 \text{ K.h}^{-1}$ ) but as the system approached the dissociation point, the temperature was increased in steps of 0.1 K. At each temperature increment of 0.1 K, the system was given 1 hour to achieve equilibrium. Two distinct slopes were observed in the heating curve. The point at which the slope changed was the hydrate dissociation point. Before this point, the increase in pressure was largely due to the hydrates dissociating and releasing the guest molecules into the vapour space. This was shown by the hydrate-liquid-vapour curve in Figure 3.3. After the dissociation point, the pressure change was primarily a function of temperature. This is shown by the vapour-liquid isochor in Figure 3-3.

In order to verify the measured results of the new systems, three methods were used. The first method used was to scatter the order in which pressure readings were taken. This was done in order to reduce any effect of hysteresis on the system. The second method used was to repeat a dissociation point in order to show reliability and repeatability in the experimental technique. Finally, the third method used consisted of conducting a linear regression on the hydrate dissociation points. The results obtained were in good agreement as they presented a highly linear relationship when plotted on a  $\ln P$  versus  $1/T$  scale.

#### 4.2.4.3 Shutdown procedure

After the hydrate measurements had been completed, the data logger was switched to manual and shutdown, and the overhead mechanical stirrer was switched off. The cold finger and programmable temperature controller were then switched off. Thereafter, the liquid bath was lowered and the drain valve was opened to empty the cell. Subsequently, the cleaning procedure mentioned in section 4.3.1.1 was followed before undertaking the next set of measurements.

### 4.3 NIST uncertainty analysis for H-L-V equilibrium data and vapour pressure measurements

The result of a measured value is only complete when accompanied by a quantitative statement of its uncertainty (Taylor and Kuyatt, 1994). A measurement's uncertainty is described by an interval around a set of measured data such that if a data point was repeated, the result should lie within the stated interval.

#### 4.3.1 Estimating uncertainty

It is of paramount importance to report all possible sources of uncertainty before presentation of the original measured data. When more than one source of uncertainty is present, the overall uncertainty is represented as the combined standard uncertainty. In this report, uncertainty was conveyed according to NIST guidelines for reporting uncertainty.

$$u_c(x) = \pm \sqrt{\sum_i u_i(x)^2} \quad (4.1)$$

The uncertainty of a measured result consists of several components, which may be grouped into two categories according to the method used to estimate their numerical values:

**Type A:** uncertainties evaluated by statistical methods

**Type B:** uncertainties evaluated by other means

Type A uncertainties for temperature and pressure arise from numerous transducer readings for a stable system, whereas type B uncertainties arise from the polynomial fitted to the calibrations as well as any manufacturers' specifications. Therefore, the combined standard uncertainty for a particular variable,  $x$ , which may be temperature or pressure, is represented by the following equation:

$$u_c(x) = \pm \sqrt{u_{instrument}(x)^2 + u_{calibration}(x)^2 + u_{repeatability}(x)^2} \quad (4.2)$$

The upper and lower uncertainty limit from the temperature calibrations was determined from the first order polynomial. In Figure 4.6, the uncertainty was found to be,  $a = \pm 0.02$  K, while in Figure 4.8, the uncertainty was found to be,  $a = \pm 0.02$  K. Similarly for the pressure calibration in Figure 4.10, the uncertainty was found to be,  $a = \pm 0.001$  MPa. From these limits, a rectangular probability distribution was formed where there was a 100% probability that the calibration uncertainty would fall in the interval. The rectangular distribution was determined by:



$$u_{calibration}(x) = \frac{b}{\sqrt{3}} \quad (4.3)$$

$$u_{instrument}(x) = \frac{b}{\sqrt{3}} \quad (4.4)$$

where

$$b = \left( \frac{a_+ \pm a_-}{2} \right) \quad (4.5)$$

During an experiment, temperature fluctuations occurred as a result of inefficient liquid circulation in the bath as well as heat loss or gain to and from the environment. Additionally, the temperature and pressure fluctuations resulted from the instrument manufacturer error. From this, the repeatability uncertainty was calculated using the following equations:

$$u_{repeatability}(x) = \left( \frac{1}{n(n-1)} \sum_{k=1}^n (x_{i,k} - \bar{x}_i)^2 \right)^{0.5} \quad (4.6)$$

where

$$\bar{x}_i = \frac{1}{n} \sum_{k=1}^n x_{i,k} \quad (4.7)$$

#### 4.3.2 Reporting uncertainty

Uncertainty may be reported as either the combined standard uncertainty or by the inclusion of a coverage factor. The coverage factor plays a role to indicate the confidence level of the measurements by expanding the uncertainty interval, for  $k > 1$ . In this report, a coverage factor was not used, as precise data measurements were required. Therefore, in this case,  $k = 1$ .

$$U(x) = k u_c(x) \quad (4.8)$$

## CHAPTER 5

## RESULTS AND DISCUSSION

In this chapter, the experimental results and discussion thereof are presented. The calibration of the pressure and temperature sensors were evaluated through comparisons of experimental vapour pressure measurements and literature data. The newly developed high-pressure cell was commissioned and tested by performing vapour pressure measurements and hydrate measurements on known test systems via the isochoric pressure search method. The measured data was compared to literature. The phase behaviour of new gas hydrate systems were also investigated and the results of these systems are presented. All systems investigated were modeled using the appropriate thermodynamic models, the results of which are also presented. In addition, the hydrate dissociation conditions of an evaporator feed sample supplied by the South African Sugar Milling Research Institute (SMRI) are presented with a discussion thereof. The unit operations involved in a hydrate separation process are also reported, along with a comparison between hydrate separation technologies and evaporation technologies. Finally, the results of an economic analysis of a typical hydrate separation process are presented.

The motivation for the measurements of these carbohydrate clathrate measurements is due to the limited amount of literature data available for such systems (Chun and Lee, 1998, 1999). In addition, the resulting phase behaviour conditions are fundamental in the process of obtaining a new energy efficient separation process in the South African sugar milling industry. The refrigerant gases used in this study were chosen as they are environmentally friendly and do not run the risk of being phased out in the near future (Doring et al., 1996; DuPont Suva, 2004; OrionAir, 2012). Sucrose concentrations of 12 wt.% and 15 wt.% were investigated as these concentrations represent typical evaporator feed compositions in a typical South African sugar milling plant.

### 5.1 Chemicals used

The sucrose ( $C_{12}H_{22}O_{11}$ ) used in this study was supplied by Sigma Aldrich. It had a stated purity of 99.5 mol%. The University of KwaZulu-Natal Chemistry Department supplied the Millipore water, which had a conductivity of  $1.5\mu S$ .

**Table 5-1: Purity and supplier of the gases used in vapour-liquid equilibrium and hydrate measurements.**

Compound	Formula	CAS number	Purity stated by supplier	Supplier
Carbon dioxide	CO <sub>2</sub>	124-38-9	0.999	AFROX Ltd
1,1,1,2-Tetrafluoroethane, R134a	C <sub>2</sub> H <sub>2</sub> F <sub>4</sub>	811-97-2	0.999	AFROX Ltd
R410a (50 wt.% Difluoromethane, 50 wt.% Pentafluoroethane)	CH <sub>2</sub> F <sub>2</sub> , CF <sub>3</sub> -CHF <sub>2</sub>	75-10-5, 354-33-6	0.998	AFROX Ltd
R507 (50 wt.% 1,1,1- Trifluoroethane, 50 wt.% Pentafluoroethane)	CF <sub>3</sub> -CH <sub>3</sub> , CF <sub>3</sub> -CHF <sub>2</sub>	420-46-2, 354-33-6	0.998	AFROX Ltd

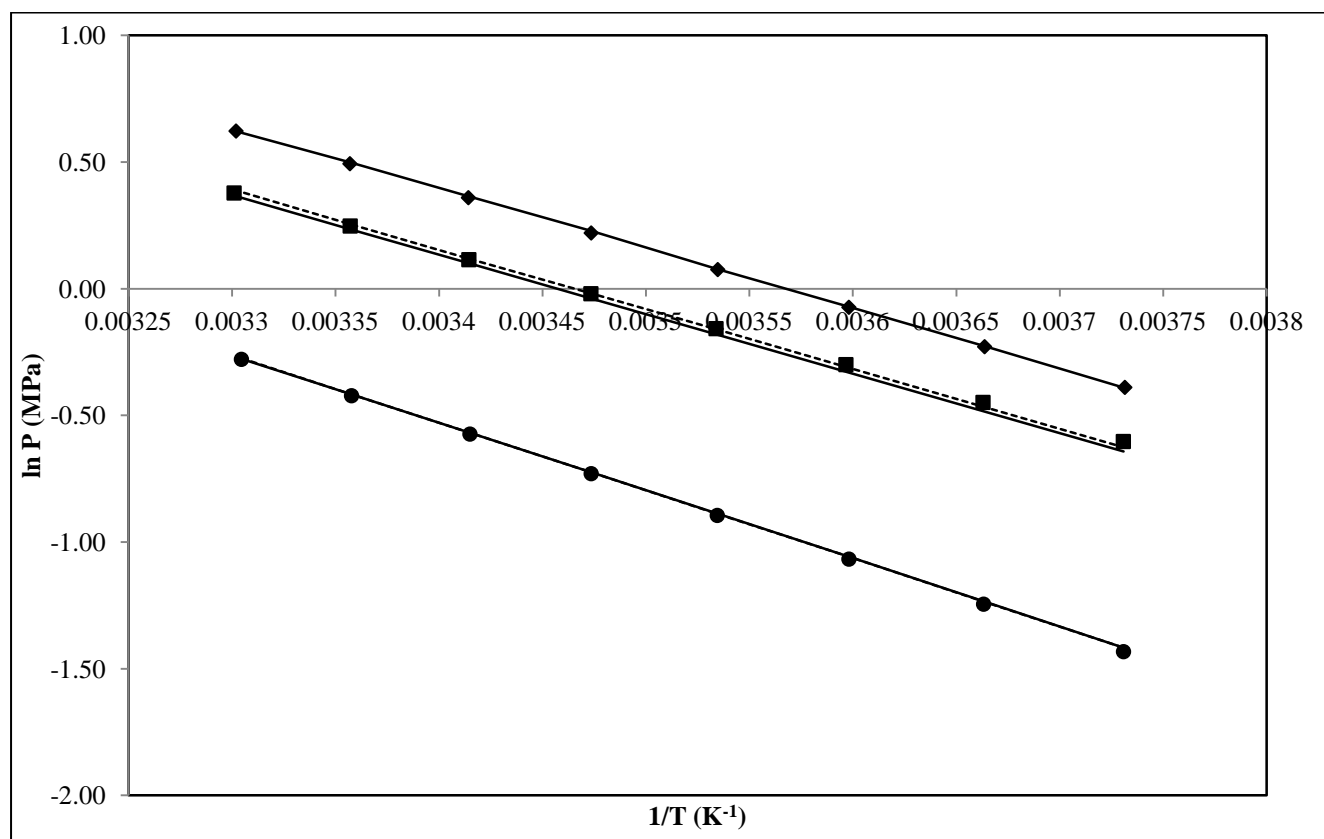
## 5.2 Calibrations

In order to verify the temperature and pressure calibrations performed in this study, isochoric data is obtained for three unary systems. A list of the gases investigated and their respective temperature and pressure ranges are given in Table 5-2. Vapour pressure measurements were conducted within the calibrated range (263.2 K – 303.2 K) of the apparatus. The gases investigated were 1,1,1,2-Tetrafluoroethane (R134a), R410a (50 wt.% Difluoromethane, 50 wt.% Pentafluoroethane) and R507 (50 wt.% 1,1,1-Trifluoroethane, 50 wt.% Pentafluoroethane). The resulting data were compared to that of published literature values.

**Table 5-2: Vapour pressure data measured in this study.**

Component	Temperature range /K	Pressure range/MPa
1,1,1,2-Tetrafluoroethane (R134a)	268.0 - 302.6	0.238 - 0.752
R410a (50wt.% Difluoromethane, 50 wt.% Pentafluoroethane)	268.0 - 302.9	0.667 - 1.854
R507 (50wt.% 1,1,1-Trifluoroethane, 50 wt.% Pentafluoroethane)	368.0 - 302.9	0.528 - 1.440

The experimental vapour pressure data for the components used in this study are presented in Tables 5-2 to 5-4 and are shown graphically in Figure 5-1. All gas hydrate measurements performed in this study were conducted at temperatures below 305 K; therefore all vapour pressure measurements were restricted to this temperature.



**Figure 5-1: Vapour pressure measurements for the components: 1,1,1,2-tetrafluoroethane: •, this study; --, (Giuliani et al., 1995); -, (NIST, 2013). R410a: ♦, this study; - (Calm, 2008). R507: ■, this study; -, (Doring et al., 1996); --, (Ngema et al., 2012).**

**Table 5-3: Vapour pressure data for 1,1,1,2-tetrafluoroethane.**

This study		Reference 1	Reference 2
T/K	P/MPa	$\Delta P$ /kPa	$\Delta P$ /kPa
302.6	0.752	1.70	3.02
297.8	0.655	3.45	3.43
292.8	0.563	2.75	2.56
287.9	0.482	2.48	2.47
282.9	0.409	2.89	2.33
277.9	0.344	3.05	3.06
273.0	0.288	3.21	3.14
268.0	0.239	3.26	3.45

$$\Delta P = |P_{\text{experimental}} - P_{\text{literature}}|$$

Reference 1: NIST (2013)

Reference 2: Giuliani et al. (1995)

The experimental vapour pressure data obtained for 1,1,1,2-tetrafluoroethane were compared to a cubic spline fit of Giuliani et al. (1995) using MATLAB and NIST software (2013). The maximum deviation from Giuliani et al. (1995) was found to be  $\pm 3.75$  kPa, while that of NIST software (2013) was found to be  $\pm 3.66$  kPa. The overall measurement temperature and pressure uncertainties were determined using Equation 4.2. These were found to be  $\pm 0.14$  K and  $\pm 0.566$  kPa respectively. The maximum deviations between this study and that of Giuliani et al. (1995) and NIST software (2013) were 1.4% and 1.3% respectively. The largest deviations were found to be in the temperature range of 268.03 K – 282.92 K. However, the results obtained in this study were found to lie between the data obtained from Giuliani et al. (1995) and NIST software (2013). Therefore, the measured vapour pressures of 1,1,1,2-tetrafluoroethane were found to be satisfactory and verified that the temperature and pressure calibrations were correct.

**Table 5-4: Vapour pressure data for R410a.**

T/K	This study		Reference 1
	P/MPa		$\Delta P$ /kPa
302.9	1.854		2.04
297.9	1.628		9.46
292.9	1.422		7.89
287.9	1.236		10.24
282.9	1.068		1.53
277.9	0.919		1.70
272.9	0.785		2.30
268.0	0.667		2.03

$$\Delta P = |P_{\text{experimental}} - P_{\text{literature}}|$$

Reference 1: Calm (2008)

There is a lack of measured vapour pressure data reported in literature for R410a. The experimental vapour pressure data obtained for R410a were compared to a cubic spline fit of Calm (2008) using MATLAB, where the maximum deviation was found to be  $\pm 10.24$  kPa. This relatively large deviation may be due to the lack of comparable data. The maximum percentage deviation between this study and that of Calm (2008) was 0.8. However, the measured vapour pressures of R410a were found to be satisfactory and verified that the temperature and pressure calibrations were correct.

**Table 5-5: Vapour pressure data for R507.**

T/K	This study		Reference 1	Reference 2
	P/MPa		$\Delta P$ /kPa	$\Delta P$ /kPa
302.9	1.440		16.18	17.23
297.9	1.262		16.22	8.76
292.9	1.102		16.15	4.55
287.9	0.961		17.95	1.77
283.0	0.835		18.89	1.84
278.0	0.722		20.13	6.29
273.0	0.619		21.34	10.77
268.0	0.528		21.15	12.63

$$\Delta P = |P_{\text{experimental}} - P_{\text{literature}}|$$

Reference 1: Doring et al. (1996)

Reference 2: Ngema et al. (2012)

The experimental vapour pressure data obtained for R507 were compared to the research of Doring et al. (1996) and Ngema et al. (2012). Doring et al. (1996) reported a form of the Wagner-equation (please see Table 5.5 below), while the data of Ngema was fitted to a spline fit using Matlab. The maximum deviation from Doring et al. (1996) was found to be  $\pm 21.34$  kPa, while that of Ngema et al. (2012) was found to be  $\pm 17.23$  kPa. Although these deviations appear to be large, the maximum deviation between the studies of Doring et al. (1996) and Ngema et al. (2012) was found to be  $\pm 33.41$  kPa. The results obtained in this study were found to lie between the measured data obtained by Doring et al. (1996) and Ngema et al. (2012). The maximum percentage deviations between this study and that of Doring et al. (1996) and Ngema et al. (2012) were 3.8 and 2.2 respectively. Therefore, the measured vapour pressures of R507 were found to be satisfactory and verified that the temperature and pressure calibrations were correct.

**Table 5-6: Wagner-equation used to determine vapour pressures of R507.**

Equation:	$P(kPa) = \exp \left[ \ln P_c + \frac{A(1 - T_R) + B(1 - T_R)^{1.5} + C(1 - T_R)^{3.5} + D(1 - T_R)^4}{T_R} \right]$	
Parameter	Value	
A	-7.342584	
B	1.046268	
C	1.999693	
D	-9.207652	
$P_c/kPa$	37.17	
$T_c/K$	343.96	

The vapour pressure data for each refrigerant gas was obtained before undertaking the respective gas hydrate measurements for the systems chosen. Therefore, the temperature probes and pressure transducer calibrations were continually monitored to ensure that they remain valid. In order to ensure that validity of the gas purity inside the cell to that in the gas cylinder, the cell was flushed numerous times with the experimental gas of choice. This was followed by the degassing of the cell contents prior to recording the measurements.

### 5.3 Measurement uncertainties

The uncertainties pertaining to temperature and pressure are discussed in *Chapter 4.3, NIST uncertainty analysis for H-L-V equilibrium data and vapour pressure measurements*. These include the instrument error, calibration and repeatability uncertainties. In addition, there exists an uncertainty in the composition of the water used in the gas hydrate measurements. Therefore, in order to reduce this uncertainty, Millipore water was used in order to minimize the amount of ions present in the water. Ions have an inhibiting effect on hydrate formation and can therefore affect the formation of hydrates in systems containing no other inhibitors, such as sucrose.

Table 5-7 below presents the uncertainty of the measurements undertaken in this study. All uncertainties were calculated using Equations 4.1 - 4.7. The combined uncertainty is applicable to all measurements performed in the study.

**Table 5-7: Measurement uncertainty applicable to this study.**

	Temperature/K		Pressure/kPa	Composition/wt. %
	Probe - Bottom	Probe - Top		
<b>Instrument error</b>	± 0.100	± 0.100	± 0.020	± 0.006
<b>Calibration uncertainty</b>	± 0.011	± 0.011	± 0.981	-
<b>Repeatability uncertainty</b>	± 0.011	± 0.013	± 0.010	± 0.017
<b>Combined Standard Uncertainty</b>	± 0.14		± 0.566	± 0.018

Chun and Lee (1998) investigated the formation of hydrates in the system R22 (1) + water (2) + sucrose (3) and reported temperature and pressure uncertainties of ± 0.2 K and 0.014 MPa respectively. Carbone et al. (2012) investigated hydrate formation in the system methane + water + glucose and reported a temperature uncertainty of ±0.1 K and a pressure uncertainty of 0.01 MPa. Therefore, the uncertainties of the measurements in this are acceptable in comparison to literature.

### 5.4 Test systems

The experimental method was confirmed by conducting hydrate measurements on two known systems. These systems included CO<sub>2</sub> (1) + water (2) and CO<sub>2</sub> (1) + water (2) + 20 wt.% sucrose (3). The measured data of the system CO<sub>2</sub> (1) + water (2) was compared to the literature data of Englezos and Hall (1994) and Mohammadi et al. (2005), while that of the system CO<sub>2</sub> (1) + water (2) + 20 wt.% sucrose (3) was compared to the literature data of Chun and Lee (1999). Measurements on these systems were performed between the systems' upper and lower quadruple points in order to ensure



that the hydrate instability region is not reached. The upper quadruple point of a system is determined through vapour pressure measurements, while the lower quadruple point is determined by the freezing point of the solution. The temperature and pressure ranges of the test systems investigated are presented below in Table 5-8.

**Table 5-8: Test systems measured for HLV equilibrium.**

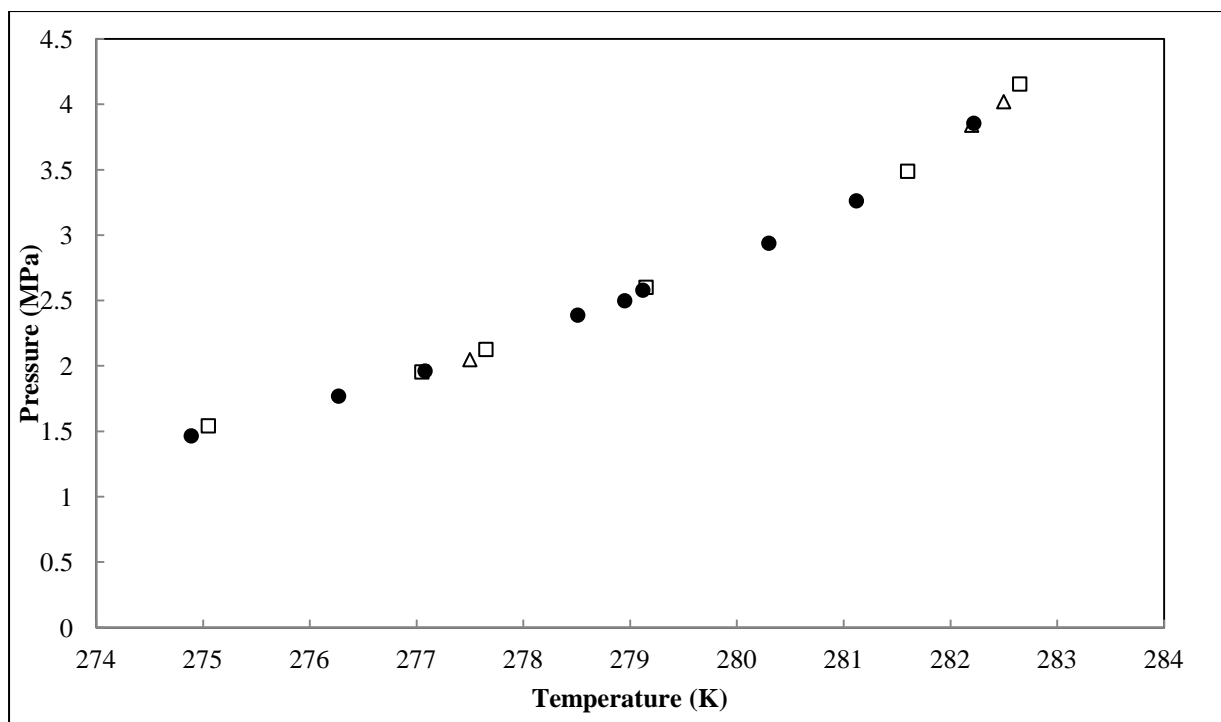
System	Temperature range/K	Pressure range/MPa
CO <sub>2</sub> (1) + water (2)	274.9 - 282.2	1.465 - 3.855
CO <sub>2</sub> (1) + water (2) + 20 wt.% sucrose (3)	275.8 - 281.9	1.925 - 4.617

The difference occurring between experimental values and those found in literature may be reported in terms of either temperature or pressure. However, since the isochoric pressure search method was used in this study, the difference was reported in terms of pressure.

#### 5.4.1 The CO<sub>2</sub>(1) + water (2) system

**Table 5-9: Hydrate dissociation measurements for the system CO<sub>2</sub> (1) + water (2).**

T/K	P/MPa
282.2	3.855
281.1	3.262
280.3	2.938
279.1	2.579
278.9	2.498
278.5	2.388
277.0	1.961
274.9	1.465



**Figure 5-2: Hydrate dissociation conditions for the system  $\text{CO}_2(1) + \text{water}(2)$ . •, this study; □, Englezos and Hall (1994); Δ, Mohammadi et al. (2005).**

A fair amount of scatter was observed when comparing the measured data to that of literature. The hydrate dissociation conditions measured in this study were subject to a combined standard measurement uncertainty of  $\pm 0.14$  K and  $\pm 0.566$  kPa. These uncertainties were acceptable when compared to the reported uncertainties of  $\pm 0.10$  K and  $\pm 0.007$  MPa of Mohammadi et al. (2005). No measurement uncertainties were reported by Englezos and Hall (1994).

The experimental hydrate dissociation conditions obtained for the system  $\text{CO}_2(1) + \text{water}(2)$  were compared to a cubic spline fit of Englezos and Hall (1994) and Mohammadi et al. (2005) using MATLAB. The maximum deviation from literature for the measured system was found to be  $\pm 20.34$  kPa when compared to the research of Englezos and Hall. The maximum pressure deviation between the reported literature data of Englezos and Hall (1994) and Mohammadi et al. (2005) was found to be  $\pm 34.87$  kPa. In addition, the measured data of Mohammadi et al. (2005) was compared to that of Deaton and Frost (1946) and Larson (1955). Due to the fact that the maximum deviation observed between measured data and literature data was smaller than the deviation between literature data, the data measured in this study were found to be in good agreement with that in literature.

The maximum pressure difference was observed in the region of 278.51 K – 280.30 K. This may be largely due to the lack of literature data available in this region. Smaller pressure deviations were observed between this study and that of Mohammadi et al. (2005), who also utilized the isochoric

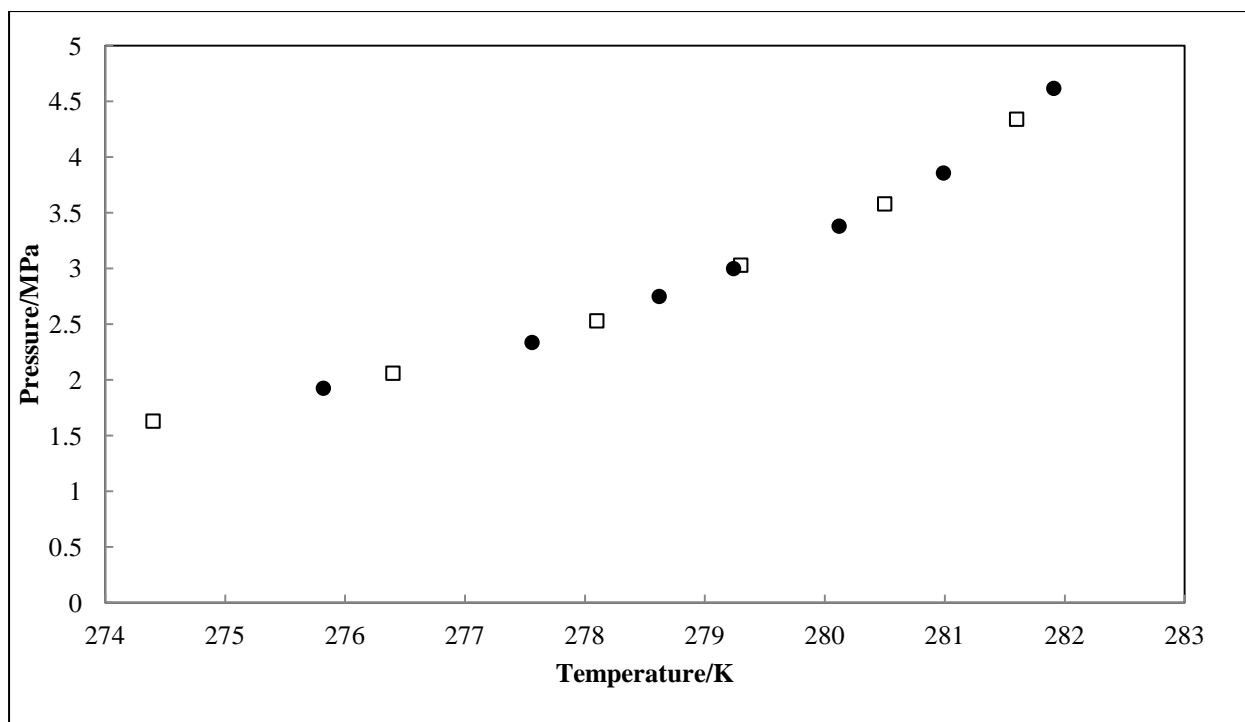
pressure search method, while Englezos and Hall (1994) made use of the isothermal pressure search method. Therefore, it is acceptable for the larger pressure deviations to occur between this study and that of Englezos and Hall (1994).

It was found that the measured hydrate dissociation conditions for the system CO<sub>2</sub> (1) + water (2) compared well in comparison to that found in literature. Therefore, the reliability of the experimental method and apparatus was confirmed.

#### 5.4.2 The CO<sub>2</sub>(1) + water (2) + sucrose (3) system

**Table 5-10: Hydrate dissociation measurements for the system CO<sub>2</sub> (1) + water (2) + 20 wt.% sucrose (3).**

T/K	P/MPa
281.9	4.617
281.0	3.857
280.1	3.380
279.2	2.999
278.6	2.749
277.6	2.336
275.8	1.925



**Figure 5-3: Hydrate dissociation conditions for the system  $\text{CO}_2(1) + \text{water}(2) + 20 \text{ wt.}\% \text{ sucrose}(3)$ . •, This study; □, Chun and Lee (1999).**

The data obtained in this work was found to agree well with that of Chun and Lee (1999). As there is limited published research on hydrate measurements for carbohydrate systems, only one literature source was available for this particular system. Chun and Lee (1999) utilized the isochoric pressure search method in their studies. No combined measurement uncertainties were reported by Chun and Lee (1999).

The experimental hydrate dissociation conditions obtained for the system  $\text{CO}_2(1) + \text{water}(2)$  were compared to a cubic spline fit of Chun and Lee (1999) using MATLAB. The maximum deviation from literature for the measured system was found to be  $\pm 20.13 \text{ kPa}$ .

It was found that the measured data compared well with that of literature, thus once again confirming the experimental method and apparatus.

### 5.5. New systems

As with the test systems, measurements on the new systems were performed between the systems' upper and lower quadruple points in order to ensure that the hydrate instability region is not reached. The temperature and pressure ranges of the new systems investigated are presented below in Table 5-11.

**Table 5-11: New HLV equilibrium data measured for systems of interest.**

System	wt.% sucrose	Temperature range/K	Pressure range/MPa
1,1,1,2-tetrafluoroethane (1) + water (2) + sucrose (3)	12	277.9 - 282.5	0.157 - 0.455
1,1,1,2-tetrafluoroethane (1) + water (2) + sucrose (3)	15	277.2 - 282.1	0.136 - 0.454
R410a (1) + water (2) + sucrose (3)	12	278.0 - 289.1	0.190 - 0.937
R410a (1) + water (2) + sucrose (3)	15	278.6 - 287.9	0.233 - 0.962
R507 (1) + water (2) + sucrose (3)	12	276.5 - 280.9	0.172 - 0.497
R507 (1) + water (2) + sucrose (3)	15	276.6 - 280.7	0.188 - 0.515

The existence of a solute in a solvent that depresses the freezing point of the solvent, such as sucrose, also depresses the formation of hydrates in the solution. Therefore, it is important to note that the greater the concentration of sucrose in the system, the greater the inhibition effect on hydrate formation. This is seen through the observation that as the sucrose concentration is increased, there exists a shift in temperature for a particular system for all pressures. It was also observed that as the pressure of the system increases, so does the temperature shift of the system.

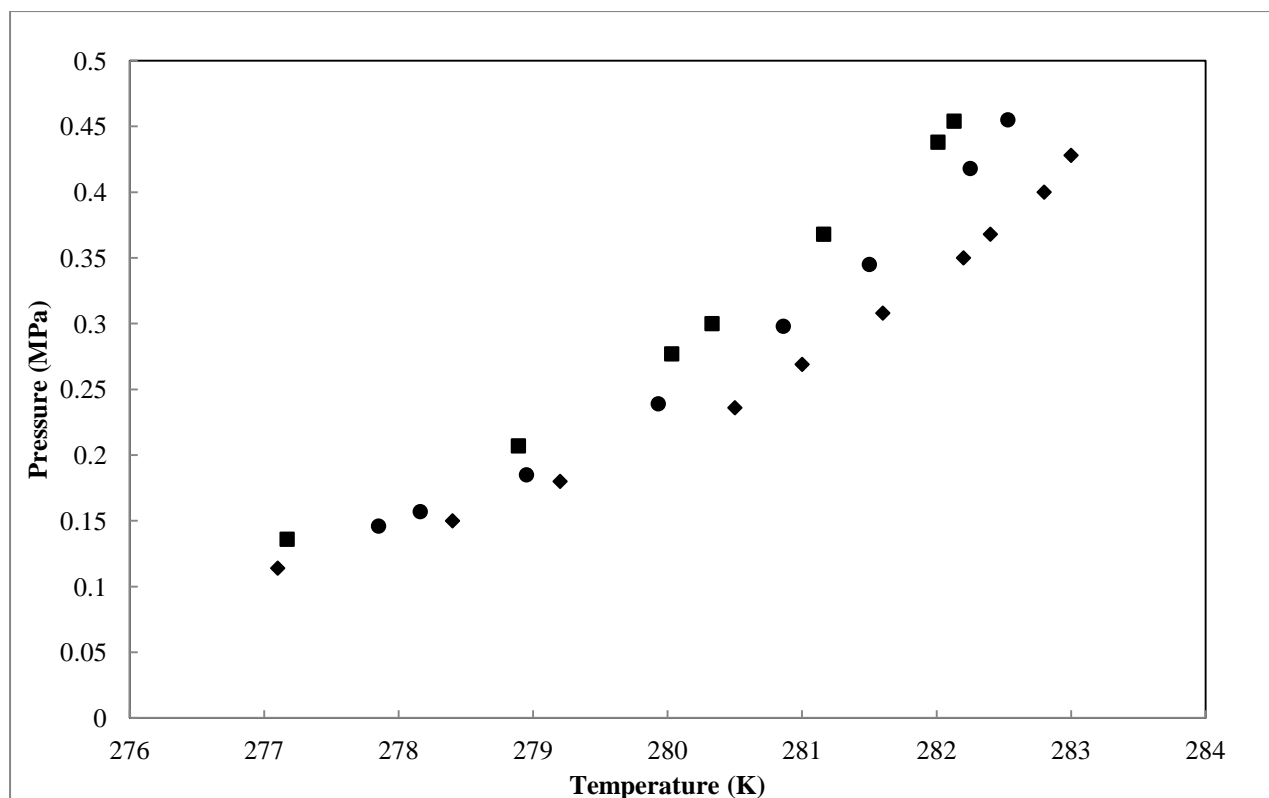
In order to verify the experimental method for use with refrigerant gases, three points for the system R410a (1) + water (2) were measured. Since CO<sub>2</sub> tends to form hydrates at high pressures (> 1 MPa), and refrigerant gases tend to form hydrate at relatively low pressures (< 1 MPa), hydrate measurements at low pressures were required in order to show confidence in the new system measurements. The results of these measurements are presented in Table 5-13 and Figure 5-6.

## 5.5.1 The 1,1,1,2-tetrafluoroethane (1) + water (2) + sucrose (3) system

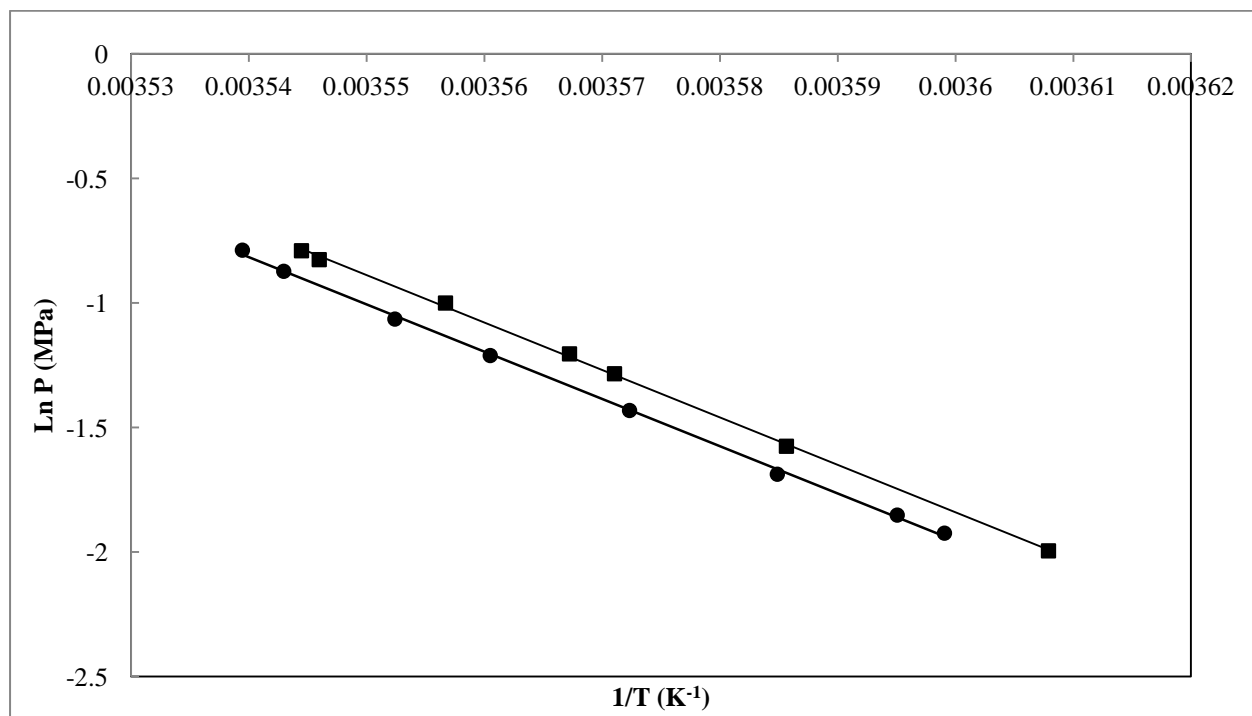
The measured data are given in Table 5-12 and plotted in Figures 5-4 and 5-5 (Ln P versus 1/T).

**Table 5-12: Hydrate dissociation measurements for the system 1,1,1,2-tetrafluoroethane (1) + water (2) + sucrose (3).**

wt.% sucrose	Temperature/K	Pressure/MPa
<b>12</b>	282.5	0.455
	282.3	0.418
	281.5	0.345
	280.9	0.298
	279.9	0.239
	279.0	0.185
	278.2	0.157
	277.9	0.146
<b>15</b>	282.1	0.454
	282.0	0.438
	281.2	0.368
	280.3	0.300
	280.0	0.277
	278.9	0.207
	277.2	0.136



**Figure 5-4:** Hydrate dissociation conditions for the system 1,1,1,2-tetrafluoroethane (1) + water (2) + sucrose (3). ♦, 0 wt.% sucrose (Ngema et al., 2012); •, 12 wt.% sucrose; ■, 15 wt.% sucrose.



**Figure 5-5:** Ln P versus 1/T plot for the system 1,1,1,2-tetrafluoroethane (1) + water (2) + sucrose (3). •, 12 wt.% sucrose; ■, 15 wt.% sucrose.

The average temperature shift between the 1,1,1,2-tetrafluoroethane system containing no sucrose (Ngema et al., 2012) and the systems containing 12 wt.% and 15 wt.% sucrose were 0.83 K and 1.01 K respectively. These shifts were found in the temperature and pressure ranges of 277.17 K – 282.53 K and 0.14 MPa – 0.46 MPa.

### 5.5.2 The R410a (1) + water (2) + sucrose (3) system

The measured data are given in Table 5-13 and plotted in Figures 5-6 and 5-7 (Ln P versus 1/T).

**Table 5-13: Hydrate dissociation measurements for the system R410a (1) + water (2) + sucrose (3).**

wt.% sucrose	Temperature/K	Pressure/MPa
<b>0</b>	281.9	0.247
	279.6	0.174
	286.3	0.493
<b>12</b>	289.1	0.937
	288.0	0.814
	287.1	0.714
	286.1	0.626
	284.9	0.533
	284.9	0.53
	283.0	0.4
	281.0	0.315
	279.2	0.242
278.0	0.19	
<b>15</b>	287.9	0.962
	287.5	0.896
	286.1	0.744
	285.4	0.682
	283.9	0.568
	282.9	0.486
	281.8	0.405
	280.5	0.333
278.6	0.233	



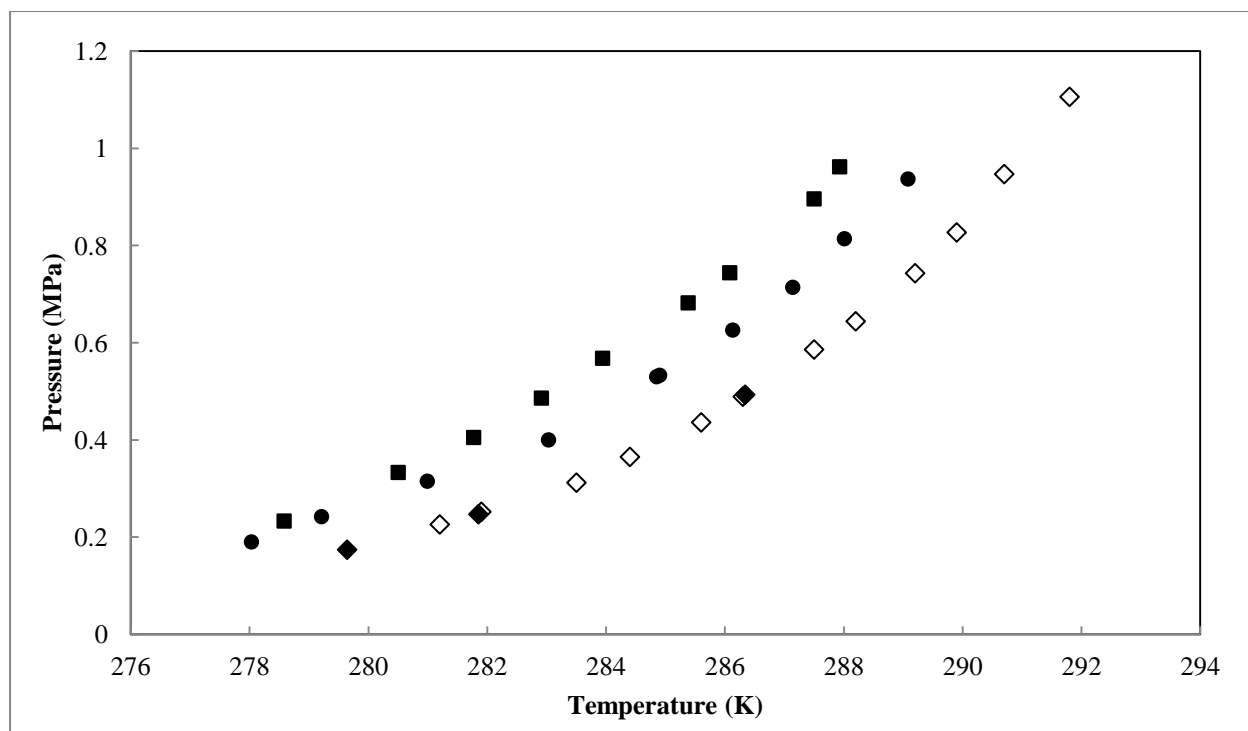


Figure 5-6: Hydrate dissociation conditions for the system R410a (1) + water (2) + sucrose (3). ♦, 0 wt.% sucrose; ◊, (Ngema et al., 2012); •, 12 wt.% sucrose; ■, 15 wt.% sucrose.

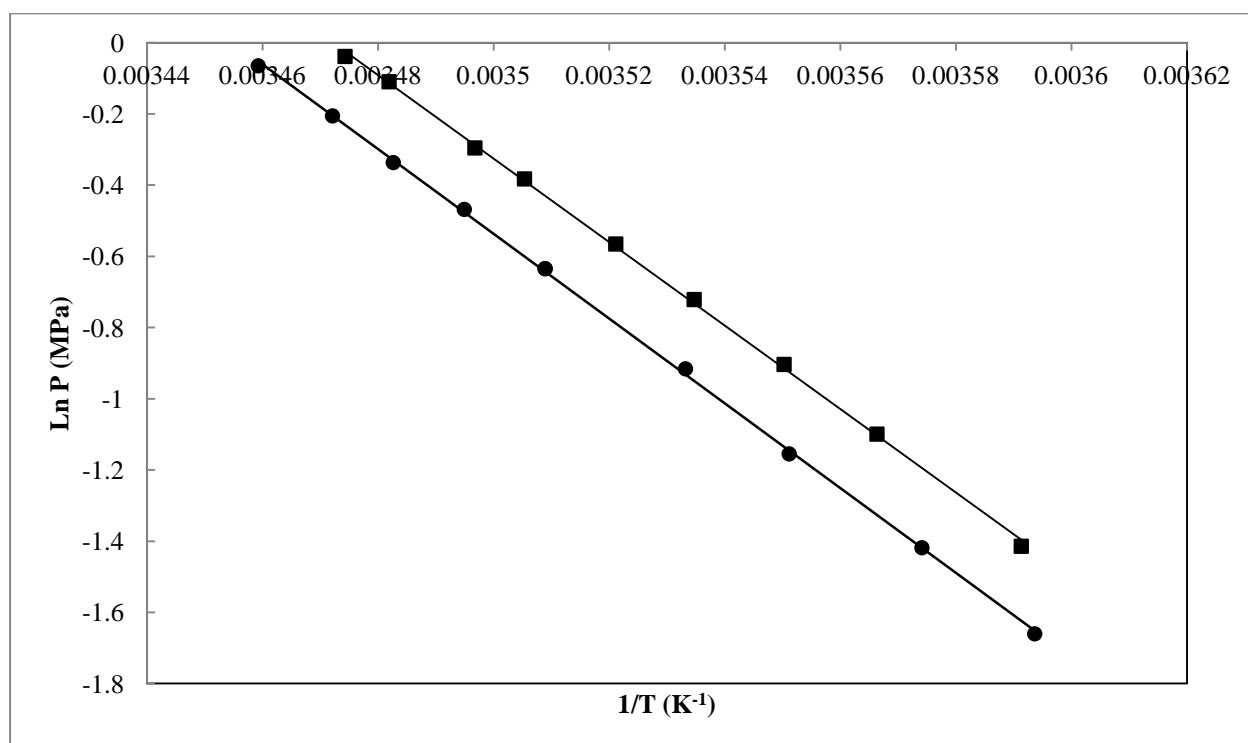


Figure 5-7: Ln P versus 1/T plot for the system R410a (1) + water (2) + sucrose (3). •, 12 wt.% sucrose; ■, 15 wt.% sucrose.

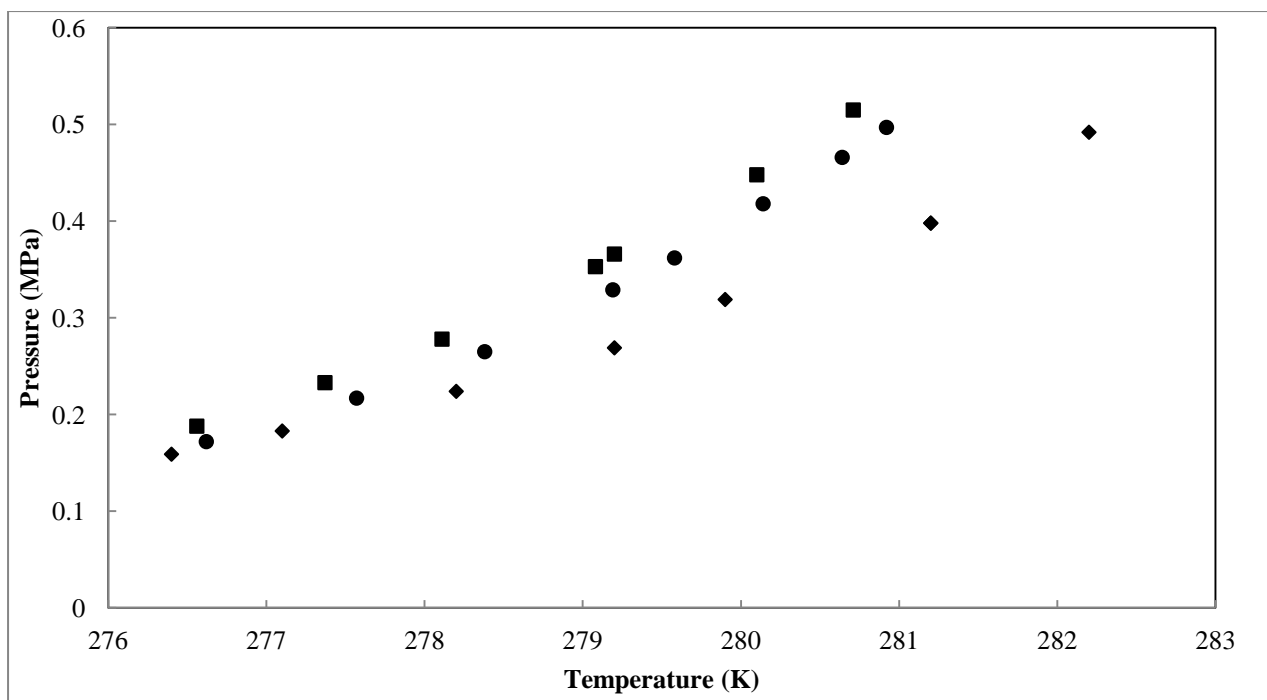
The average temperature shift between the R410a system containing no sucrose (Ngema et al., 2012) and the systems containing 12 wt.% and 15 wt.% sucrose were 0.78 K and 0.99 K respectively. These shifts were observed in the temperature and pressure ranges of 278.03 K – 281.77 K and 0.19 MPa – 0.41 MPa.

### 5.5.3 The R507 (1) + water (2) + sucrose (3) system

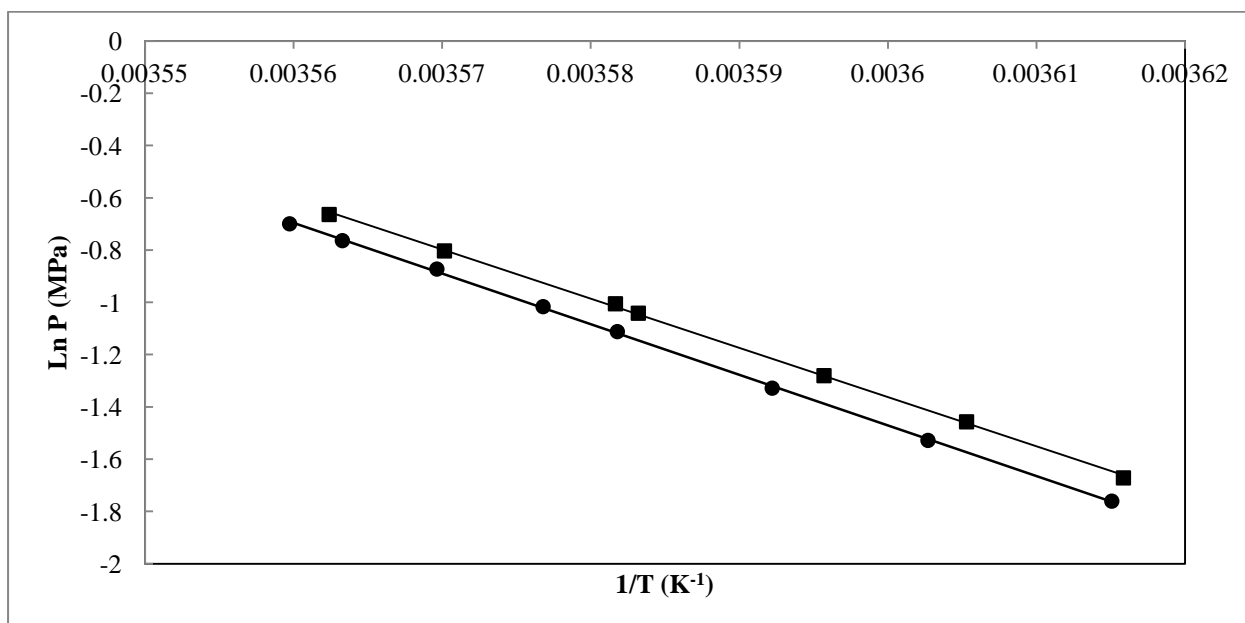
The measured data are given in Table 5-14 and plotted in Figures 5-8 and 5-9 (Ln P versus 1/T).

**Table 5-14: Hydrate dissociation measurements for the system R507 (1) + water (2) + sucrose (3).**

wt.% sucrose	Temperature/K	Pressure/MPa
<b>12</b>	280.9	0.497
	280.6	0.466
	280.1	0.418
	279.6	0.362
	279.2	0.329
	278.4	0.265
	277.6	0.217
	276.5	0.172
<b>15</b>	280.7	0.515
	280.1	0.448
	279.2	0.366
	279.1	0.353
	278.2	0.278
	277.5	0.233
	276.6	0.188



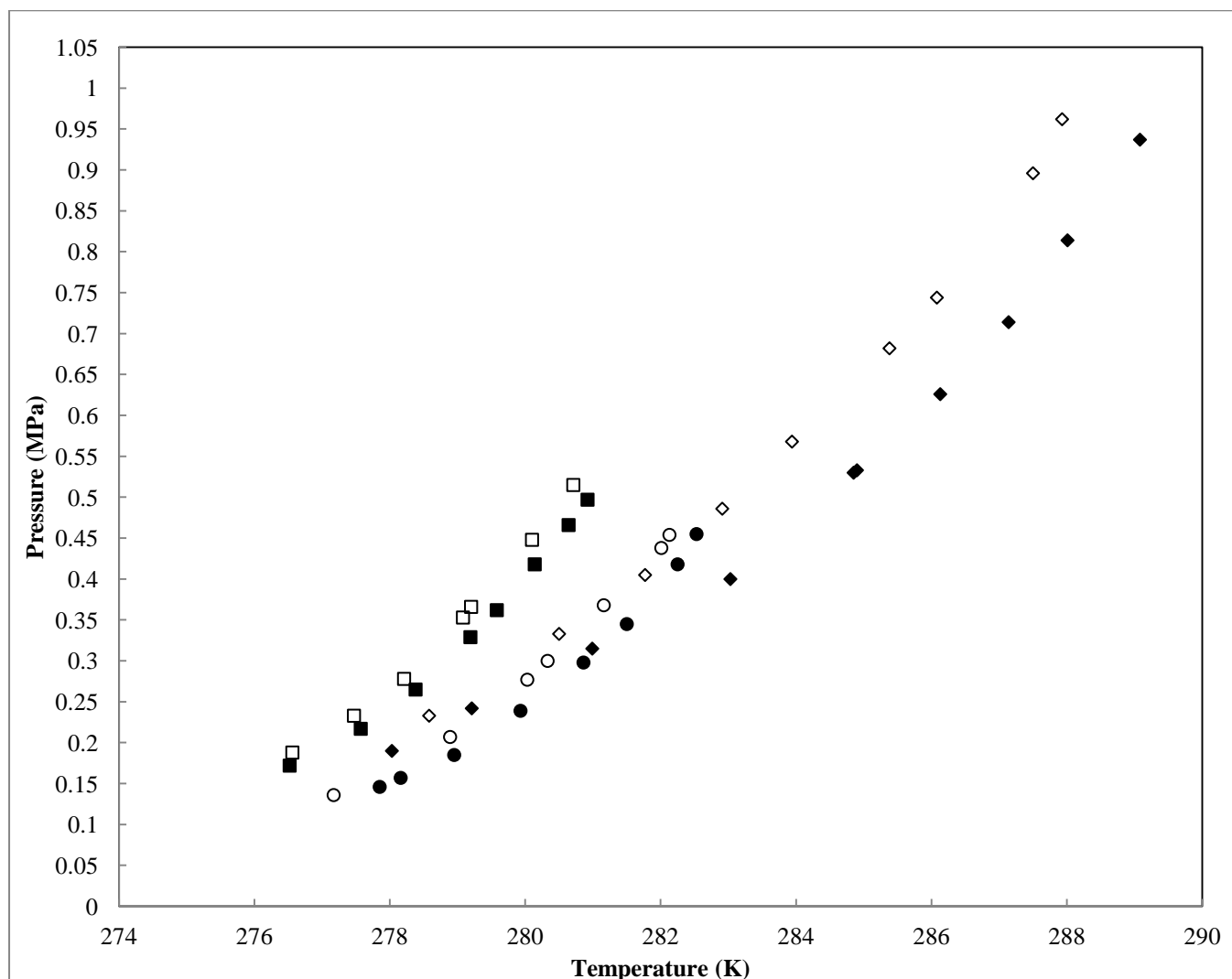
**Figure 5-8: Hydrate dissociation conditions for the system R507 (1) + water (2) + sucrose (3). ♦, 0 wt.% sucrose (Ngema et al., 2012); •, 12 wt.% sucrose; ■, 15 wt.% sucrose.**



**Figure 5-9: Ln P versus 1/T plot for the system R507 (1) + water (2) + sucrose (3). •, 12 wt.% sucrose; ■, 15 wt.% sucrose.**

The average temperature shift between the R507 system containing no sucrose (Ngema et al., 2012) and the systems containing 12 wt.% and 15 wt.% sucrose were 0.82 K and 1.07 K respectively. These shifts were observed in the temperature and pressure ranges of 276.52 K – 280.92 K and 0.17 MPa – 0.52 MPa.

## 5.5.4. Comparison of the data measured for the systems consisting of refrigerant formers



**Figure 5-10: Hydrate dissociation conditions for the systems 1,1,1,2-tetrafluoroethane (1) + water (2) + sucrose (3), R410a (1) + water (2) + sucrose (3) and R507 (1) + water (2) + sucrose (3). 1,1,1,2-tetrafluoroethane: ●, 12 wt. %; ○, 15 wt.%. R410a: ◆, 12 wt.%; ◇, 15 wt.%. R507: ■, 12 wt.%; □, 15 wt.%.**

When all three refrigerant formers are compared, the best performing refrigerant is found to be R410a. This is due to the observation that at higher temperatures, i.e. temperatures closer to ambient, the inhibiting effect of sucrose on hydrate formation is less than that when compared to 1,1,1,2-tetrafluoroethane and R507. In addition, the temperature shift for R410a is the least in the examined range when compared to 1,1,1,2-tetrafluoroethane and R507. The second best performing refrigerant former is R134a. This is seen by the fact that at lower temperatures, the inhibiting effect of sucrose is the least when compared to R410a and R507. Also, the temperature shift for 1,1,1,2-tetrafluoroethane

is the second in the examined range when compared to R410a and R507. In this study, R507 is the least efficient refrigerant former for carbohydrate systems.

The feasible operating region for the proposed system lies in the temperature range of 280 K – 282 K and the corresponding pressure range of 0.3 MPa – 0.5 MPa. In this region, the increased sucrose concentration begins to play less of an inhibiting role on hydrate formation. In addition, this region represents the crossover point for the two best performing refrigerants, R134a and R410a.

## 5.6 Data modeling

In this study, two modeling methodologies were used. For the systems containing carbon dioxide, the Peng-Robinson EOS in combination with the van der Waals mixing rules was used to measure the vapour phase. This methodology followed the modeling approach of Parrish and Prausnitz (1972). For the systems containing refrigerant gases, the vapour phase was assumed to be an ideal gas ignoring its water content. In order to model the liquid phase, the UNIFAC group-contribution model was chosen. The methodology followed the modeling approach of Eslamimanesh et al. (2011).

For the system where no sucrose was present ( $\text{CO}_2$  (1) + water (2)), the direct ( $\phi$ - $\phi$ ) method was employed whereby Equation 2.13 was used to describe the fugacity coefficient of water in the liquid phase. For the remaining systems where sucrose was present, the combined ( $\gamma$ - $\phi$ ) method was employed whereby Equation 2.28 was used to describe the fugacity coefficient of water in the liquid phase.

### 5.6.1 Modeling approach of Parrish and Prausnitz (1972)

The predictive modeling approach of Parrish and Prausnitz (1972) was used to model the test systems  $\text{CO}_2$  (1) + water (2) and  $\text{CO}_2$  (1) + water (2) + 20 wt.% sucrose (3). The solubility of carbon dioxide was taken into account using the PR EOS with the classical mixing rules of van der Waals. Carbon dioxide is known to form both small and large structure I type hydrates. The flow diagram presenting the approach used to predict the pressure was given in Figures 5-11 and 5-12 for the systems  $\text{CO}_2$  (1) + water (2) and  $\text{CO}_2$  (1) + water (2) + 20 wt.% sucrose (3) respectively.

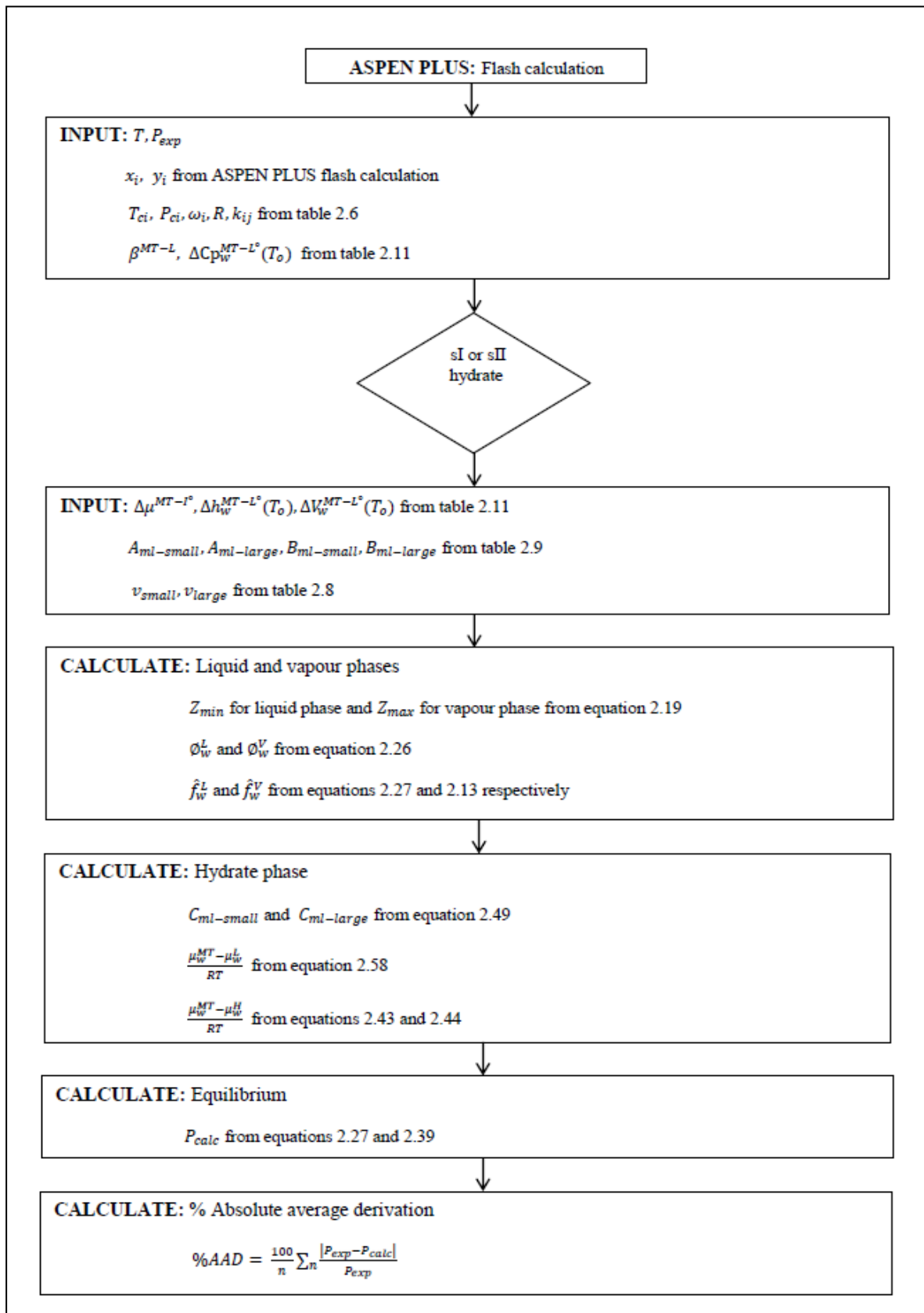
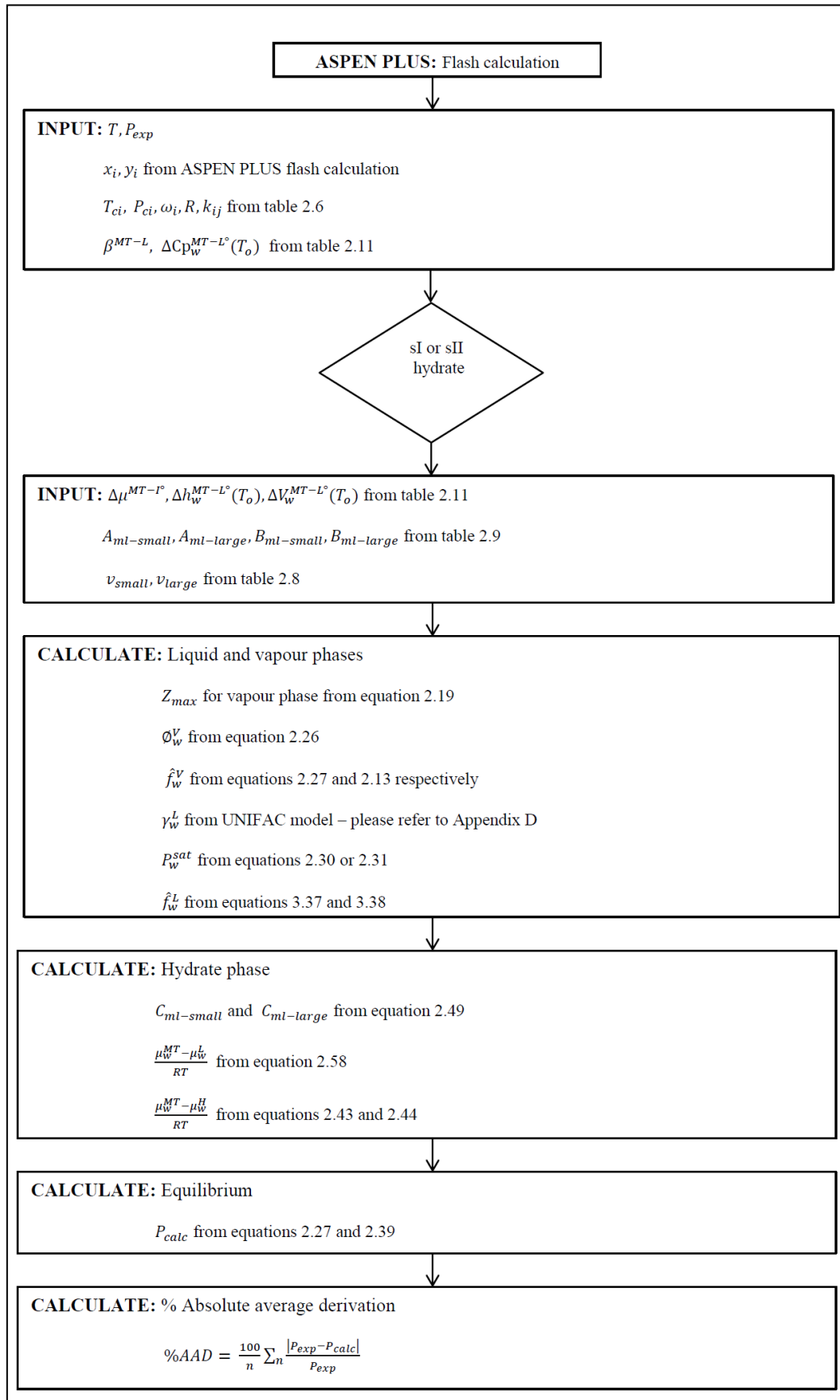


Figure 5-11: Computation flow chart for the predictive model for CO<sub>2</sub> (1) + water (2).



**Figure 5-12: Computation flow chart for the predictive model for CO<sub>2</sub> (1) + water (2) + 20 wt.% sucrose (3).**

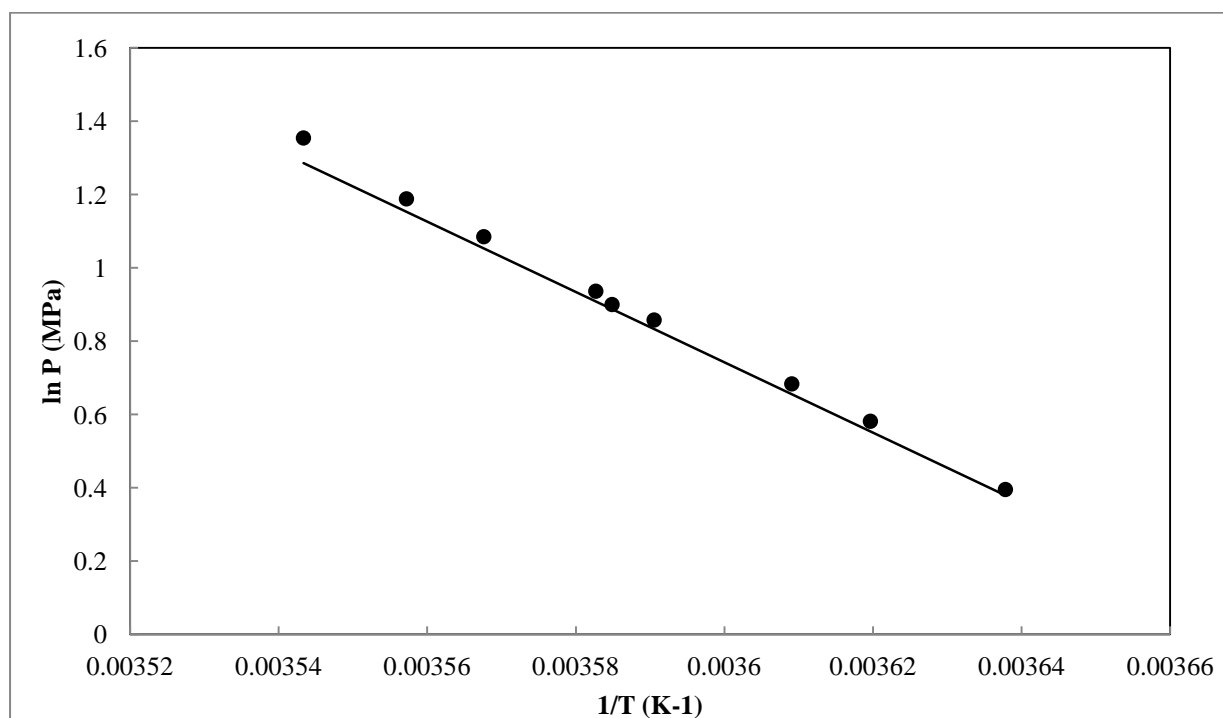


Figure 5-13: H-V-L equilibrium data for the system CO<sub>2</sub> (1) + water (2). •, this study; - , Parrish and Prausnitz (1972) predictive model.

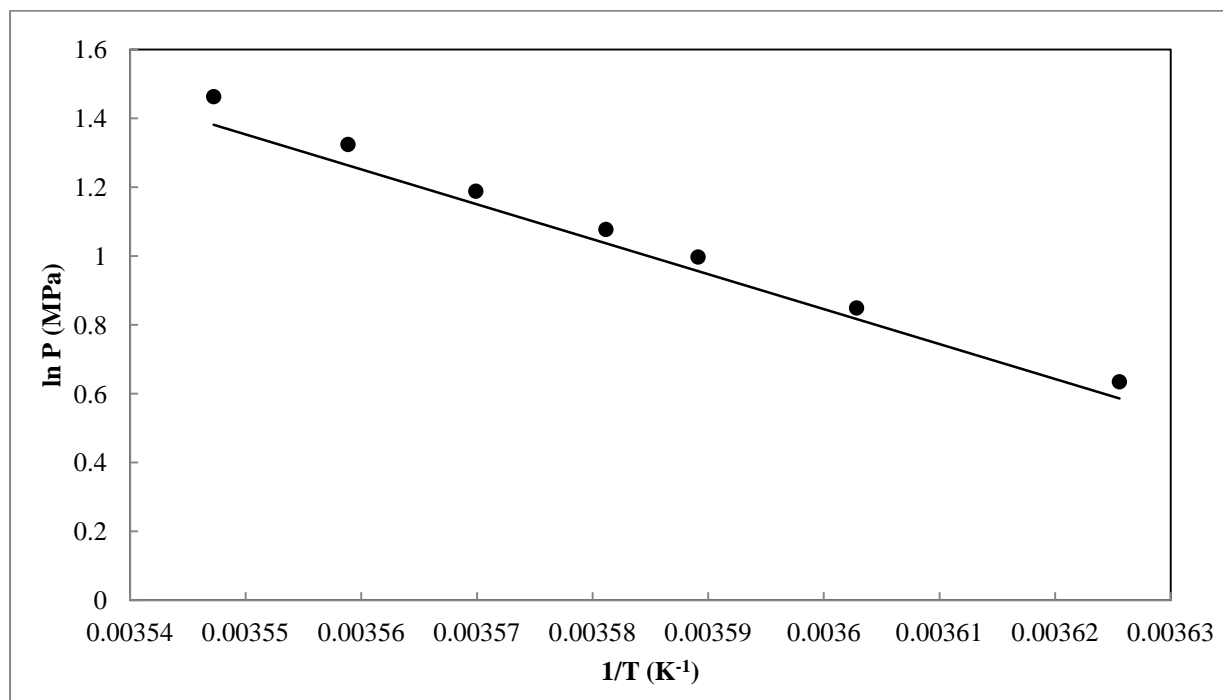


Figure 5-14: H-V-L equilibrium data for the system CO<sub>2</sub> (1) + water (2) + 20 wt.% sucrose (3). •, this study; - , Parrish and Prausnitz (1972) predictive model.



The experimental data as well as the results of the predictive model for the systems CO<sub>2</sub> (1) + water (2) and CO<sub>2</sub> (1) + water (2) + 20 wt.% sucrose (3) are shown in Figures 5-13 and 5-14 respectively. The predictive model used described the solubility of the system at lower temperatures and pressure well, however, as the temperatures and pressures began to increase, the model deviated from the measured results. This was not surprising as at high temperatures and pressures, the significance of phase non-ideality becomes increasingly apparent and the PR EOS with van der Waals mixing rules was not adequate in defining the liquid phase density. It can also be observed that the presence of sucrose results in deviation from the experimental results. This is expected as the UNIFAC model does not take into account the effects of intramolecular hydration bonding and steric hindrance on saccharide molecule component interactions (Chun and Lee, 1998).

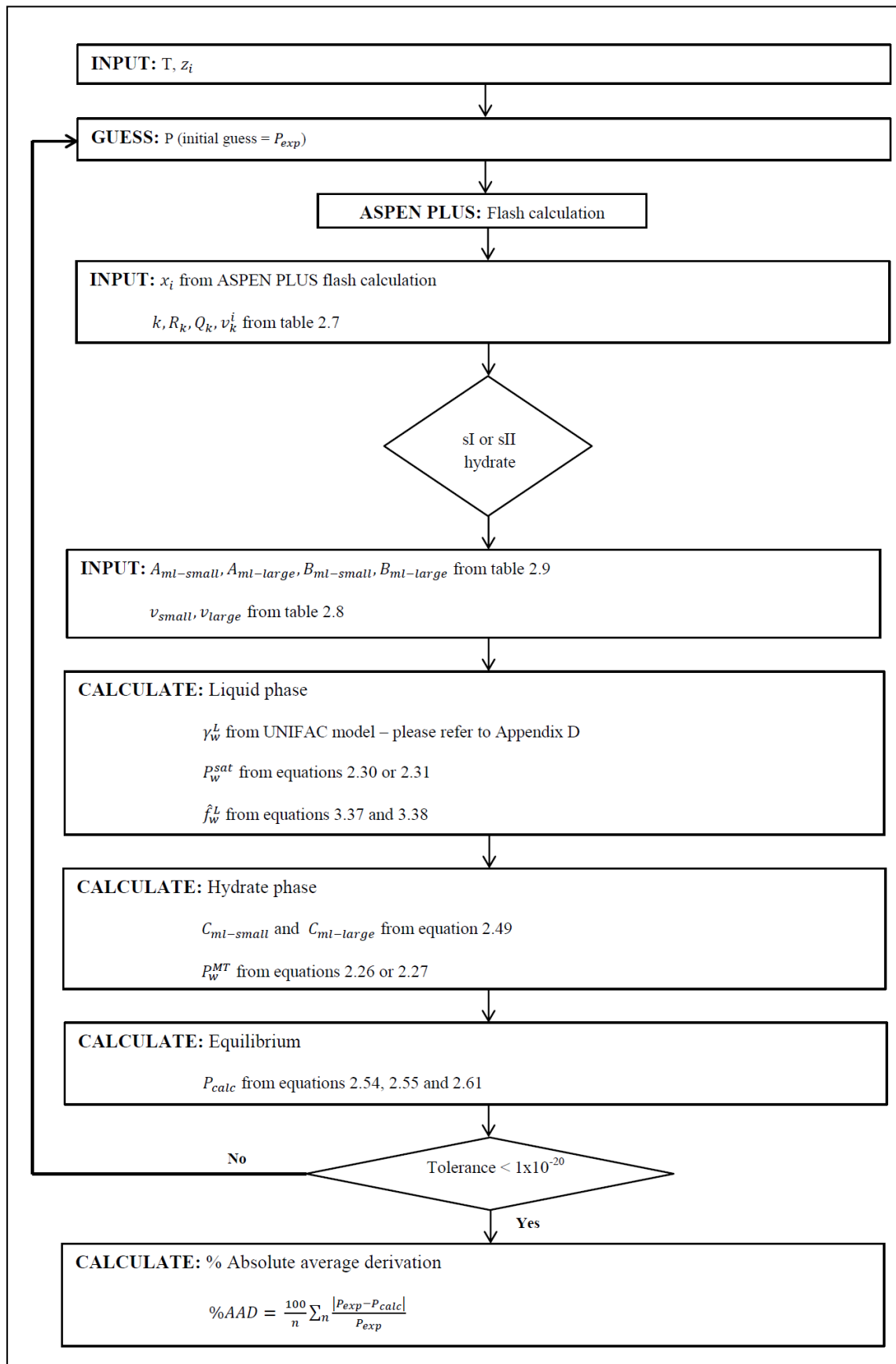
For the system CO<sub>2</sub> (1) + water (2) the resulting percent absolute average deviation (%AAD) was found to be 3.00 while that of the system CO<sub>2</sub> (1) + water (2) + 20 wt.% sucrose (3) was found to be 4.72.

#### *5.6.2 Modeling approach of Eslamimanesh et al. (2011)*

The predictive modeling approach of Eslamimanesh (2011) was used to model the systems 1,1,1,2-tetrafluoroethane (1) + water (2) + sucrose (3), R410a (1) + water (2) + sucrose (3) and R507 (1) + water (2) + sucrose (3). In this approach, the vapour phase is assumed ideal. All three refrigerants are known to form large structure II type hydrates. The flow diagram presenting the approach used to predict the pressure was given in Figure 5-15.

In this modeling approach, the Poynting factor is assumed to equal one for systems where the pressure was below 2 MPa. However, if this value was varied, the %AAD was found to change significantly. Due to the fact that the vapour phase was assumed ideal, the fugacity of the refrigerant was taken equal to the dissociation pressure. Any variations in this assumption had no effect on the %AAD.

Due to the solubility of the refrigerant gases in the water-sucrose systems, the initial sucrose concentration in the aqueous phase was slightly altered from the sucrose concentration at the hydrate dissociation point. However, although refrigerant solubility cannot be ignored, the change in sucrose concentration in the aqueous phase due to this occurrence was found to be negligible.



**Figure 5-15: Computation flow chart for the predictive model for the hydrate formers R134a, R410a and R507 (1) + water (2) + various concentrations of sucrose (3).**

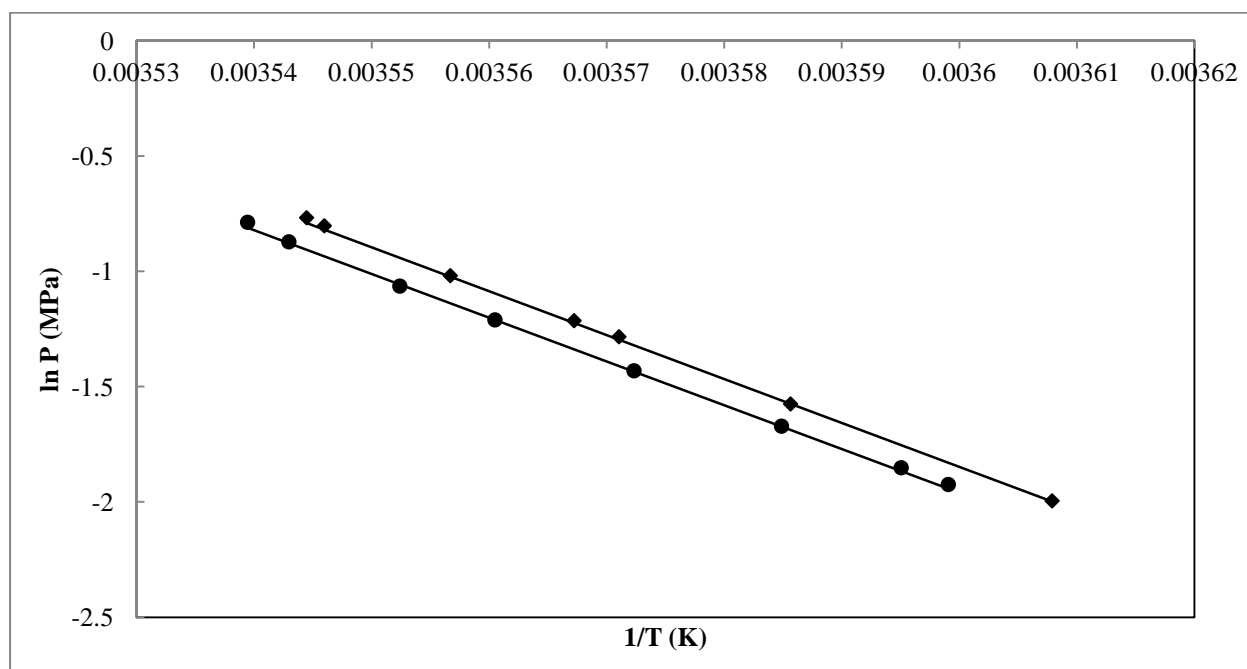


Figure 5-16: H-V-L equilibrium data for the system 1,1,1,2-tetrafluoroethane (1) + water (2) + sucrose (3). •, 12 wt.%; ♦, 15 wt.%; - , Eslamimanesh et al. (2011) predictive model.

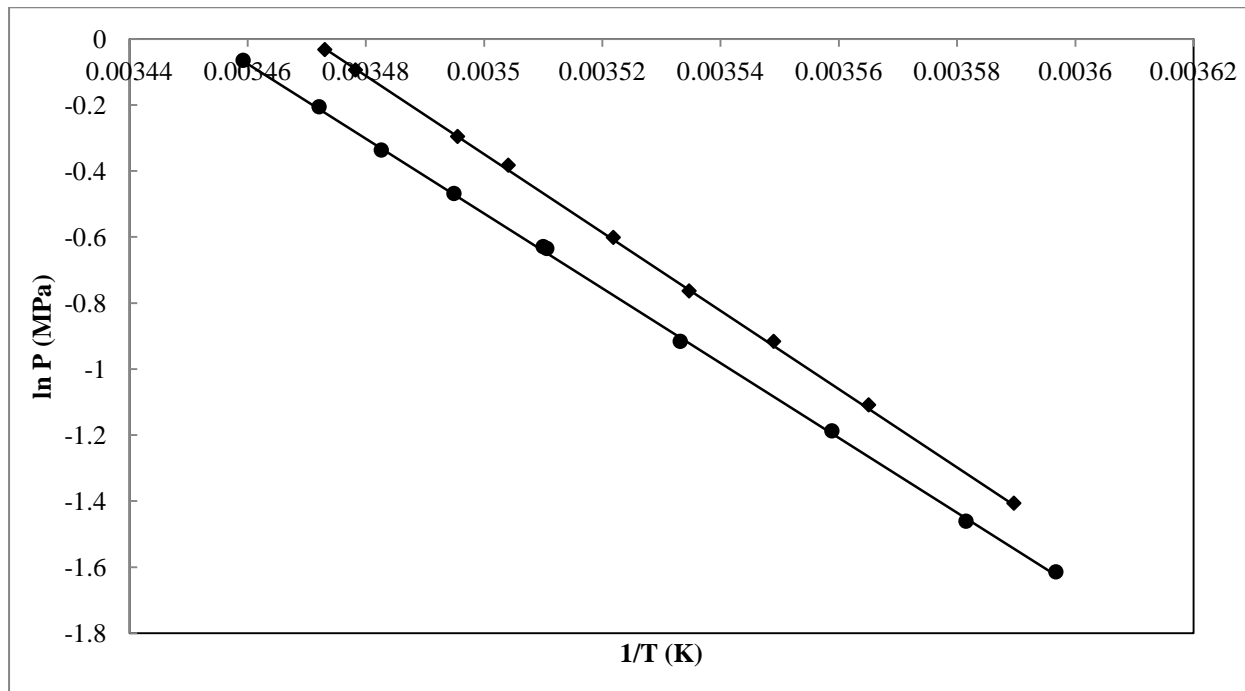
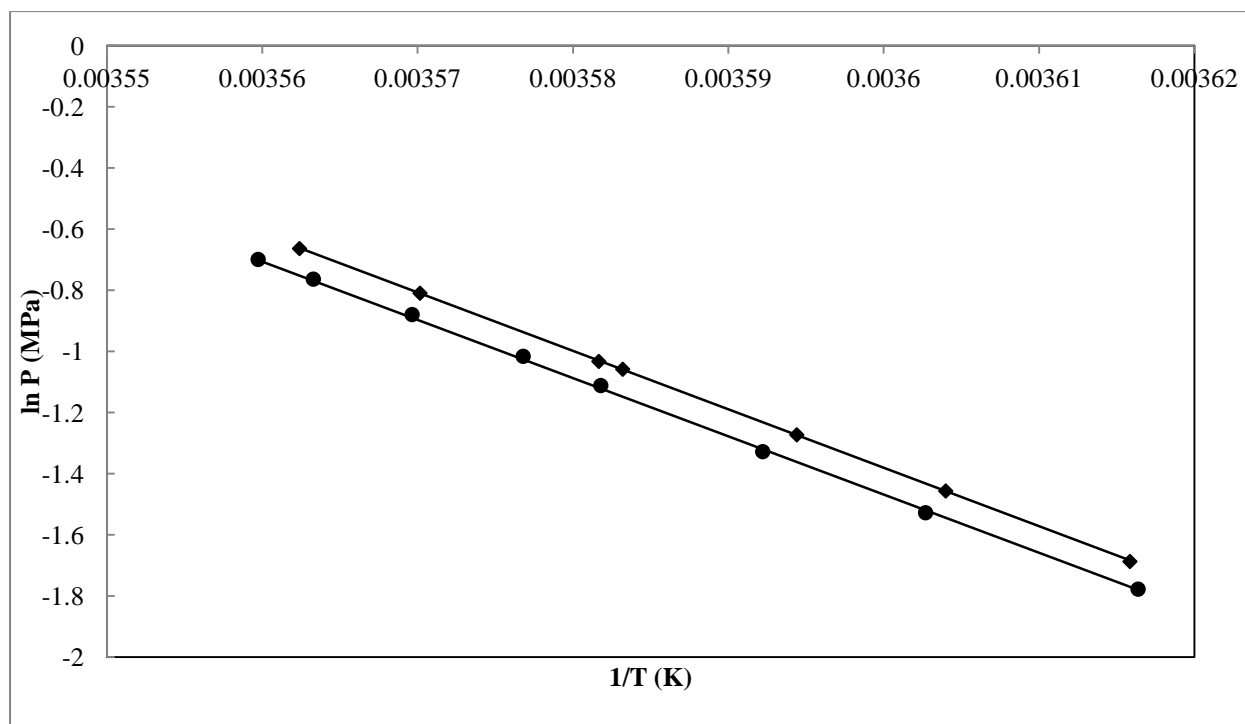


Figure 5.17: H-V-L equilibrium data for the system R410a (1) + water (2) + sucrose (3). •, 12 wt.%; ♦, 15 wt.%; - , Eslamimanesh et al. (2011) predictive model.



**Figure 5.18: H-V-L equilibrium data for the system R507 (1) + water (2) + sucrose (3). •, 12 wt.%; ♦, 15 wt.%; - , Eslamimanesh et al. (2011) predictive model.**

The experimental data as well as the results of the predictive model for the systems 1,1,1,2-tetrafluoroethane (1) + water (2) + sucrose (3), R410a (1) + water (2) + sucrose (3) and R507 (1) + water (2) + sucrose (3) are shown in Figures 5-16 to 5-18. Overall, the predictive model of Eslamimanesh et al. (2012) used in this study predicted the experimental hydrate dissociation data accurately. In literature, the %AAD of the system R22 (1) + water (2) + sucrose (3) investigated by Chun and Lee (1998) resulted in values of 3.03 and 2.82 for the sucrose concentrations of 20 and 40 wt.% respectively. In this study, the resulting %AAD for all new systems are presented below in Table 5-15. The predictive model used in this study appeared to better predict the hydrate dissociation pressures than that used by Chun and Lee (1998). This may be due to their usage of the Redlich-Kwong-Saove EOS with the modified Huron-Vidal mixing rules in comparison to the model approach of Eslamimanesh et al. (2012). In addition, the correction method used to account for the inhibition effect of sucrose on hydrate formation may not accurately predict the system at higher concentrations of sucrose. Therefore, at the lower concentrations (12 and 15 wt.%), the inhibition effect is better accounted for resulting in less deviation between experimental and predicted pressures.

**Table 5-15: Percent absolute average deviation for measured systems using the predictive model approach of Eslamimanesh et al. (2012).**

System	wt.% sucrose	%AAD
1,1,1,2-tetrafluoroethane (1) + water (2) + sucrose (3)	12	1.21
1,1,1,2-tetrafluoroethane (1) + water (2) + sucrose (3)	15	1.38
R410a (1) + water (2) + sucrose (3)	12	1.18
R410a (1) + water (2) + sucrose (3)	15	1.40
R507 (1) + water (2) + sucrose (3)	12	1.29
R507 (1) + water (2) + sucrose (3)	15	1.45

### 5.7 Industrial application

In order to meet the high demands of a developing society, more energy efficient and cost effective technologies need to be implemented into industry. The only manner in which this can be achieved is through research and development. Research is of paramount importance for the application of new technologies into industry. However, before any new technologies can attain industrial application, a large amount of testing and evaluation needs to take place. This includes economic analyses, pilot plant testing and safety assessments to name but a few. Therefore, in order to determine the feasibility of implementing hydrate separation technologies into industry, various comparisons to existing separation techniques need to be undertaken.

#### 5.7.1 "SMRI" sample analysis

A sucrose sample was supplied by the SMRI (known as the "SMRI" sample) in order to determine if hydrate crystals would form in the desired process stream. A sample with a solids content of 63 °Brix was supplied. The solids content comprised of the following carbohydrate groups; fructose 1.26 wt.%, glucose 0.46 wt.% and sucrose 60.71 wt.%. This high solids content solution was obtained from the evaporator product stream. The reason for this is due to the fact that the evaporator feed is relatively unstable. This would affect the storage of this sample. Therefore, for the purposes of this study, the evaporator product stream sample was diluted to the desired concentrations. Unfortunately, at the time that the sample was collected, the sugar mills were experiencing large concentrations of polysaccharides in their factories due to microbiological activity. This leads to several processing difficulties. Therefore, the hydrate dissociation measurements conducted on this sample were performed on the worst-case scenario basis.

The refrigerant gas used in the mixed sucrose sample provided by SMRI was R410a; the best performing refrigerant from the hydrate results performed earlier in the study. Measurements performed on the R410a hydrate systems were conducted over a large temperature and pressure range of 278.03 K – 289.08 K and 0.19 MPa – 0.96 MPa respectively. Therefore, a substantial range over which measurements on the “SMRI” sample could be performed was available for comparison.

**Table 5-16: “SMRI” systems measured for HVL equilibrium.**

System	wt. % sucrose	Temperature/K	Pressure/MPa
R410a (1) + water (2) + “SMRI” sample (3)	12	284.36 – 288.79	0.51 – 0.98
R410a (1) + water (2) + “SMRI” sample (3)	15	283.84 – 288.07	0.80 – 1.01

Initially great difficulty was found in forming hydrate crystals in the sample supplied by the SMRI. This was noticed at measurements performed at lower pressures (< 0.5 MPa). Therefore, higher pressures (> 0.5 MPa) were investigated and hydrates were found to form easily at these conditions.

**Table 5-17: Hydrate dissociation measurements for the system R410a (1) + water (2) + “SMRI” sample (3).**

System	wt.% sucrose	Temperature/K	Pressure/MPa
<b>R410a (1) + water (2) + “SMRI” sample</b>	<b>12</b>	284.4	0.511
		285.6	0.605
		285.7	0.641
		287.3	0.78
		287.8	0.838
		288.8	0.976
<b>R410a (1) + water (2) + “SMRI” sample</b>	<b>15</b>	283.8	0.595
		285.3	0.696
		286.4	0.795
		287.6	0.935
		288.1	1.006



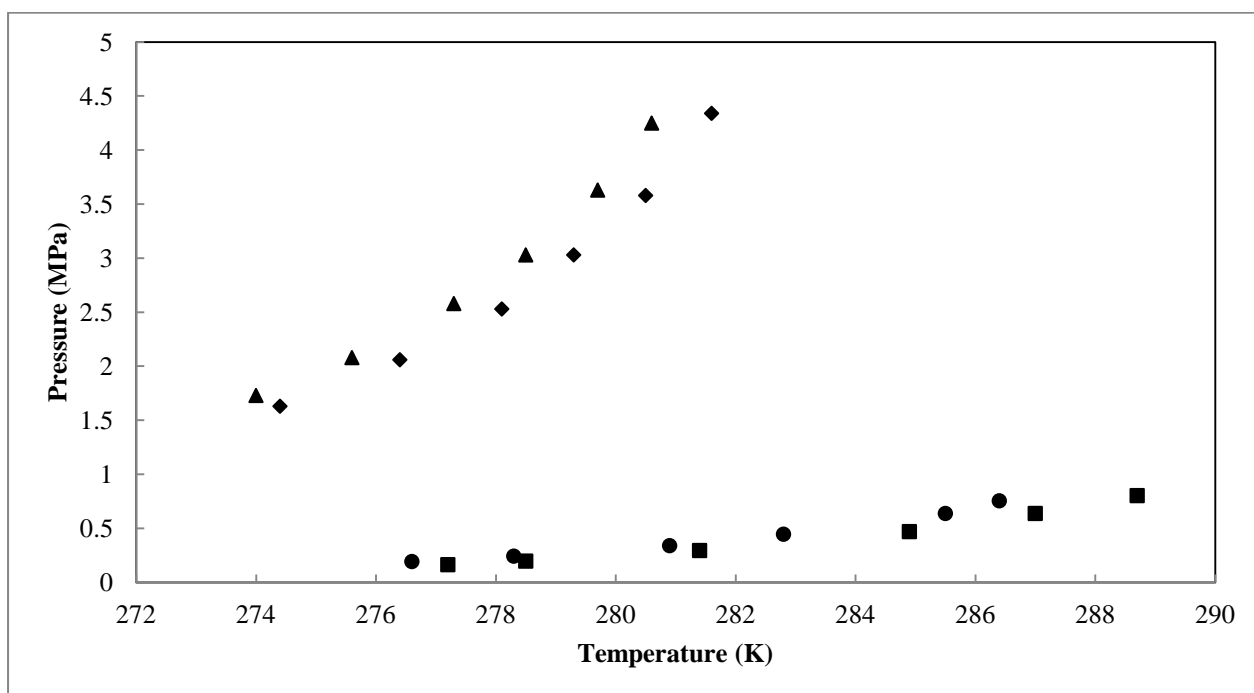


Figure 5-20: Hydrate dissociation conditions for the system former (1) + water (2) + sucrose (3).

20 wt.% sucrose: ♦, CO<sub>2</sub>; ■, R22. 30 wt.% sucrose: ▲, CO<sub>2</sub>. 40 wt.% sucrose: ●, R22.

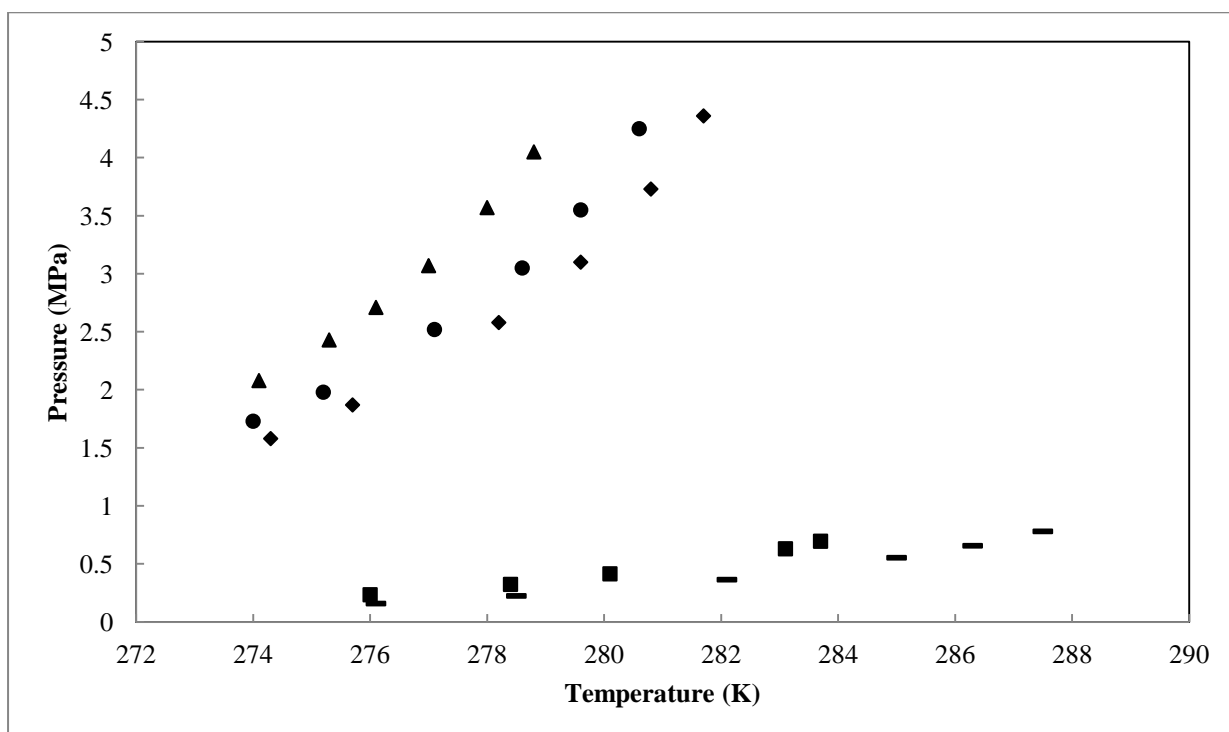
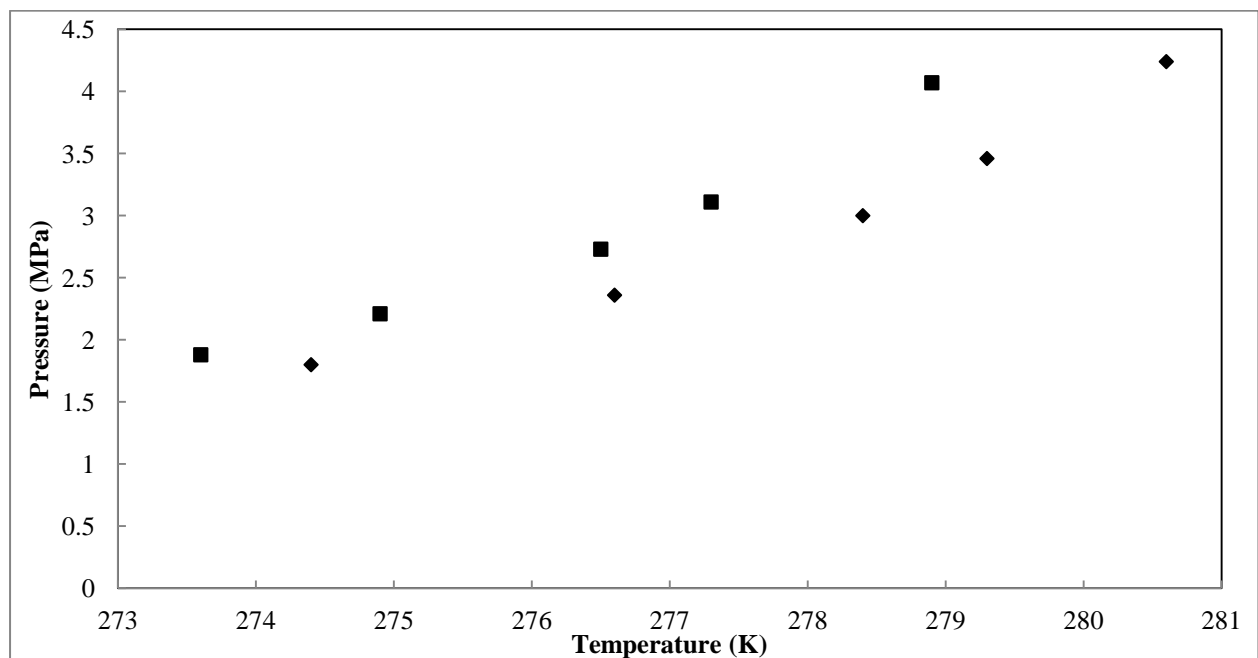


Figure 5-21: Hydrate dissociation conditions for the system former (1) + water (2) + glucose (3).

10 wt.% glucose: ♦, CO<sub>2</sub>. 20 wt.% glucose: ●, CO<sub>2</sub>; ■, R22. 30 wt.% glucose: ▲, CO<sub>2</sub>. 40 wt.% glucose: ■, R22.





**Figure 5-22: Hydrate dissociation conditions for the system CO<sub>2</sub> (1) + water (2) + fructose (3). ♦, 20 wt.%; ■, 30 wt.%.**

### 5.7.2 Energy comparison

As previously mentioned, in most circumstances, the heat of fusion is less than that of evaporation. The concentration process currently being used in South African sugar mills to concentrate a 12 °Brix solution to a 62 °Brix solution is evaporation. This is a highly energy intensive separation method. Therefore, by introducing a fusion-based separation technology to replace the evaporation process, a substantial energy saving may be achieved.

In the hydrate separation process, it is assumed that only water and former gas takes part in the formation of hydrate crystals; while in the evaporation process, it is also assumed that only water is vaporised. Therefore, the heats of fusion and evaporation of water can be directly compared for each process. This comparison is presented in Table 5-18 below. For this comparison, a basis of 1 ton of HP steam is required to evaporate 5 tons of water (SMRI, 2012).

**Table 5-18: Simple energy comparison between evaporation and fusion.**

<b>Evaporation</b>		<b>Fusion</b>	
Heat of vaporization (kJ/kg) <sup>a</sup>	1025	Heat of fusion (kJ/kg) <sup>a</sup>	151
Energy needed to evaporate 5 ton of water (kJ)	5125000	Energy needed to fuse 5 ton of water (kJ)	755000

<sup>a</sup> Reference: Perry et al. (1997)

Therefore, through a basic comparison, it can be seen that the energy required for fusion is 14.73 % of the total energy required for evaporation. Hence, the energy requirement for the separation of aqueous sucrose solutions can be reduced by approximately 85 % through the use of gas hydrate separation technologies.

### 5.7.3 Hydrate separation technology

A wide range of inherent design flexibility accompanies the hydrate separation process. Therefore, instead of viewing it like evaporators, which are commercially produced standards allowing for minimal optimization, it should be viewed in terms of fractional distillation trains, and thus optimized for each application (Barron and Wrobel, 1985). Therefore, the hydrate process may eventually be a ‘building block’ technology, which comprises standard and custom mechanisms that can be assembled into complete process technologies. These complete technologies can then be optimized for each area of application (Barron and Wrobel, 1985). The unit operations that comprise that hydrate separation process are reviewed below.

## 5.7.3.1 Unit operations

A general process diagram of the hydrate separation process is shown below in Figure 5-23.

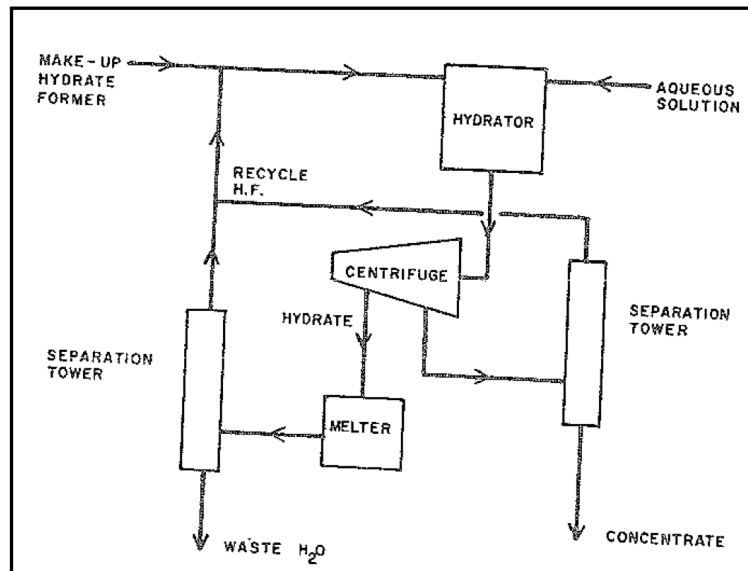


Figure 5-23: Hydrate separation process diagram (Werezak, 1969).

The major unit operations of a hydrate separation process include a hydrator or crystallizer, a separator, a melter and a stripper or recycle column.

The hydrate separation process is comprised of four stages. The first stage involves gas hydrate formation, where hydrate nucleation and growth occur. This reaction can either be a homogenous crystallization from a miscible former, or a multiphase reaction involving aqueous solution, solid hydrate and one or more hydrate former phases. This is dependent on the hydrate former used. The second stage is concerned with the separation of the concentrated liquid and the solid hydrate phase. Various separation techniques are available, such as centrifugation, filtration, or by means of a wash column. However, it has been found that centrifugation is the most promising method for this separation (Huang et al., 1965; Werezak, 1969). During the third stage, the solid hydrates are dissociated to produce a water-former mixture. This is achieved by either raising the temperature or lowering the pressure. The final stage involves stripping and recycling of the hydrate former. Although the former gas is recycled, a small amount of make-up gas may be required.

## 5.7.3.2 Comparison between hydrate separation processes and conventional evaporation technologies

A comparison between hydrate separation processes and conventional evaporation techniques is presented in Table 5-19. The primary difference between these two processes is the occurring phase change; vaporization versus fusion.

**Table 5-19: Characteristics of vaporization process versus fusion processes (Barron and Wrobel, 1985).**

<b>Characteristics</b>	<b>Vaporization</b>	<b>Fusion</b>
Number of applications	Many	Many
Selectivity of making separations	Usually good	Usually good
Corrosion potential	High	Low
Scaling potential	High	Low
Ability to handle sensitive materials	Low	High
Affected by viscosity	No	Yes
Complexity of equipment	Moderate	Moderate
Base of retrofit	Easy	Easy
Commercial status	Yes	Beginning phase
Number of suppliers	Many	Few
Product purity and value	Moderate	High
Capital cost	High	Low
Energy cost	High	Low
Operations and maintenance cost	High	Moderate

#### 5.7.4 Industrial cost analysis

The industrial cost analysis performed in this study was taken from the cost estimation proposed by Barron and Wrobel (1985). The data used by Barron and Wrobel in estimating the costs of constructing and operating a hydrate separation process was obtained from numerous published and unpublished sources. The data attained was reduced to a collective set of assumptions and scope of costing. These are presented in Tables 5-20 and 5-21 below.

**Table 5-20: Cost analysis assumptions (Barron and Wrobel, 1985).**

<b>Project life</b>	20 years
<b>Design and construction time</b>	Zero
<b>Ownership</b>	Private
<b>Amortization factor</b>	7.469 (20 years and 12%)
<b>Stream factor</b>	0.90 (7885 hrs./yr.)
<b>Contingency</b>	Zero
<b>Contracting approach</b>	Single contract to design and build
<b>System maturity</b>	Not the first installation

**Table 5-21: Cost analysis scope (Barron and Wrobel, 1985).**

<b>Included costs</b>
<ul style="list-style-type: none"> <li>• Fabrication of process equipment, including vessels, heat exchangers, pumps, compressors, pipes and fittings, electrical systems, controls and structural work for support of the above.</li> <li>• Shipment to job site, including loading, truck, freight and off-loading at the jobsite.</li> <li>• Erection of equipment, including labour, materials and construction equipment needed to place, align and connect process equipment.</li> <li>• Start-up testing, including labour and materials.</li> <li>• Construction indirects, including field overhead, shared site equipment and miscellaneous consumable materials.</li> <li>• Design, procurement and construction services, including overhead and profit.</li> </ul>
<b>Excluded costs</b>
<ul style="list-style-type: none"> <li>• Site development, such as clearing, excavation, fill, hauling and disposal.</li> <li>• Foundations, structures and architectural features, such as non-equipment footings, buildings and enclosures.</li> <li>• Off-site facilities, such as water supply</li> <li>• Ancillary systems, such as utilities and lighting</li> <li>• Unrelated process systems</li> <li>• Owner's costs, such as land, permits, fees, taxes, tax credits, insurances, interest during construction and working capital</li> </ul>

The costs associated with the construction and maintenance of a hydrate separation process are primarily affected by the following variables (Barron and Wrobel, 1985):

- Plant capacity or size
- Freezing and melting temperatures of the crystallizing system
- Viscosity of the mother liquor from which the component is being crystallized
- Latent heat of fusion for the material being crystallized
- Material of construction requirements

## 5.7.4.1 Capital costs

The capital cost associated with the construction of the hydrate separation process equipment was determined using the following equation:

$$\text{Capital cost} = (\text{Base cost})(F_s)(F_t)(F_v)(F_{hf})(F_{mat}) \quad (6.1)$$

where  $F_s$  is the size factor,  $F_t$  is the temperature factor,  $F_v$  is the viscosity factor,  $F_{hf}$  is the latent heat factor and  $F_{mat}$  is the material of construction factor.

## 5.7.4.2 Operation and maintenance costs

The operation and maintenance costs associated with the operation of the hydrate separation process equipment were determined using the following equation:

$$\text{Operations and maintenance costs} = L + E + M + A \quad (6.2)$$

$$\text{where } L = (\text{average labour rate})(C_s)(\text{overhead rate}) \quad (6.3)$$

$$E = (\text{Local energy cost})(C_t)(7.20) \quad (6.4)$$

$$M = (0.035)(\text{capital cost})(\text{Annual hydrate production rate})^{-1} \quad (6.5)$$

$$M = (\text{amortized capital cost})(\text{Annual hydrate production rate})^{-1} \quad (6.6)$$

where  $C_s$  is the size-labour cost factor and  $C_t$  is the energy-temperature cost factor.

## 5.7.4.3 Hydrate separation process cost analysis

The cost analysis performed was based on a feed flow rate of 20 000 lb./hr. (9072 kg./hr.) of 12 %Brix aqueous sucrose solution. This feed was concentrated to a final product of 65 °Brix. The evaporation process concentrates the feed to approximately 62 °Brix, therefore 65 °Brix was chosen as the final concentration in order to cost for the most expensive situation. These concentrations were chosen they represent typical evaporator feed and product streams. Imperial measurements were used as all cost factors were based on flow rates of lb./hr. The reader is referred to Appendix D for the detailed calculation procedure.

$$\begin{aligned} \text{Capital costs} &= R19607894(1.25)(1.08)(1.26)(1)(1) \\ &= R33\,353\,028 \end{aligned}$$

$$\begin{aligned} \text{Operation and maintenance costs} &= R\,7.55 + R0 + R8.16 + 31.21 \\ &= R38.26 \text{ per } 454 \text{ kg of feed processed} \end{aligned}$$

The average capital cost for the construction of an evaporator train in a sugar mill is R100 million (SMRI, 2012). Therefore, the capital cost for the construction of a hydrate separation process fares very well in comparison to that of an evaporation process. The operating cost for a typical evaporation process in a sugar mill is R3 per ton cane processed. However, this figure does not include the maintenance costs. Therefore, an accurate comparison between the two processes cannot be made regarding operating and maintenance costs. Please refer to *Appendix D, Economic Cost Analysis* for a detailed description of the calculation procedure used.

The above cost analysis is a crude estimate based on many ideal assumptions. However, further research into this technology, such as forming stable hydrates, as well as research into the use of refrigerants in food products must be fully investigated before costing exercises can be covered in detail.



## CHAPTER 6

### CONCLUSIONS

A temperature calibration for the Pt-100 temperature sensors and a pressure calibration for the 0-10 MPa pressure transducer were conducted. The Overall Standard Uncertainty, including calibration and manufacturer uncertainty, was determined to be  $\pm 0.14$  K and  $\pm 0.566$  kPa for temperature and pressure respectively. The calibrations were verified through measurement of vapour pressures for the pure components: 1,1,1,2-tetrafluoroethane (R134a), R410a and R507.

Hydrate-liquid-vapour equilibrium measurements were conducted using the isochoric pressure search method. All measurements were performed using a ( $64 \text{ cm}^3$ ) stainless steel equilibrium cell. The experimental method, apparatus and calibrations were verified through measurement of known test systems;  $\text{CO}_2$  (1) + water (2) + {0 and 20} wt.% sucrose (3) and R410a (1) + water (2). The resulting data compared well to that of literature.

Three new refrigerants were selected for measurements in the presence of sucrose. These included 1,1,1,2-tetrafluoroethane (1) + water (2) + {12 and 15}wt.% sucrose (3), R410a (1) + water (2) + {12 and 15}wt.% sucrose (3) and R507 (1) + water (2) + {12 and 15}wt.% sucrose (3).

The best performing refrigerant was found to be R410a. It was found that at higher temperatures, i.e. temperatures closer to ambient, the inhibiting effect of sucrose on hydrate formation is less than that for R410a when compared to 1,1,1,2-tetrafluoroethane and R507. In addition, the temperature shift for R410a is the least in the examined range when compared to 1,1,1,2-tetrafluoroethane and R507. In addition, it was determined that the feasible operating region for the proposed system lies in the temperature range of 280 K – 282 K and the corresponding pressure range of 0.3 MPa – 0.5 MPa. In this region, the increased sucrose concentration begins to play less of an inhibiting role on hydrate formation.

The presence of sucrose in the system resulted in an inhibition effect on hydrate formation. This is seen by the shift of the HVL equilibrium phase boundary to either higher pressures or lower temperatures. Additionally, through measurements performed on the sample supplied by the SMRI it was observed that the presence of additional carbohydrates (glucose and fructose) in the system increased the effect of inhibition on hydrate formation.

In this study, the van der Waals-Platteeuw solid solution theory was used to model the hydrate phase. For systems containing carbon dioxide, the vapour phase was modeled using the Peng-Robinson Equation of State (Peng and Robinson, 1976), while for systems containing refrigerants, the modifications of Eslamimanesh et al. (2011) were used and the vapour phase was assumed to be ideal, ignoring its water content. In all systems, the liquid phase was modeled using the UNIFAC model. The inhibition effect of sucrose was accounted for using a purely empirical correction method proposed by Englezos and Hall (1994). The predicted results compared well to the experimental results.

An approximate cost analysis, based on the findings of Barron and Wrobel (1985), was conducted. This analysis determined that the capital costs associated with the construction of a hydrate separation technology would amount to approximately R33 million with the operations and maintenance costs amounting to R00.08 per kg of feed processed.

It is recommended that for the implementation of the hydrate process as a concentration technology, various kinetic properties such as particle size and quality need to be known. Therefore, project limitations were present in the fact that since the isochoric pressure cell is fully sealed and non-visual, crystal size and quality cannot be examined. These crystal properties are important in determining whether or not the crystals will be stable and large enough for separation from the concentrated solution after hydrate formation. In addition, since the cell cannot be opened during hydrate formation, due to the temperature and pressure considerations, the concentration of the solution, and thus the degree of separation, cannot be determined.

## CHAPTER 7

### RECOMMENDATIONS

Various measurements may be conducted as a continuation of this study. Further hydrate measurements for systems containing sucrose with various refrigerant formers, i.e. R134a, R410a and R507, as well other fluorinated hydrate formers such as R32, are recommended. Additionally, systems consisting of a mixture of carbohydrates, such as sucrose, glucose and fructose, should be investigated.

In order for hydrate separation technologies to be implemented into industry, crystal size and quality need to be determined. In addition, techniques to determine the concentration of the final solution need to be established. Possible solutions to be investigated in order to overcome these limitations include molecular and mesoscopic experimental methods. Molecular level experimental methods for studying hydrate properties include Solid-State NMR Spectroscopy, Raman Spectroscopy and X-Ray Diffraction. By use of these methods, hydrate properties such as structure identification and changes in hydrate structure during formation and decomposition can be obtained. On a mesoscopic level, Laser Scattering and Particle Video Microscope can be used to determine hydrate crystal size during formation and decomposition.

In terms of determining the extent of separation, and thus the concentration of the final solution, two methods have been presented in literature by Huang et al. (1965). These methods are discussed in *Chapter 3.3, Extent of separation*, and include the direct and indirect methods. Investigations into the above mentioned methods are recommended in order to acquire an accurate and repeatable method to determine the solids content of the final solution.

In addition, the development of a new model to account for the inhibition effect of sucrose would be valuable for the prediction of hydrate dissociation pressures in aqueous carbohydrate solutions. The only approach used to date is based on a purely empirical correction method proposed by Englezos and Hall (1994). Therefore, it is recommended that additional HLV measurements be performed on aqueous carbohydrate solutions in order for a more accurate model to be developed.

Finally, investigations into industrially supplied evaporator feed sugar samples must be performed. Such investigations would provide a better understanding regarding hydrate formation in evaporator process streams.

## REFERENCES

- Adisasmito, S, Frank, R. J and Sloan, D, 1991, Hydrates of carbon dioxide and methane mixtures, *J. Chem. Eng. Data*, 36, (1), 68-71.
- Akiya, T., Shimazaki, T., Oowa, M., Matsuo, M. and Yoshida, Y., 1999. Formation Conditions of Clathrates Between HFC Alternative Refrigerants and Water. *International Journal of Thermophysics*, 20, 1753-1763.
- Barron, T. S. and Wrobel, P. J., 1985. *Separation Process Economics*. Houston, pp. 27-41.
- Beltran, J. G. and Servio, P., 2008. Equilibrium studies for the system methane + carbon dioxide + neohexane + water. *Journal of Chemical Engineering Data*, Volume 53, pp. 1745-1749.
- Bishnoi, P. R., Gupta, A. K., Englezos, P. and Kalogerakis, N., 1989. Multiphase equilibrium flash calculations for systems containing gas hydrates. *Fluid Phase Equilibria*, Volume 53, pp. 97-104.
- Bishnoi, P. R. and Natarajan, V., 1996. Formation and Decomposition of Gas Hydrates. *Fluid Phase Equilibria*, Volume 117, pp. 168-177.
- Calm, J. E., 2008. Properties and efficiencies of R410a, R421a, R422b and R422d compared to R22. *Refrigerant Management Services*, pp. 1-14.
- Cambray, G., 2007. Green with Energy. [Online]  
Available at: <http://scienceinafrica.com/old/2007/june/greenenergy2.htm>  
[Accessed 6 June 2013].
- Carbone, A. S., Ivall, J. R. and Servio, P. D., 2012. H-Lw-V Equilibrium Measurements of Pure Methane Gas in the Presence of D-(+)-Glucose. *Journal of Chemical and Engineering Data*, pp. 974-977.
- Carroll, J. J., 2003. *Natural Gas Hydrates: A Guide for Engineers*. Burlington: Gulf Professional Publishing.
- Chen, G.-J. and Guo, T.-M., 1996. Thermodynamic modeling of hydrate formation based on new concepts. *Fluid Phase Equilibria*, Volume 122, pp. 43-65.
- Chen, G.-J. and Guo, T.-M., 1998. A new approach to gas hydrate modelling. *Chemical Engineering Journal*, Volume 71, pp. 145-151.
- Chen, L.-J., Hsieh, M.-K., Lin, S.-T. and Chen, Y.-P., 2001. Prediction of Gas Hydrate Phase Behaviour in the Presence of Alcohols and Glycols with PRSV Equation of State and the VDW-P Model. Edinburgh.
- Chung, C. C., 2000. *Handbook of Sugar Refining: A Manual for the Design and Operation of Sugar Refining Facilities*, John Wiley and Sons Inc.
- Chun, M.-K. and Lee, H., 1998. Phase equilibria of R22 (CHClF<sub>2</sub>) hydrate system in the presence of sucrose, glucose and lactic acid. *Fluid Phase Equilibria*, pp. 361-370.
- Chun, M.-K. and Lee, H., 1999. Phase equilibria of carbon dioxide hydrate system in the presence of sucrose, glucose and fructose. *Journal of Chemical Engineering Data*, pp. 1081-1084.

## REFERENCES

- Chun, M.-K., Yoon, J.-H. and Lee, H., 1996. Clathrate Phase Equilibria for the Water + Deuterium Oxide + Carbon Dioxide and Water + Deuterium Oxide + Chlorodifluoromethane (R22) Systems. *Journal of Chemical Engineering Data*, pp. 1114-1116.
- Cole, W. A. and Goodwin, S. P., 1990. Flash calculations for gas hydrates: A rigorous approach. *Chemical Engineering Science*, pp. 569-573.
- Dalmazzone, D., Kharrat, M., Lachet, V., Fouconnier, B. and Clause, D., 2002. DSC and PVT Measurements: Methane and Trichlorofluoromethane Hydrate Dissociation Equilibria. *Journal of Thermal Analysis and Calorimetry*, 70, pp. 493-505.
- Deaton, W. H. and Frost, E. M., 1946. Gas hydrates and their relation to the operation of natural gas pipe lines, U.S. Bureau of Mines Monograph 8.
- Delahaye, A., Fournaison, L., Marinha, S. and Chatti, I., 2006. Effect of THF on Equilibrium Pressure and Dissociation Enthalpy of CO<sub>2</sub> Hydrates Applied to Secondary Refrigeration. *Industrial and Engineering Chemical Research*, pp. 391-397.
- Deshpande, S. S., Cheryan, M., Sathe, S. K. and Salunkhe, D. K., 1984. Freeze concentration of fruit juices. *Critical Reviews in Food Science and Nutrition*, 20(3), pp. 173-248.
- Dharmawardhana, P. B., Parrish, W. R. and Sloan, E. D., 1980. Experimental thermodynamic parameters for the prediction of natural gas hydrate dissociation conditions. *Ind. Eng. Chem. Fundam.*, Volume 19, pp. 410-414.
- Dhima, A., de Hemptinne, J.-C. and Jose, J., 1999. Solubility of Hydrocarbons and CO<sub>2</sub> Mixtures in Water under High Pressure. *Industrial and Engineering Chemical Research*, Volume 38, pp. 3144-3161.
- Dixon, M. C., 2008. Quartz Crystal Microbalance with Dissipation Monitoring: Enabling Real-Time Characterization of Biological Materials and Their Interactions. *Journal of Biomolecular Techniques*, 19(3), pp. 151-158.
- Dohrn, R., Peper, S., Fonseca, J.M.S., 2010. High-pressure phase equilibria: experimental methods and systems investigated (2000-2004). *Fluid Phase Equilibria*, 288, 1-54.
- Doring, R., Buchwald, H. and Hellman, J., 1996. Results of experimental and theoretical studies of the azeotropic refrigerant R507. *International Journal of Refrigeration*, 20(2), pp. 78-84.
- Englezos, P., 1992. Computation of the Incipient Equilibrium Carbon Dioxide Hydrate Formation Conditions in Aqueous Electrolyte Solutions. *Industrial and Engineering Chemistry Research*, 31(9), pp. 2232-2237.
- Englezos, P., 1993. Clathrate hydrates. *Industrial and Engineering Chemical Research*, pp. 1251-1274.
- Englezos, P., 1994. The Freeze Concentration Process and its Applications. *Developments in Chemical Engineering and Mineral Processing*, 2(1), pp. 3-15.
- Englezos, P. and Bishnoi, P. R., 1991. Experimental Study on the Equilibrium Ethane Hydrate Formation Conditions in Aqueous Electrolyte Solutions. *Industrial and Engineering Chemistry Research*, Volume 30, pp. 1655-1659.
- Englezos, P. and Hall, S., 1994. Phase Equilibrium Data on Carbon Dioxide Hydrate in the Presence of Electrolytes, Water Soluble Polymers and Monmorillonite. *Canadian Journal of Chemical Engineering*, Volume 72, pp. 887-893.

- Englezos, P., Huang, Z. and Bishnoi, P. R., 1991. Prediction of natural gas hydrate formation conditions in the presence of methanol using the Trebble-Bishnoi equation of state. *Journal of Canadian Petroleum Technology*, Volume 30, pp. 148-155.
- Englezos, P., Kalogerakis, P. N., Dholabhai, P. D. and Bishnoi, P. R., 1987. Kinetics of Formation of Methane and Ethane Gas Hydrates. *Chemical Engineering Science*, Volume 42, pp. 2647-2658.
- Eslamimanesh, A., Mohammadi, A. H. and Richon, D., 2011. Thermodynamic model for predicting phase equilibria of simple clathrate hydrates of refrigerants. *Chemical Engineering Science*, Volume 66, pp. 5439-5445.
- Eslamimanesh, A., Mohammadi, A. H., Richon, D., Naidoo, P. and Ramjugernath, D., 2012. Application of gas hydrate formation in separation processes: A review of experimental studies. *Journal of Chemical Thermodynamics*, 46, pp. 62-71.
- Fan, S. and Guo T.-M., 1999. Hydrate Formation of CO<sub>2</sub>-Rich Binary and Quaternary Gas Mixtures in Aqueous Sodium Chloride Solutions. *Journal of Chemical Engineering Data*, 44, (4), pp. 829-832.
- Fredenslund, A. and Sørensen, J. M., 1993. Group Contribution Estimation Methods. In *Models for Thermodynamic and Phase Equilibria Calculations*; Sandler, S. I., Ed.; Marcel Dekker: New York, pp. 287-361.
- Giuliani, G., Kumar, S. and Polonara, F., 1995. A constant volume apparatus for vapour pressure and gas phase P-v-T measurements: validation with data for R22 and R134a. *Fluid Phase Equilibria*, Volume 109, pp. 265-279.
- Guo, T.-M., Wu, B.-H., Zhu, Y.-H., Fan, S.-S. and Chen, G.-J., 2004. A review of gas hydrate research in China. *Journal of Petroleum and Science*, Volume 41, pp. 11-20.
- Heist Engineering Corp, 1988. *Beet Sugar Refining Applications*, Springfield: US Department of Commerce.
- Heist, J. A., 1979. Freeze Crystallisation. *Chemical Engineering*, pp. 72-82.
- Heist, J. A., 1981. Freeze Crystallization: Improving the energy efficiency of a low-energy separation process. *Houston*, pp. 97-105.
- Heist, J. A. and Barron, T. S., 1983. *Freeze Crystallization Processes: Efficiency by Flexibility*. *Houston*, pp. 837-845.
- Herri, J. -M., Bouchemoua, A., Kwaterski, M., Fezoua, M., Ouabbas, Y. and Cameiro, A., 2011. Gas hydrate equilibria for CO<sub>2</sub>-N<sub>2</sub> and CO<sub>2</sub>-CH<sub>4</sub> gas mixtures—Experimental studies and thermodynamic modelling. *Fluid Phase Equilibria*, Volume 301, pp. 171-190.
- Hirai, S., Okazaki, K., Araki, N., Yoshimoto, K., Ito, H. and Hijikata, K., 1995. Experiments for dynamic behaviour of carbon dioxide in deep sea. *Energy Conversion and Management*, 36(6-9), pp. 471-474.
- Holder, G. D. and Grigoriou, G. C., 1980. Hydrate Dissociation Pressures of (Methane + Ethane + Water) Existence of a Locus of Minimum Pressures. *Journal of Chemical Thermodynamics*, Volume 12, pp. 1093-1104.
- Huang, C. P., Fennema, O. and Powrie, W. D., 1965. Gas Hydrates in Aqueous-Organic Systems: 1. Preliminary Studies. *Cryobiology*, 2(3), pp. 109-115.

- Huang, C. P., Fennema, O. and Powrie, W. D., 1966. Gas Hydrates in Aqueous-Organic Systems: 2. Concentration by Gas Hydrate Formation. *Cryobiology*, pp. 240-245.
- Huo, Z. Freer, E., Lamar, M., Sannigrahi, B. and Knauss, D.M., 2001. Hydrate plug prevention by anti-agglomeration. *Chemical Engineering Science*, 56(17), pp. 4979-4991.
- Ivanic, J., Huo, Z. and Sloan, E. D., 2004. Improved hydrate equilibrium measurements in ternary gas and black oil systems. *Fluid Phase Equilibria*, Volume 222-223, pp. 303-310.
- Javanmardi, J., Ayatollahi, S., Motealleh, R. and Moshfeghian, M., 2004. Experimental Measurement and Modeling of R22 (CHClF<sub>2</sub>) Hydrates in Mixtures of Acetone + Water. *Journal for Chemical Engineering Data*, Volume 49, pp. 886-889.
- Javanmardi, J., Babaei, S., Eslamimanesh, A. and Mohammadi, A. H., 2012. Experimental measurements and predictions of gas hydrate dissociation conditions in the presence of methanol and ethane-1,2-diol aqueous solutions. *Journal of Chemical Engineering Data*, Volume 57, pp. 1474-1479.
- Kamath, V. A. and Holder, G. D., 1987. Dissociation heat transfer characteristics of methane hydrates. *AIChE Journal*, 33(2), pp. 347-350.
- Kamath, V. A., Holder, G. D. and Angert, P. F., 1984. Three phase interfacial heat transfer during the dissociation of propane hydrates. *Chemical Engineering Science*, 39(10), pp. 1435-1442.
- Khalil, W., 2006. Développement d'un appareil automatisé de mesure simultanée d'équilibres de phases et de propriétés volumétriques. Exploitation des données volumétriques pour le calcul prédictif de grandeurs thermodynamiques dérivées. PhD Dissertation, Ecole Nationale Supérieure des Mines de Paris, France .
- Khokhar, A. A., 1998. Gas storage in structure H hydrates. *Fluid Phase Equilibria*, pp. 383-392.
- Khosravani, E., Moradi, G. and Sajjadifar, S., 2013. An accurate thermodynamic model to predict phase behaviour of clathrate hydrates in the absence and presence of methanol based on the genetic algorithm. *Journal of Chemical Thermodynamics*, Volume 57, pp. 286-294.
- Kim, H. C., Bishnoi, P. R., Heidemann, R. A. and Rizvi, S. S. H., 1987. Kinetics of methane hydrate decomposition. *Chemical Engineering Science*, 42(7), pp. 1645-1653.
- Klauda, J. B. and Sandler, S. I., 2000. A Fugacity Model for Gas Hydrate Phase Equilibria. *Industrial and Engineering Chemical Research*, Volume 39, pp. 3377-3386.
- Klauda, J. B. and Sandler, S. I., 2002. Ab Initio Intermolecular Potentials for Gas Hydrates and Their Predictions. *Journal of Physical Chemistry*, Volume 106, pp. 5722-5732.
- Klauda, J. B. and Sandler, S. I., 2003. Phase behaviour of clathrate hydrates: a model for single and multiple gas component hydrates. *Chemical Engineering Science*, Volume 58, pp. 27-41.
- Larson, S. D., 1955, Phase studies of the two-component carbon dioxide-water system involving the carbon dioxide hydrate, Ph.D. Thesis, University of Illinois.
- Le Parlouer, P., Dalmazzone, C., Herzhaft, B., Rousseau, L. and Mthonat, C., 2004. Characteristics of gas hydrates formation using a new high-pressure micro-DSC. *Journal of Thermal Analysis and Calorimetry*, pp. 165-172.

## REFERENCES

- Lee, B. R., Sa, J. H., Park, D. H., Cho, S., Lee, J., Kim, H. J., Oh, E., Jeon, S., Lee, J. D., Lee K. H., 2012, Continuous Method for the Fast Screening of Thermodynamic Promoters of Gas Hydrates Using a Quartz Crystal Microbalance. *Energy Fuels* 26, pp. 767-772.
- Lee, J. D., Susilo, R. and Englezos, P., 2005. Kinetics of Structure H gas Hydrate. *Energy and Fuels*, pp. 1008-1015.
- Lewis, A. E., Khodabocus, F., Dhokun, V. and Khalife, M., 2010. Thermodynamic simulation and evaluation of sugar refinery evaporators using a steady state modeling approach. *Applied Thermal Engineering*, pp. 2180-2186.
- Liang, D., Guo, K., Wang, R. and Fan, S., 2001. Hydrate equilibrium data of 1,1,1,2-tetrafluoroethane (HFC-134a), 1,1-dichloro-1-fluoroethane (HCFC-141b) and 1,1-difluoroethane (HFC-152a). *Fluid Phase Equilibria*, 187-188, pp. 61-70.
- Long, J. P. and Sloan, E. D., 1996. Hydrates in the ocean and evidence for the location of hydrate formation. *International Journal of Thermophysics*, 17(1), pp. 1-13.
- Maekawa, T., 2013. Equilibrium conditions of clathrate hydrates formed from xenon and aqueous solutions of acetone, 1,4-dioxane and 1,3-dioxolane. *Fluid Phase Equilibria*, Volume 339, pp. 15-19.
- Ma, Q.-L., Chen, G.-J. and Guo, T.-M., 2003. Modeling the gas hydrate formation of inhibitor containing systems. *Fluid Phase Equilibria*, 205(2), pp. 291-302.
- Martinez, M. C., Dalmazzone, D., Furst, W., Delahaye, A. and Fournaison, L., 2008. Thermodynamic properties of THF + CO<sub>2</sub> hydrates in relation with refrigeration applications. *AIChE J*, pp. 1088-1095.
- Mayoufi, N., Dalmazzone, D., Furst, W., Delahaye, A. and Fournaison, L., 2010. CO<sub>2</sub> Enclathration in Hydrates of Peralkyl-(Ammonium/Phosphonium) Salts: Stability Conditions and Dissociation Enthalpies. *Journal of Chemical Engineering Data*, pp. 1271-1275.
- McCormack, R. A. and Andersen, R. K., 1995. Clathrate Desalination Plant: Preliminary Research Study.
- McNamee, K. and Conrad, P., 2011. The effect of autoclave design and test protocol on hydrate test results. Edinburgh.
- Michelsen, M. L., 1990. A Modified Huron-Vidal Mixing Rule for Cubic Equations of State. *Fluid Phase Equilibria*, Volume 60, pp. 213-219.
- Mohammadi, A. H., Anderson, R. and Tohidi, B., 2005. Carbon monoxide clathrate hydrates: Equilibrium data and thermodynamic modeling. *AIChE Journal*, 51, pp. 2825-2833.
- Mohammadi, A. H. and Richon, D., 2008. Thermodynamic Model for Predicting Liquid Water-Hydrate Equilibrium of the Water-Hydrocarbon System. *Industrial and Engineering Chemical Research*, Volume 47, pp. 1346-1350.
- Mohammadi, A. H. and Richon, D., 2009. Equilibrium Data of Nitrous Oxide and Carbon Dioxide Clathrate Hydrates. *Journal of Chemical Engineering Data*, Volume 54, pp. 279-281.
- Mohammadi, A. H., Tohidi, B. and Burgass, R. W., 2003. Equilibrium Data and Thermodynamic Modeling of Nitrogen, Oxygen, and Air Clathrate Hydrates. *Journal of Chemical Engineering Data*, Volume 48, pp. 612-616.



- Mooijer-van den Heuvel, M. M., 2004. Phase Behaviour and Structural Aspects of Ternary Clathrate Hydrate Systems, The Role of Additives. PhD Thesis, Delft University of Technology.
- Mooijer-van den Heuvel, M. M., Sawirjo, N. M. and Peters, C. J., 2006. Influence of fluoroalkanes on the phase behaviour of methane gas hydrate systems. *Fluid Phase Equilibria*, Volume 241, pp. 124-137.
- Najibi, H., Chapoy, A., Haghghi, H. and Tohidi, B., 2009. Experimental determination and prediction of methane hydrate stability in alcohols and electrolyte solutions. *Fluid Phase Equilibria*, pp. 127-131.
- Ngema, P. T., Petticrew, C., Naidoo, P., Mohammadi, A.H. and Ramjugernath, D., 2012. Experimental measurements and thermodynamic modeling of the dissociation conditions of clathrate hydrates for (refrigerant + NaCl + water) systems, Durban: Thermodynamic Research Unit, School of Engineering, University of KwaZulu-Natal.
- Ng, H. J. and Robinson, D. B., 1980. A Method for Predicting the Equilibrium Gas Phase Water Content in Gas-Hydrate Equilibrium. *Industrial and Engineering Chemistry Fundamentals*, Volume 19, pp. 33-36.
- Nixdorf, J. and Oellrich, L. R., 1997. Experimental determination of hydrate equilibrium conditions for pure gases, binary and ternary mixtures and natural gases. *Fluid Phase Equilibria*, Volume 139, pp. 325-333.
- Oellrich, L.R., 2004, Natural Gas Hydrates and their Potential for Future Energy Supply, in Proc. 17th National and 6th ISHMT/ASME Heat and Mass Transfer Conference (HMT), IGCAR, Kalpakkam, Jan. 5-7.
- Ohgaki, K., Makihara, Y and Takano, K., 1993, Formation of CO<sub>2</sub> Hydrate in Pure and Sea Waters, *Journal of Chemical Engineering of Japan*, 26, (5), pp. 558-564.
- OrionAir, 2012. Refrigerant gas phase out (January 1995 to 2015). [Online] Available at: <http://www.orionair.co.uk/gas%20regulations.htm> [Accessed 4 March 2013].
- Ostergaard, K. K., Tohidi, B., Burgass, R.W., Danesh, A. and Todd, A.C., 2001. Hydrate Equilibrium Data of Multicomponent Systems in the Presence of Structure-II and Structure-H Heavy Hydrate Formers. *Chemical and Engineering Data*, 46(3), pp. 703-708.
- Parker, D., 2009. How SA could liberate power and fuel from its sugar cane fields. [Online] Available at: <http://www.engineeringnews.co.za/article/how-sa-could-liberate-power-and-fuel-from-its-sugar-cane-fields-2009-08-07> [Accessed 6 June 2013].
- Parrish, W. R. Ostergaard, K. K. et al., 2001. Hydrate Equilibrium Data of Multicomponent Systems in the Presence Prusnitz, J. M., 1972. Dissociation Pressures of Gas Hydrates Formed by Gas Mixtures. *Industrial and Engineering Chemical Process Design Development*, 11(1), pp. 26-35.
- Patel, N. C. and Teja, A. S., 1982. A new cubic equation of state for fluids and fluid mixtures. *Chemical Engineering Science*, Volume 37, pp. 463-473.
- Peng, D.-Y. and Robinson, D. B., 1976. A New Two-Constant Equation of State. *Industrial and Engineering Chemical Fundamentals*, 15(1), pp. 59-64.
- Perry, R.H. and Green, D.W., 1997. *Perry's Chemical Engineering Handbook*, McGraw-Hill, New York.

- Peters, C. J., Mooijer-van den Heuvel, M. M. and de Swaan Aarons, J., 2000. Influence of water-insoluble organic components on the gas hydrate equilibrium conditions of methane. *Fluid Phase Equilibria*, pp. 73-91.
- Peters, C. J., Mooijer-van den Heuvel, M. M. and Sawirjo, N. M., 2006. Influence of fluoroalkanes on the phase behaviour of methane gas hydrates. *Fluid Phase Equilibria*, pp. 124-137.
- Petticrew, C., 2012. An investigation into the use of fluorinated hydrating agents in the desalination of industrial wastewater. Masters dissertation, University of KwaZulu-Natal.
- Phillips, L., 2011. Can South Africa run on sugar power?. [Online] Available at: <http://www.farmersweekly.co.za/article.aspx?id=10940&h=Can-South-Africa-run-on-sugar-power> [Accessed 6 June 2013].
- Poling, B. E., Prausnitz, J. M. and O'Connell, J. P., 2001. *The Properties of Gases and Liquids*. 5th ed. New York: McGraw-Hill.
- Prausnitz, J. M. and Chueh, P. L., 1968. *Computer calculations for high-pressure vapour-liquid equilibria*. Englewood Cliffs, Prentice-Hall.
- Purwanto, Y. A., Oshita, S., Seo, Y. and Kawagoe, Y., 2001. Concentration of liquid foods by the use of gas hydrate. *Journal of Food Engineering*, Volume 47, pp. 133-138.
- Raal, J. D. and Muhlbauer, A. L., 1998, *Phase Equilibria: Measurement and Computation*, Taylor & Francis: Bristol, PA.
- Richon, D., 1996. New experimental developments for phase equilibrium measurements. *Fluid Phase Equilibria*, 116, pp. 421-428.
- Richon, D., 2009. Experimental techniques for the determination of thermophysical properties to enhance chemical processes. *Pure Applied Chemistry*, pp. 1769-1782.
- Rivollet, F., 2005. Etude des propriétés volumétriques (PVT) d'hydrocarbures légers (C1- C4), du dioxyde de carbone et d'hydrogène sulfure, PhD Thesis, Ecole Nationale Supérieure des Mines de Paris, France.
- Robinson, D. B. and Mehta, B. R., 1971. Hydrates In the Propane, Carbon Dioxide- Water System. *Journal of Canadian Petroleum Technology*, 10, pp. 33-35.
- Ruffine, L., Donval, J.P., Charlou, A., Cremiere, A. and Zehnder, B.H., 2010. Experimental study of gas hydrate formation and destabilisation using a novel high-pressure apparatus. *Marine and Petroleum Geology*, 27(6), pp. 1157-1165.
- Sabil, M. and Bin, K., 2009. Phase Behaviour, Thermodynamics and Kinetics of Clathrate Hydrate Systems of Carbon Dioxide in Presence of Tetrahydrofuran and Electrolytes. PhD Thesis, Delft University of Technology.
- SASA, 2012. The Sugarcane Industry: a sustainable source of renewable energy. SASA, 30 July.
- Schroeter, J. P., Kobayashi, R. and Hildebrand, M. A., 1983. Hydrate decomposition conditions in the system hydrogen sulfide-methane-propane. *Industrial and Engineering Chemistry Fundamentals*, 22 (4), pp. 361-364.

- Sloan, E. D. and Koh, C. A., 2008. Clathrate Hydrates of Natural Gases. Boca Raton: CRC Press.
- Sloan, E. D., Sparks, K. A. and Johnson, J. J., 1987. 2-phase liquid-hydrocarbon hydrate equilibrium for ethane and propane. *Industrial and Engineering Chemistry Research*, 26(6), pp. 1173-1179.
- Sloan, E., Khoury, F. and Kobayashi, R., 1976. Water Content of Methane Gas in Equilibrium with Hydrates. *Industrial and Engineering Chemical Fundamentals*, 15(4), pp. 318-323.
- Smith, J. M., Van Ness, H. C. and Abbott, M. M., 2005. *Introduction to Chemical Engineering Thermodynamics*. 7 ed. New York: McGraw-Hill.
- SMRI, 2012. The Manufacture of Raw and Refined Sugar in SA. [Online] Available at: <http://www.smri.org/rawsuagrfacts.php> [Accessed 7 February 2013].
- Soave, G., 1972. Equilibrium constants from a modified Redlich-Kwong equation of state. *Chemical Engineering Science*, Volume 27, pp. 1197-1203.
- Stryjek, R. and Vera, J. H., 1986. PRSV: An improved Peng—Robinson equation of state for pure compounds and mixtures. *The Canadian Journal of Chemical Engineering*, 64(2), pp. 323-333.
- Sugahara, T., Murayama, S., Hashimoto, S. and Ohgaki, K., 2005. Phase equilibria for H<sub>2</sub>+CO<sub>2</sub>+H<sub>2</sub>O system containing gas hydrates. *Fluid Phase Equilibria*, Volume 233, pp. 190-193.
- Sun, R. and Duan, Z., 2007. An accurate model to predict the thermodynamic stability of methane hydrate and methane solubility in marine environments. *Chemical Geology*, Volume 244, pp. 248-262.
- Taylor, B. N. and Kuyatt, C. E., 1994. *Guidelines for Evaluating and Expressing the Uncertainty of NIST Measurement Results*. NIST Technical Note 1297.
- Tohidi, B., Danesh, A. and Todd, A. C., 1995. Modeling Single and Mixed Electrolyte Solutions and its Applications to Gas Hydrates. *ICHEME*, 73(A), pp. 464-472.
- Tohidi, B., Burgass, R. W., Danesh, A. and Todd, A. C., 2002. Application of Quartz Crystal Microbalance to Gas Hydrate Stability Zone Measurements. *Yokohama*, pp. 380-383.
- Tongaat Hulett Sugar, 2012. Sugar Manufacture Process. [Online] Available at: [http://www.huletts.co.za/car/sm\\_process/asp](http://www.huletts.co.za/car/sm_process/asp) [Accessed 7 February 2013].
- Tongaat Hulett Sugar, 2013. Energising for Growth. [Online] Available at: [http://www.tongaat.co.za/imc/annual\\_reports/ar02/hulett\\_sugar/sugar\\_main.htm](http://www.tongaat.co.za/imc/annual_reports/ar02/hulett_sugar/sugar_main.htm) [Accessed 16 January 2013].
- Treble, M. A. and Bishnoi, P. R., 1988. Thermodynamic property prediction with the Treble Bishnoi equation of state. *Fluid Phase Equilibria*, Volume 39, pp. 111-128.
- Tumba, A. K., 2010. Application of Gas Hydrates to the Separation of close boiling components in petroleum streams. KwaZulu-Natal: Thermodynamics research department, school of Chemical Engineering, University of KwaZulu-Natal
- Unruh, C. H. and Katz, D. L., 1949. Gas hydrates of carbon dioxide-methane mixture, . *Pet. Trans. AIME*, 186, 83.

## REFERENCES

- Valderrama, J. O., 1990. A generalized Patel-Teja equation of state for polar and nonpolar fluids and their mixtures. *Journal of Chemical Engineering of Japan*, 23, pp. 87-91.
- van der Waals, J. H. and Platteeuw, J. C., 1959. Clathrate Solutions. *Advances in Chemical Physics*, 2, pp. 1-57.
- Villano, L. D. and Kelland, M. A., 2011. An investigation into the laboratory method for the evaluation of the performance of kinetic hydrate inhibitors using super heated gas hydrates. *Chemical Engineering Science*, 66, pp. 1973-1985.
- Vlahakis, J. G., Chen, H.-S, Suwandi, M. S and Barduhn, A. J., 1972. The growth rate of ice crystals: properties of carbon dioxide hydrate, a review of properties of 51 gas hydrates, Syracuse University Research and Development Report 8330, US Department of the Interior.
- Vysniauskas, A. and Bishnoi, P. R., 1983. A kinetic study of methane hydrate formation. *Chemical Engineering Science*, 38, pp.1061-1072.
- Wendland, M., Hasse, H. and Maurer, G., 1999. Experimental Pressure–Temperature Data on Three- and Four-Phase Equilibria of Fluid, Hydrate, and Ice Phases in the System Carbon Dioxide–Water. *Journal of Chemical & Engineering Data*, 44, pp.901-906.
- Werezak, G. N., 1969. Unusual Methods of Separation. *AIChE Symposium Series*, 65(91), pp. 6-18.

**APPENDIX A**

**CRITERIA FOR POTENTIAL FLUORINATED HYDRATE FORMERS**

In order to determine the most suitable fluorinated hydrate formers, a detailed analysis of each property and criteria for each potential former needs to be performed. This is shown in Table A.1 below.

Table A.1: Detailed analysis of specific criteria used to determine potential fluorinated hydrate formers.

Commercial name	R32	R125	R134a	R290
Chemical formula	CH <sub>2</sub> F <sub>2</sub>	CHF <sub>2</sub> CF <sub>3</sub>	CH <sub>2</sub> FCF <sub>3</sub>	C <sub>3</sub> H <sub>8</sub>
Ecological effect	ODP = 0 GWP = 220	ODP = 0 GWP = 860	ODP = 0 GWP = 1300	ODP = 0 GWP = 3
Toxicity effect	Freeze burns from liquid contact. Anaesthetic effects. Abnormal heart beat.	Skin irritation. Freeze burns from liquid contact. Nervous symptoms. Increased pulse rate.	Skin irritation. Freeze burns from liquid contact. Nervous symptoms. Increased pulse rate.	Acts as simple asphyxiant.
Flammability	Flammable liquefied gas.	Non-flammable	Non-flammable	Flammable
Chemical stability	Stable.	Stable. Do not mix with oxygen or air above atmospheric pressure.	Stable. Do not mix with oxygen or air above atmospheric pressure.	Stable. Forms explosive mixtures with air.
Hydrate former class	I	II	II	II
Compatibility	Incompatible with aluminium, zinc, magnesium, sodium, potassium and barium.	Incompatible with freshly abraded aluminium surfaces, potassium, calcium, powdered aluminium, magnesium and zinc.	Incompatible with freshly abraded aluminium surfaces, potassium, calcium, powdered aluminium, magnesium and zinc.	Incompatible with air and oxidisers.
Water solubility (25 °C, 1 atm)	4.4 g/L	0.097 wt. %	0.15 wt. %	75 mg/L
Upper quadruple point	294.09 K 1.489 MPa	Not available in examined literature.	283.13 K 0.4144 MPa	278.4 K 0.562 MPa
Critical point	351.55 K 5.38 MPa	339.19 K 3.595 MPa	374.30 K 4.06 MPa	369.75 K 4.247 MPa

Table A.1 (continued): Detailed analysis of specific criteria used to determine potential fluorinated hydrate formers.

<b>Commercial name</b>	<b>R407c</b>	<b>R410a</b>	<b>R507</b>
<b>Chemical formula</b>	23 wt.% R23, 23 wt.% R125, 52 wt.% R134a	50 wt.% R23, 50 wt.% R125	50 wt.% R125, 50 wt.% R143a
<b>Ecological effect</b>	ODP = 0 GWP = 1610	ODP = 0 GWP = 1890	ODP = 0 GWP = 3300
<b>Toxicity effect</b>	Skin irritation. Freeze burns from liquid contact. Nervous symptoms. Increased pulse rate.	Skin irritation. Nervous symptoms. Increased pulse rate.	Irregular heartbeat and nervous symptoms
<b>Flammability</b>	Non-flammable	Non-flammable	Non-flammable
<b>Chemical stability</b>	Stable. Do not mix with oxygen or air above atmospheric pressure.	Stable. Do not mix with oxygen or air above atmospheric pressure.	Stable, release toxic decomposition gases
<b>Hydrate former class</b>	Not available in examined literature.	II	II
<b>Compatibility</b>	Incompatible with freshly abraded aluminum surfaces, potassium, calcium, powdered aluminum, magnesium and zinc.	Incompatible with freshly abraded aluminum surfaces, potassium, calcium, powdered aluminum, magnesium and zinc.	Incompatible with alkaline metals and alloy, alkali earth metals,
<b>Water solubility (25 °C, 1 atm)</b>	Insoluble	430 mg/L	
<b>Upper quadruple point</b>	Not available in examined literature.	Not available in examined literature.	Not available in examined literature.
<b>Critical point</b>	359.20 K 4.634 MPa	343.32 K 4.770 MPa	343.95 K 3.720 MPa

## APPENDIX B

MEASURED HL<sub>V</sub> EQUILIBRIUM DATA**Table B.1: Measured HL<sub>V</sub> equilibrium data for the system CO<sub>2</sub>(1) + water (2) cited in literature.**

System	Temperature range/K	Pressure range/MPa	Reference
CO <sub>2</sub> (1) + water (2)	273.7 - 282.9	1.32 - 4.32	Deaton and Frost (1946)
	277.2 - 281.9	2.04 - 3.69	Unruh and Katz (1949)
	273.4 - 283.2	1.23 - 4.50	Larson (1955)
	273.9 - 282.0	1.38 - 3.84	Robinson and Mehta (1971)
	279.6 - 282.8	2.74 - 4.36	Ng and Robinson (1985)
	273.6 - 283.2	1.30 - 4.51	Vlahakis et al. (1972)
	274.3 - 282.9	1.42 - 4.37	Adisasmito et al. (1991)
	273.4 - 281.1	1.34 - 4.09	Ohgaki et al. (1993)
	275.1 - 282.7	1.54 - 4.16	Englezos and Hall (1994)
	275.4 - 283.3	1.56 - 4.52	Chun et al. (1996)
	273.6 - 282.0	1.31 - 4.02	Fan and Guo (1999)
	273.9 - 282.2	1.37 - 3.85	Wendland et al. (1999)
	274.7 - 279.7	1.50 - 2.78	Fan et al. (1999)
	276.5 - 282.5	1.82 - 4.01	Mooijer-van den Heuvel et al. (2002)
	277.5 - 298.3	2.05 - 47.86	Mohammadi et al. (2005)

**Table B.2: Measured HL<sub>V</sub> equilibrium data for the system 1,1,1,2-tetrafluoroethane (1) + water (2) cited in literature.**

System	Temperature range/K	Pressure range/MPa	Reference
1,1,1,2-tetrafluoroethane (1)	273.5 - 283.1	0.06 - 0.41	Liang et al. (2001)
+ water (2)	273.5 - 283.5	0.04 - 0.42	Akiya et al. (1999)
	279.4 - 282.9	0.18 - 0.38	Eslamimanesh et al. (2011)
	277.1 - 282.0	0.11 - 0.43	Ngema et al. (2013)

**Table B.3: Measured HL<sub>V</sub> equilibrium data for the system R410a (1) + water (2) cited in literature.**

System	Temperature range/K	Pressure range/MPa	Reference
R410a (1) + water (2)	277.5 - 293.0	0.18 - 1.42	Ngema et al. (2013)



**Table B.4: Measured HL<sub>V</sub> equilibrium data for the system R507 (1) + water (2) cited in literature.**

System	Temperature range/K	Pressure range/MPa	Reference
R507 (1) + water (2)	277.7 - 283.7	0.221 - 0.873	Ngema et al. (2013)

**Table B.5: Measured HL<sub>V</sub> equilibrium data for the system Former (1) + water (2) + sucrose (3) cited in literature.**

System	Temperature range/K	Pressure range/MPa	Reference
R22 (1) + water (2) + 20 wt.% sucrose (3)	277.2 - 288.7	0.16 - 0.80	Chun and Lee (1998)
R22 (1) + water (2) + 40 wt.% sucrose (3)	276.6 - 286.4	0.19 - 0.76	Chun and Lee (1998)
CO <sub>2</sub> (1) + water (2) + 20 wt.% sucrose	274.4 - 281.6	1.63 - 4.34	Chun and Lee (1999)
CO <sub>2</sub> (1) + water (2) + 30 wt.% sucrose	274.0 - 280.6	1.73 - 4.25	Chun and Lee (1999)

**Table B.6: Measured HL<sub>V</sub> equilibrium data for the system Former (1) + water (2) + glucose (3) cited in literature.**

System	Temperature range/K	Pressure range/MPa	Reference
R22 (1) + water (2) + 20 wt.% glucose (3)	276.1 - 287.5	0.16 - 0.78	Chun and Lee (1998)
R22 (1) + water (2) + 40 wt.% glucose (3)	276.0 - 283.7	0.24 - 0.70	Chun and Lee (1998)
CO <sub>2</sub> (1) + water (2) + 10 wt.% glucose	274.3 - 281.7	1.58 - 4.36	Chun and Lee (1999)
CO <sub>2</sub> (1) + water (2) + 20 wt.% glucose	274.0 - 280.6	1.73 - 4.25	Chun and Lee (1999)
CO <sub>2</sub> (1) + water (2) + 30 wt.% glucose	274.1 - 278.8	2.08 - 4.05	Chun and Lee (1999)
CH <sub>4</sub> (1) + water (2) + 10 wt.% glucose	275.4 - 281.3	3.43 - 6.02	Carbone et al. (2012)
CH <sub>4</sub> (1) + water (2) + 20 wt.% glucose	275.3 - 280.9	3.81 - 6.61	Carbone et al. (2012)
CH <sub>4</sub> (1) + water (2) + 30 wt.% glucose	275.2 - 280.9	4.43 - 7.77	Carbone et al. (2012)

**Table B.7: Measured HLV equilibrium data for the system Former (1) + water (2) + fructose (3) cited in literature.**

<b>System</b>	<b>Temperature range/K</b>	<b>Pressure range/MPa</b>	<b>Reference</b>
CO <sub>2</sub> (1) + water (2) + 20 wt.% fructose	274.4 - 280.6	1.80 - 4.24	Chun and Lee (1999)
CO <sub>2</sub> (1) + water (2) + 30 wt.% fructose	273.6 - 278.9	1.88 - 4.07	Chun and Lee (1999)

## APPENDIX C

## UNIFAC METHOD

The UNIFAC group-contribution method treats solution non-ideality as being comprised of two additive parts; a combinatorial term,  $g^C$ , to account for molecular size and shape differences, and a residual term,  $g^R$ , to account for molecular interactions.

$$g = g^C + g^R \quad (\text{C.1})$$

The UNIFAC method for estimation of activity coefficients depends on the concept that a liquid mixture may be considered as a solution of the structural units from which the molecules are formed, rather than a solution of the molecules themselves. The UNIFAC method is based on the UNIQUAC method equation, for which the activity coefficients are given by (Smith et al., 2005):

$$\ln \gamma_i = \ln \gamma_i^C + \ln \gamma_i^R \quad (\text{C.2})$$

where

$$\ln \gamma_i^C = 1 - J_i + \ln J_i - 5q_i \left( 1 - \frac{J_i}{L_i} + \ln \frac{J_i}{L_i} \right) \quad (\text{C.3})$$

$$\ln \gamma_i^R = q_i \left[ 1 - \sum_k \left( \theta_k \frac{\beta_{ik}}{s_k} - e_{ki} \ln \frac{\beta_{ik}}{s_k} \right) \right] \quad (\text{C.4})$$

In the calculation of the activity coefficients using the UNIFAC model the basic subgroups are presented in Table 2.7.

The parameters  $J_i$  and  $L_i$  are given by the following equations:

$$J_i = \frac{r_i}{\sum_j r_j x_j} \quad (\text{C.5})$$

$$L_i = \frac{q_i}{\sum_j q_j x_j} \quad (\text{C.6})$$

The following definitions apply to Equations B.3 and B.4:

$$r_i = \sum_k v_k^{(i)} R_k \quad (\text{C.7})$$

$$q_i = \sum_k v_k^{(i)} Q_k \quad (\text{C.8})$$

$$e_{ki} = \frac{v_k^{(i)} Q_k}{q_i} \quad (\text{C.9})$$

$$\beta_{ik} = \sum_m e_{mi} \tau_{mk} \quad (\text{C.10})$$

$$\theta_k = \frac{\sum_i x_i q_i e_{ki}}{\sum_j x_j q_j} \quad (\text{C.11})$$

$$s_k = \sum_m \theta_m \tau_{mk} \quad (\text{C.12})$$

$$\tau_{mk} = \exp \frac{-a_{mk}}{T} \quad (\text{C.13})$$

The values for the parameter,  $a_{mk}$ , are presented below in Table C.1.

**Table C.1: UNIFAC interactions parameters,  $a_{mk}$ , in Kelvins (Fredenslund et al.,1993).**

	<b>2</b>	<b>3</b>	<b>15</b>	<b>17</b>	<b>24</b>	<b>50</b>
<b>2 CH2</b>	0.00	0.00	986.50	1318.00	677.00	387.10
<b>3 CH</b>	0.00	0.00	986.50	1318.00	677.00	387.10
<b>15 OH</b>	156.40	156.40	0.00	353.50	-203.60	190.30
<b>17 H2O</b>	300.00	300.00	-229.10	0.00	-116.00	-197.50
<b>24 CHO</b>	505.70	505.70	529.00	480.80	0.00	-275.50
<b>50 COO</b>	529.00	529.00	88.63	284.40	577.50	0.00

The subscript  $i$  identifies the species in solution, while the subscript  $j$  is a ‘dummy’ index which covers the range of species. In the same manner, the subscript  $k$  identifies the solution subgroups, while the subscript  $m$  is a ‘dummy’ index which covers the range of subgroups. The quantity denoted by  $v_k^{(i)}$  represents the number of subgroups of type  $k$  in one molecule of species  $i$ .

## APPENDIX D

## ECONOMIC COST ANALYSIS

The cost analysis performed on the proposed hydrate separation process was based on concentrating a feed stream at 12 %Brix to a product stream at 65 %Brix. The feed flow rate was taken to be 20000 lb./hr. (9072 kg./hr.). Imperial measurements were used, as all cost factors used from the research of Barron and Wrobel were based on flow rates of lb./hr.

**D.1 Capital costs**

The capital cost associated with the construction of the hydrate separation process equipment was determined using the following equation:

$$\text{Capital cost} = (\text{Base cost})(F_s)(F_t)(F_v)(F_{hf})(F_{mat}) \quad (\text{D.1})$$

*D.1.1 Base cost*

For a direct freeze process, such as a hydrate separation process, the base cost was given as US\$1035000. Since this figure was based on the economic situation in 1985, the base cost had to be converted into its present day monetary value. This was performed through price indexing.

$$\text{Present day base cost} = \text{past price} \times \frac{\text{present day CEPCI}}{\text{past CEPCI}} \quad (\text{D.2})$$

$$\text{Present day base cost} = 1035000 \times \frac{567.3}{325.8}$$

$$\text{Present day base cost} = \$1802196$$

*D.1.2 Size factor (Fs)*

The size factor was based on the amount of water being crystallised and thus removed from the system. In order to concentrate a feed flow rate of 20000 lb./hr. at 12 %Brix to a product stream at 65 %Brix, the amount of water removed is calculated using the following equation:

$$\text{water removed} = \text{feed flow rate} - \left( \text{feed flow rate} \times \frac{\text{feed conc.}}{\text{product conc.}} \right) \quad (\text{D.3})$$

$$\text{water removed} = 20000 - \left( 20000 \times \frac{0.12}{0.65} \right)$$

$$\text{water removed} = 16308 \text{ lb/hr}$$

Therefore, from Figure E.1, the size factor was found to be,  $F_s = 1.25$ .

*D.1.3 Temperature factor (Ft)*

The temperature factor was based on the crystalliser freezing temperature. This temperature is determined from freezing point depression data. The freezing point depression for a 65 %Brix aqueous sucrose solution is 18.16 F, resulting in a freezing point of +13.84 F (Perry et al., 1997).

Therefore, from Figure E.2, the temperature factor was found to be,  $F_t = 1.08$ .

*D.1.4 Viscosity factor (Fv)*

The viscosity factor was based on the viscosity of the aqueous solution at the crystalliser operating temperature. From the HLV results obtained for this study, a typical operating temperature for a hydrate separation process is 15 °C. Therefore, the viscosity of 65 %Brix solution at 15 °C is equal to 21.13 centipoise (Perry et al., 1997).

Therefore, from Figure E.3, the viscosity factor was found to be,  $F_v = 1.26$ .

### D.1.5 Latent heat factor ( $F_{hf}$ )

The latent heat factor was based on the latent heats of fusion of the constituents being crystallised. In this case, only water is crystallised, resulting in a latent heat of fusion of 144 Btu/lb. (Barron and Wrobel, 1985).

Therefore, from Figure E.4, the latent heat factor was found to be,  $F_{hf} = 1.00$ .

### D.1.6 Material of construction factor ( $F_{mat}$ )

The material of construction factor was based on material corrosion at low temperatures. These factors are shown below in Table D.1.

**Table D-1: Material of construction cost factors (Barron and Wrobel, 1985).**

Material	Material of construction factor
Carbon steel	0.60
Line carbon steel	0.70
316 Stainless steel	1.00

Therefore, since the material of construction chosen for this process is 316 stainless steel, the material of construction factor was found to be,  $F_{mat} = 1.00$ .

## D.2 Operating and maintenance costs

The operation and maintenance costs associated with the operating and maintaining the hydrate separation process equipment were determined using the following equation:

$$\text{Operations and maintenance costs} = L + E + M + A \quad (\text{D.4})$$

### D.2.1 Labour component

The labour component was comprised of three variables; average labour rate, labour cost size factor (Cs) and overhead rate.

The average labour rate was taken as R75 per hour (UKZN, 2013) and the overhead rate was taken as 1.2 (Barron and Wrobel, 1985).

The labour cost size factor was based on the amount of water being crystallised and thus removed from the system (please refer to *D.1.2*). Therefore, from Figure E.5, the labour cost size factor was found to be,  $C_s = 0.09$ .

Therefore, the labour component was calculated as follows:

$$L = R74 \times 1.2 \times 0.09$$

$$L = R7.55$$

### *D.2.2 Energy component*

Since burning bagasse provides for all fuel requirements on a sugar mill, the energy component was taken to equal zero for this process.

### *D.2.3 Maintenance component*

The maintenance component was comprised of two variables; capital cost and annual hydrate production rate.

The annual hydrate production rate was found from the following equation (Barron and Wrobel, 1985):

$$\text{annual hydrate production rate} = 8.768 \times \text{amount of water removed} \quad (\text{D.5})$$

$$\text{annual hydrate production rate} = 8.768 \times 16308$$

$$\text{annual hydrate production rate} = 142986 \text{ lb}$$

Therefore, the maintenance component was calculated as follows:

$$M = \frac{0.035 \times R33353028}{142986}$$

$$M = R8.16$$



*D.2.4 Amortisation component*

The amortisation component was dependent on four variables; plant capacity, capital cost, project lifetime (20 years) and interest rate (12%).

Therefore, the amortisation component was calculated as follows:

$$A = \frac{R33353028 \times 0.035}{142986}$$

$$A = R31.21$$

APPENDIX E

FIGURES

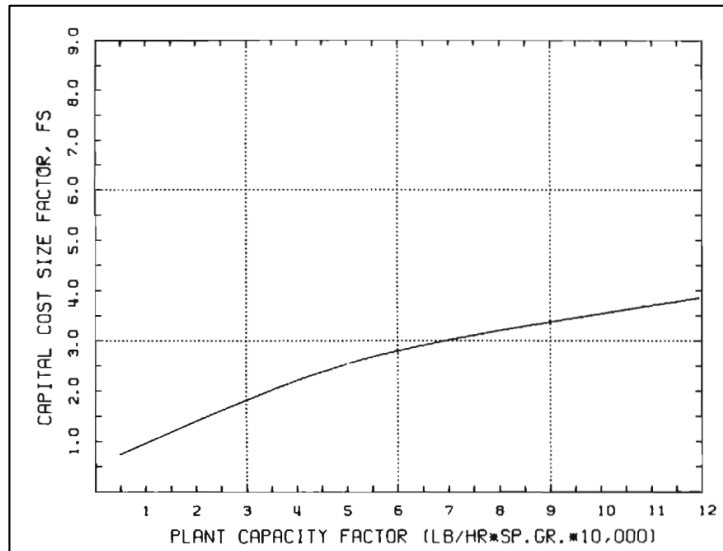


Figure E-1: Capital cost factor – size (Barron and Wrobel, 1985).

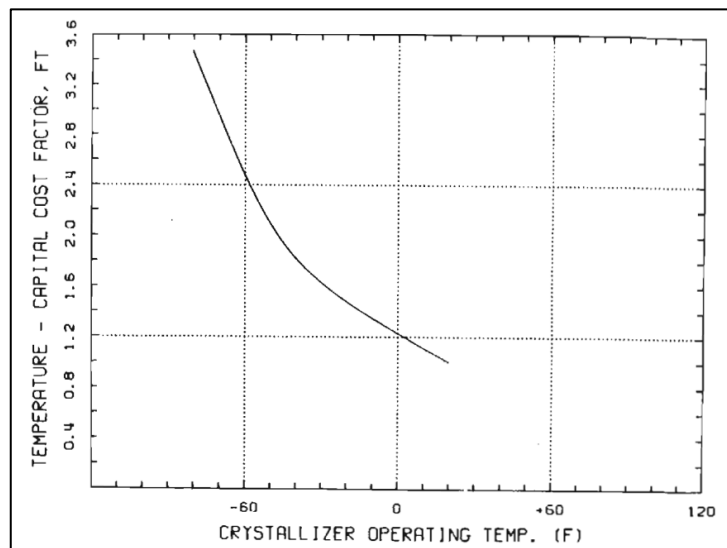


Figure E-2: Capital cost factor – temperature (Barron and Wrobel, 1985).

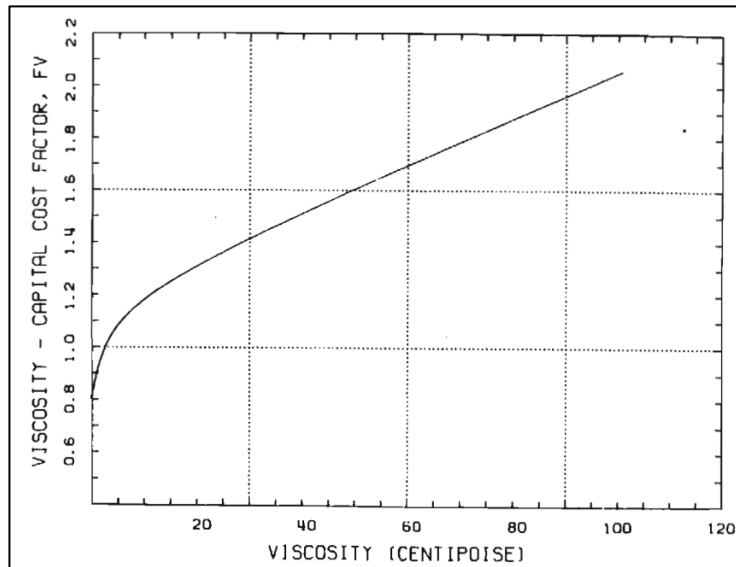


Figure E-3: Capital cost factor – viscosity (Barron and Wrobel, 1985).

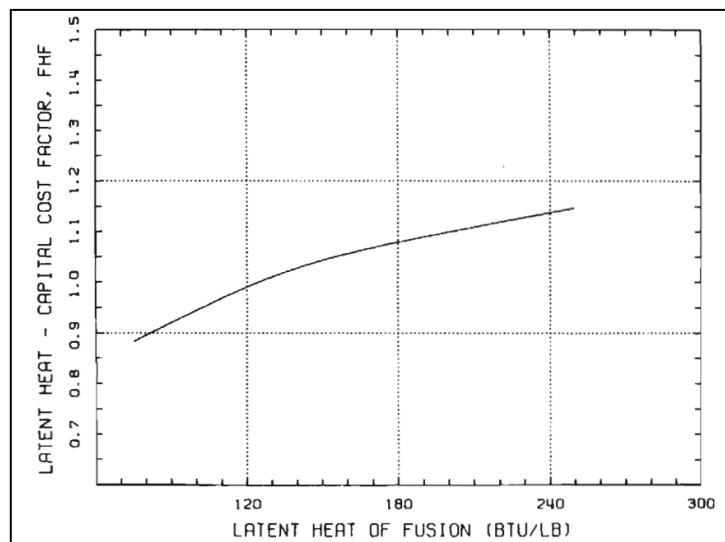


Figure E-4: Capital cost factor – latent heat (Barron and Wrobel, 1985).

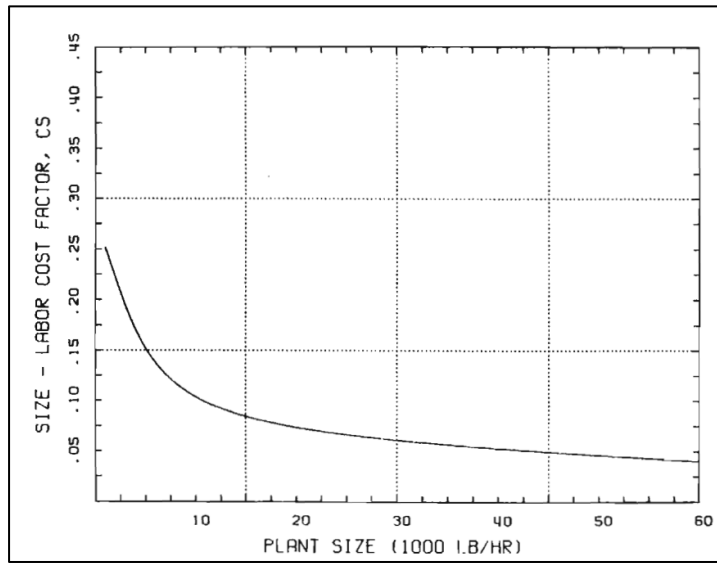


Figure E-5: Labour cost factor – size (Barron and Wrobel, 1985).